UNIVERSIDADE DE SÃO PAULO
INSTITUTO OCEANOGRÁFICO

SILVANA SIMONE BATISTA PENNINCK

Influence of environmental drivers on the plankton distribution on the inner shelf off Ubatuba, southeastern Brazil

São Paulo
2022

SILVANA SIMONE BATISTA PENNINCK

Influence of environmental drivers on the plankton distribution on the inner shelf off Ubatuba, southeastern Brazil

Corrected Version

A thesis submitted to the Instituto Oceanográfico of the Universidade de São Paulo in partial fulfilment for the degree of Doctor of Science, Oceanography, with emphasis in Biological Oceanography.

Supervisor: Dr. Rubens M. Lopes

São Paulo

2022

PENNINCK, Silvana Simone Batista. **Influence of environmental drivers on the plankton distribution on the inner shelf off Ubatuba, southeastern Brazil.** Tese (Doutorado) apresentada ao Instituto Oceanográfico da Universidade de São Paulo para obtenção do título de Doutor em Ciências, Programa de Oceanografia, área de Oceanografia Biológica.

Aprovado em 17/08/2022

Versão Corrigida

Banca Examinadora

Prof. Dr. Rubens Mendes Lopes Instituição IO - USP

Presidente Assinatura _____

Prof. Dr. José Juan Barrera Alba Instituição UNIFESP

Conceito: _____ Assinatura_____

Prof. Dra. Áurea Maria Ciotti Instituição CEBIMar - USP

Conceito: _____ Assinatura_____

Prof. Dr. Lohengrin Dias de Almeida Fernandes Instituição IEAPM

Conceito: _____ Assinatura_____

Aos meus avós paternos, Geralda e Miguel (*in memoriam*).

AGRADECIMENTOS

Ao Prof. Dr. Rubens Mendes Lopes, meu orientador, por ter me apresentado as camadas finas e aceitado me orientar nesse projeto; obrigada pelas oportunidades, pelo apoio, pela confiança e enorme paciência.

À Profa. Dra. Margaret McManus, supervisora no meu doutorado sanduíche, por ter aceitado minha proposta de colaboração e ter me recebido em seu laboratório na Universidade do Hawaii; obrigada pelo grande exemplo de mentoria e dedicação, e por sua paciência com o meu inglês.

A Coordenação de aperfeiçoamento de Pessoal de Nível Superior - CAPES pela concessão das bolsas de doutorado no Brasil e doutorado sanduíche no exterior. Aos funcionários da Secretaria de Pós-graduação do IOUSP (Ana Paula, Daniel e Leticia) pelo apoio nas questões burocráticas da pós.

À Dra. Flávia Saldanha-Correa, e às professoras Dras. Áurea Ciotti e Gleyci Moser pelas valiosas contribuições no meu exame de qualificação.

Ao professor Dr. Hidekatsu Yamazaki, por ceder o perfilador multiparâmetro para minhas coletas e pelas contribuições sobre a metodologia apropriada para observação de camadas finas.

Aos técnicos do departamento de Oc. Biológica do IO/USP, Mayza Pompeu, Tomás Silva, Mateus Chuqui por me ajudar com as análises químicas. Aos técnicos do Laboratório de Instrumentação do IO/USP pelo empréstimo dos materiais para meus trabalhos de campo, e por me ensinar a lidar com o ADCP.

À profa Dr. Camila Signori pelo incentivo e apoio com o processo do doutorado sanduíche.

Ao prof. Dr. Joseph pelas cartas de recomendação e por disponibilizar dados de satélite e de modelos.

À Luciana Frazão pela grande ajuda com a classificação taxonômica do fitoplâncton e pelo apoio nas análises no citômetro. À Maiá Medeiros e Alessandra Gomes pela ajuda com o sistema de imageamento durante as coletas. À Josiane Lima e ao Leandro de la Cruz pela ajuda com o processamento e classificação das imagens do plâncton. A todos os colegas do LAPS que participaram direta ou indiretamente nas minhas coletas em campo – Josiane, Cláudia, Yonara, Yumi, Caroline e Gelaysi. À Marta Stephan pela ajuda com a logística dos meus trabalhos de campo e pelo apoio com outros assuntos de pesquisa.

Aos funcionários da Base de Ubatuba e à tripulação do B.Pq. Veliger II, em especial ao mestre Oziel do Carmo Santos (in memoriam) que nos conduziu seguramente pelos mares de Ubatuba em todas as campanhas.

Aos meus amados pais, Maria e José, pelo apoio incondicional, educação e valores passados.

Ao meu marido Felipe pelo suporte, compreensão e presença ao longo do período de elaboração deste trabalho.

O presente trabalho foi realizado com apoio da Coordenação de Aperfeiçoamento de Pessoal de Nível Superior – Brasil (CAPES) – Código de Financiamento 001.

This study was financed in part by the Coordenação de Aperfeiçoamento de Pessoal de Nível Superior - Brasil (CAPES) - Finance Code 001.

"[...]
Não sou eu quem me navega
Quem me navega é o mar
Não sou eu quem me navega
Quem me navega é o mar

É ele quem me carrega
Como nem fosse levar
É ele quem me carrega
Como nem fosse levar

Timoneiro nunca fui
Que eu não sou de velejar
O leme da minha vida
Deus é quem faz governar

E quando alguém me pergunta
Como se faz pra nadar
Explico que eu não navego
Quem me navega é o mar [...]"

Trecho de "Timoneiro"
(Paulinho da viola & Hermínio
Bello de Carvalho)

RESUMO

PENNINCK, Silvana Simone Batista. **Influência de fatores ambientais na distribuição do plâncton na plataforma interna de Ubatuba, Brasil.** 2022. 154 f. Tese (Doutorado) – Instituto Oceanográfico, Universidade de São Paulo, São Paulo, 2022.

Com o objetivo geral de avaliar a distribuição espaço-temporal do plâncton em diferentes condições ambientais, governadas por processos físicos, na plataforma interna de Ubatuba (SP), considerando resoluções verticais e espaciais detalhadas, foram conduzidos três estudos independentes, que são apresentados ao longo desta tese na forma de artigos científicos, nos capítulos II a IV. No capítulo II, a ocorrência de camadas finas de fitoplâncton e sua evolução temporal foram investigadas ao longo de dois dias de observações em fevereiro/2019. No capítulo III foram analisadas as variações sazonais (entre inverno e verão) e de curto prazo (horas) na abundância e distribuição do plâncton e sua relação com condições hidrodinâmicas, a partir de observações realizadas em julho/2018 e janeiro/2019. No capítulo IV avaliou-se a influência das condições ambientais na abundância e distribuição vertical e horizontal das populações de *Synechococcus*, *Prochlorococcus*, pico- e nanoeucariotos, comparando diferentes cenários obtidos em dezembro/2018 e janeiro/2019. No geral, o levantamento de dados contou com técnicas de observação em campo em estações fixas e espaciais, perfilagens contínuas com sensores ópticos e acústicos de alta-resolução, além de coletas discretas de amostras para análise em laboratório. A abundância dos principais grupos que compõem o plâncton, de microrganismos autotróficos ao mesozooplâncton, foi estimada usando um sistema de imageamento *in situ* e citometria de fluxo (pico-nanoplâncton). Os resultados gerais sugerem que o vento é a principal forçante das variabilidades na abundância e distribuição vertical e horizontal do plâncton na zona costeira de Ubatuba, impulsionando fenômenos de submesoscala relacionados à intrusão e retração da Água Central do Atlântico Sul ao longo da plataforma interna, e processos de mistura vertical em eventos de mudança no padrão dos ventos, principalmente quando associados a sistemas frontais. A presente tese traz uma contribuição original ao conhecimento sobre a influência de processos físicos na distribuição do plâncton em alta resolução espaço-temporal em um ecossistema costeiro subtropical.

Palavras-chave: Distribuição do plâncton. Variação espaço-temporal. Camadas finas. Acoplamento físico-biológico. Imageamento do plâncton. Região costeira de Ubatuba.

ABSTRACT

PENNINCK, Silvana Simone Batista. **Influence of environmental drivers on the plankton distribution on the inner shelf off Ubatuba, southeastern Brazil.** 2022. 154 f. Tese (Doutorado) – Instituto Oceanográfico, Universidade de São Paulo, São Paulo, 2022.

With the general objective of evaluating the spatiotemporal distribution of plankton under different environmental conditions, governed by physical processes, on the inner shelf off Ubatuba (SP), Brazil, considering more detailed vertical and spatial resolutions, three independent studies were carried out. These studies are presented throughout this thesis in the form of scientific articles, in chapters II to IV. In chapter II, the occurrence of thin layers of phytoplankton and their temporal evolution were investigated over two days of observations in February/2019. Chapter III analyzed seasonal (winter/summer) and short-term variation (hours) in the plankton abundance and distribution and their relationship with hydrodynamic conditions, based on observations carried out in July/2018 and January/2019. In chapter IV the influence of environmental conditions on the abundance and vertical and horizontal distributions of the *Synechococcus*, *Prochlorococcus*, picoeukaryotes, and nanoeukaryotes populations was evaluated, comparing different scenarios obtained in December/2018 and January/2019. Overall, the data collection relied on field observation techniques at fixed and spatial stations, continuous high-resolution profilings with optical and acoustic sensors, in addition to discrete sample collection for analysis in laboratory. The abundance of the main plankton groups, from autotrophic microorganisms to mesozooplankton, was estimated using an *in situ* imaging system and flow cytometry (pico-nanoplankton). The general results suggest that the wind is the primary forcing of the variability in the plankton abundance and vertical and horizontal distribution in the coastal zone of Ubatuba, driving submesoscale phenomena related to the intrusion and retreat of the South Atlantic Central Water along the inner shelf and vertical mixing processes in events of change in the wind pattern, especially when associated with frontal systems. The present thesis makes an original contribution to the knowledge about the influence of physical processes on plankton distribution in high spatio-temporal resolution in a subtropical coastal ecosystem.

Keywords: Plankton distribution. Spatiotemporal variability. Thin layers. Physical-biological coupling. Plankton imaging. Ubatuba coastal region.

INDEX OF FIGURES

Chapter I

Chapter II

Chapter III

Chapter IV

Appendix A

Appendix B

Appendix C

INDEX OF TABLES

Chapter IV

Appendix A

Appendix B

Appendix C

LIST OF ABBREVIATIONS AND ACRONYMS

ADCP	Acoustic Doppler Current Profiler
AOU	Apparent Oxygen Utilization
Chl-a	Chlorophyll-a
Chl-Flu	Chlorophyll-a Fluorescence
CMEMS	Copernicus Marine Environment Monitoring Service
CW	Coastal water
DO	Dissolved Oxygen
Feb.	February
Fig.	Figure
IOUSP	Oceanographic Institute of the University of São Paulo
LAPS	Laboratory of Plankton Systems
LCR	LAPS Camera Recorder
LLS	LAPS Learning Set
LPD	LAPS Plankton Detector
MVBS	Mean Volume Backscattering Strength
N	Brunt-Väisälä frequency or Buoyancy Frequency
NanoEuk	Nanoeukaryotes
PicoEuk	Picoeukaryotes
Pro	*Prochlorococcus*
Ri	Richardson Number
ROI	Region of interest
RVBS	Relative Volume Backscatter Strength
S^2	Vertical Current Shear
SACW	South Atlantic Central Water
SBCS	Southeastern Brazilian Continental shelf
SBS	Southern Brazilian shelf
SCM	Subsurface Chlorophyll Maximum
SW	Shelf Water
Syne	*Synechococcus*
Temp.	Temperature
Tur.	Turbidity
TW	Tropical Water
USP	University of São Paulo
Zeu	Euphotic Zone Depth

SUMMARY

1. Chapter I – Introduction

1.1. Overview

The distribution and dynamics of plankton communities in the marine environment are deeply related to the physical conditions of the environment they live in. Physical-biological coupling relationships have implications for interactions within the ecosystem, influencing fisheries (WHITE et al., 2019), distribution of biogeochemical properties (HAAS et al., 2021), and carbon fluxes (EHRNSTEN et al., 2019). Biophysical interactions have been identified as drivers in the formation of phytoplankton patches and zooplankton aggregates in temperate, subtropical, and tropical environments, from the open ocean to coastal and estuarine systems (BENOIT-BIRD; SHROYER; MCMANUS, 2013; MCMANUS et al., 2021; KASAI et al., 2010; MULLIN; BROOKS, 1976).

Physical processes impact plankton biology from very small spatial scales, such as the microscale (centimeters or less) and the fine-scale (meters scale), to large scales, such as the submesoscale (0.1-10 km) and the mesoscale (of tens to hundreds of kilometers) (PRAIRIE et al., 2012). Regarding the temporal scales, there are long-term and interannual components (e.g., climate changes and oscillations), seasonal (complete seasons of the year), related to (sub)mesoscale (e.g., vortices and ocean fronts), and short-term (e.g., tidal cycles and rare or extreme events). The temporal and spatial scales are interconnected, considering that a certain biological parameter, when transported by the flow, undergoes a displacement in time and space from a fixed reference point (MAHADEVAN, 2016).

In coastal zones, drivers interact at different spatiotemporal scales, constituting a complex and heterogeneous ecosystem (MANN; LAZIER, 2006). In these regions, short-term variations can be greater than seasonal ones, leading to strong spatiotemporal variations in nutrient concentration and phytoplankton biomass (NOGUEIRA; BRANDINI, 2018). The influence of physical processes on plankton variability at smaller temporal and spatial scales has been little explored in the coastal zone of Ubatuba, Southeastern Brazil, which has a strong seasonal and short-term variability in water masses and hydrodynamic conditions (CASTRO FILHO; MIRANDA; MIYAO, 1987; CERDA; CASTRO, 2014; MAZZINI, 2009). The transient intrusions of the South

Atlantic Coastal Water (SACW) on the continental shelf off Ubatuba mediated by submesoscale processes provide an opportunity to evaluate mechanisms of physical-biological coupling.

Thus, the general objective of this thesis is to study the high-resolution spatiotemporal distribution of plankton and its relationship with different submesoscale and small-scale processes on the inner shelf off Ubatuba. The specific objectives are addressed in three independent chapters in the form of scientific articles (Table 1.1). Chapter II deals with the physical and biological mechanisms of formation and dissipation of thin layers of phytoplankton, observed in the summer of February/2019. In Chapter III, the short-term variability of the spatial distribution and abundance of plankton (phytoplankton and zooplankton) and their relationship with oceanographic conditions observed in July/2018 (winter) and January/2019 (summer) are analyzed. In Chapter IV, the spatial distributions of the pico- and nanoplankton in response to physical-chemical conditions are studied in two different scenarios between late spring and summer, in December/2018 and January/2019.

For data collection, high-resolution environmental sensors and imaging techniques were used, in addition to water samplings for analysis in the laboratory, at fixed oceanographic stations and in transects along the inner shelf. In Chapters II and III the abundances of the main micro- and mesoplankton groups were estimated using an *in situ* imaging system. In Chapter II, the temporal plankton variability was evaluated over 12 h, considering vertical scales from ~0.5 to 1 m, while in Chapter III, the temporal and spatial variability of plankton was evaluated at fixed stations of 12 and 24 h, and along a cross-shore transect with stations at intervals of about 1.5 km. In Chapter IV, the flow cytometry technique was used to estimate pico- and nanoplankton abundances and study their variability along the inner shelf between 7 stations at ~1.5 km apart (see Table 1.1).

Assessing the plankton distribution variability using high-resolution spatiotemporal sampling techniques is critical to understanding biophysical interactions and their consequences for planktonic community structure. This work aims to add more knowledge of the dynamics of physical and biological processes operating in the coastal ecosystem of Ubatuba, contributing to future assessments of the plankton response to changes in physical and physicochemical conditions in coastal zones induced by climate change, in addition to serving as a database for plankton monitoring.

Table 1.1. Objectives, sampling date, temporal and spatial scales, environmental variables, plankton size groups, and data collection methods for the chapters II to IV of this doctoral thesis.

Chapter	Objective	Date	Temporal scale	Vertical scale	Horizontal scale	Environmental variables	Plankton size groups	Methods
II - Thin layers in the coastal zone of Ubatuba, Brazil: mechanisms of formation and dissipation	To investigate the occurrence and temporal variability of fine-scale micro- and mesoplankton aggregations and the physical and biological processes involved in their formation and dissipation.	Feb/2019	12 h	0.5 - 1 m	-	Temperature, salinity, dissolved oxygen, turbidity, chlorophyll-a, nutrients, Brunt–Väisälä frequency, Richardson number, current shear, wind data, sea surface height, and Ekman transport	Microplankton (mainly > 100 µm) Mesoplankton (0.2-20 mm)	High-resolution environmental sensors; Water sampling; Satellite data; *In situ* imaging system
III - Short-term variability in plankton abundance on the inner shelf off Ubatuba, Brazil	To assess short-term variations in the distribution of the main micro- and mesoplankton groups on the inner shelf and their relationship with submesoscale processes.	Jul/2018 and Jan/2019	12/24 h	1 m	~1.5 km	Temperature, salinity, dissolved oxygen, turbidity, chlorophyll-a, nutrients, Brunt–Väisälä frequency, Richardson number, wind data, and sea surface height	Microplankton (mainly > 100 µm) Mesoplankton (0.2-20 mm)	High-resolution environmental sensors; Water sampling; Satellite data; *In situ* imaging system
IV - Influence of environmental conditions on the pico-nanophytoplankton distribution on the inner shelf off Ubatuba, Brazil	To address the relationships between environmental conditions and the vertical distribution of pico- and nanoplankton abundance at small spatial scales along the inner shelf.	Dec/2018 and Jan/2019	-	few meters	~1.5 km	Temperature, salinity, dissolved oxygen, turbidity, chlorophyll-a, nutrients, euphotic zone, apparent oxygen utilization, Brunt–Väisälä frequency, and wind data	Picoplankton (0.2-2 µm) Nanoplankton (2-20 µm)	High-resolution environmental sensors; Water sampling; Satellite data; Flow cytometry

1.2.Study site

The study area, in the coastal region of Ubatuba, state of São Paulo, is located on the Southeastern Brazilian Continental shelf (SBCS), in the southwestern Atlantic Ocean (Fig. 1.1). The internal and external sections of the SBCS have different dynamics. The outer shelf is influenced by the Brazil Current, while the inner shelf has the dynamics controlled by the winds (CASTRO, 1997). The tidal currents on the continental shelf are low in energy and there are no large river discharges. Thus, winds have been identified as the most energetic forcing of circulation on the SBCS (CASTRO, 1985; MAZZINI, 2009).

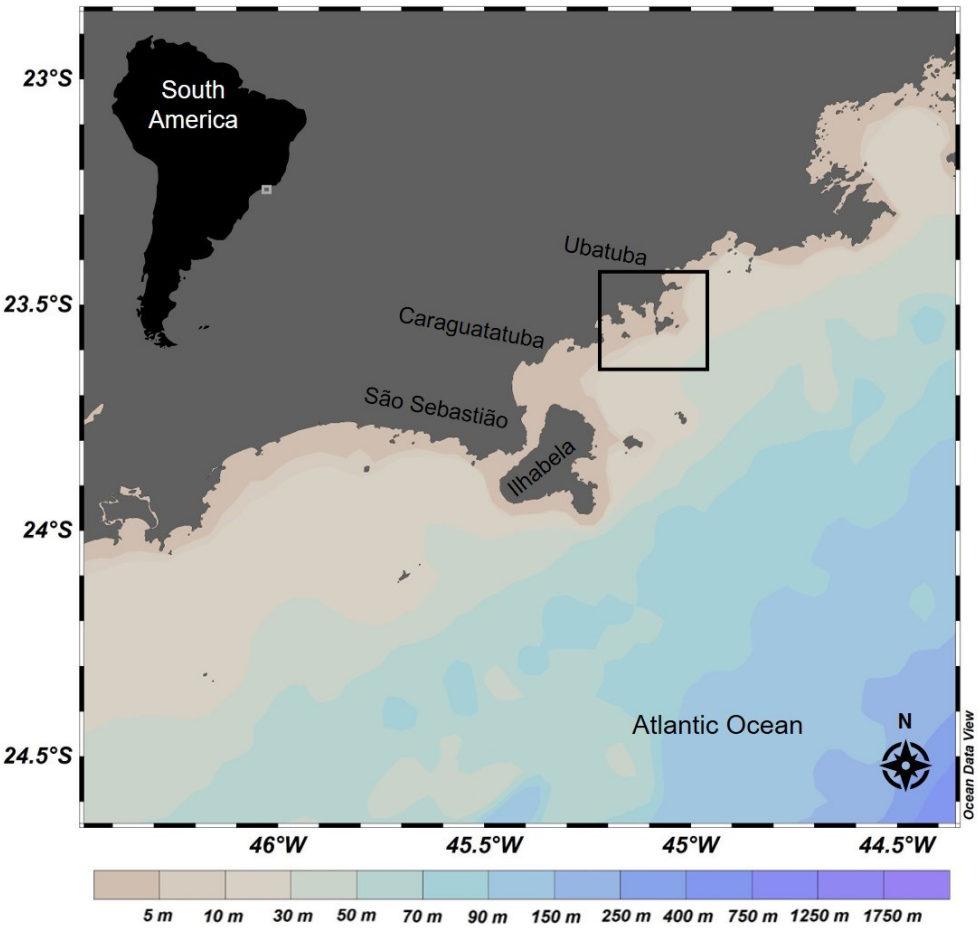

Fig. 1.1. Bathymetric map of the northern coast of the state of São Paulo, southeastern Brazil, with the delimitation of the study area (square) located on the inner shelf off Ubatuba.

Observational studies off Ubatuba have shown that on the inner shelf the direction of currents is predominantly to the southwest, with inversion events to the northeast (anticyclonic rotation) at the passage of frontal systems (CASTRO, 1997; CASTRO; MIRANDA, 1998). Moreover, hydrodynamic energy in this region is considered low to moderate, due to the presence of islands (Ilhabela, Mar Virado, and Anchieta Islands), which act as a barrier to the action of waves from the open ocean (BATISTA; HARARI, 2017; MAHIQUES, 1995).

The shelf off Ubatuba is characterized by the presence of three water masses that interact with each other, modifying temperature, salinity, and nutrient concentrations: (CASTRO FILHO; MIRANDA; MIYAO, 1987): Tropical Water (TW; relatively high salinity, high temperature, low nutrient concentration), Coastal Water (CW; relatively low salinity, high temperature, variable nutrient concentration) and South Atlantic Central Water (SACW; relatively low temperature, high nutrient concentration). The presence of oceanic SACW on the coast occurs from late spring to late summer induced by prevailing winds from E-NE, which via Ekman transport move the CW at the surface to offshore, causing the bottom intrusion of the SACW onto the shelf, towards the euphotic zone (MIRANDA; KATSURAGAWA, 1991; QUINTANA et al., 2015).

SACW intrusions are the most relevant (sub)mesoscale phenomenon in this region (CERDA; CASTRO, 2014), affecting the dynamics of the entire ecosystem. When SACW penetrates onshore from the slope up to the inner shelf a strong stratification is established at midwater. In the euphotic zone, phytoplankton respond to enrichment in nutrient concentration (mainly nitrate) with an increase in biomass (AIDAR et al., 1993; BRANDINI et al., 2014), enhancing primary production (GAETA et al., 1999) and stimulating an increase in zooplankton biomass and abundance (LOPES et al., 2006; MELO JÚNIOR et al., 2016). Furthermore, the association between the availability of nutrients provided by SACW and the physical processes of stratification and current shear through the water column can lead to the formation of particle aggregation (MARCOLIN; LOPES; JACKSON, 2015).

1.3.Objectives

The general objective is to evaluate the high-resolution spatiotemporal distribution of plankton under different submesoscale and small-scale processes in the coastal system of Ubatuba, southeastern Brazil. Specifically, the objectives are:

1. To investigate the occurrence and temporal variability of fine-scale micro- and mesoplankton aggregations (thin layers) and the physical and biological processes involved in their formation and dissipation.
2. To assess short-term (hours) variations in the vertical and horizontal distribution of the main micro- and mesoplankton groups on the inner shelf and their relationship with submesoscale processes.
3. To address the relationships between environmental conditions and the vertical distribution of pico- and nanoplankton abundance at small spatial scales along the inner shelf.

2. Chapter II - Thin layers in the coastal zone of Ubatuba, Brazil: mechanisms of formation and dissipation.

2.1. Abstract

Thin layers are vertically compressed, horizontally extensive highly concentrated features comprised of plankton and/or particles. They are critical components of the marine ecosystem, likely playing a key role in the life histories and evolutionary trajectories of species found in, or, interacting with them. These structures have been reported in diverse marine environments around the globe. However, the mechanisms of thin layer formation/dissipation in the southwestern Atlantic Ocean were unknown until this contribution. To assess the temporal evolution of thin phytoplankton layers on the inner shelf off Ubatuba, Brazil, we conducted two oceanographic fixed station cruises, including optics, acoustics, and imaging techniques. Over a period of two days, three thin layers were observed: within the pycnocline, close to the maximum stratification, and below the pycnocline where phytoplankton were affected by the enhanced nutrient supply provided by the South Atlantic Central Water (SACW). Changes in regional wind patterns influenced the presence of SACW, which directly affected shear and stratification: the main physical mechanisms we attribute to thin layer formation in this region. The associated biological mechanisms contributing to thin layer formation were biomass accumulation (*in situ* growth) and likely the mobility of dinoflagellates. The dominant organisms in the thin layer depths and surroundings, by our *in-situ* imaging system, were cyanobacteria, diatoms, dinoflagellates, and crustaceans. Thin Layers likely have crucial importance for meso-oligotrophic environments, representing important feeding resources for higher trophic levels.

This chapter was published in *Limnology and Oceanography* and can be accessed via the link: **https://doi.org/10.1002/lno.11623**.

Keywords: Physical–biological coupling, thin layers, phytoplankton, South Atlantic Central Water, southeastern Brazilian continental shelf.

2.2.Introduction

The vertical distribution of plankton is influenced by an interplay of physical, chemical, and biological factors that can lead to the formation of structures called “thin layers”. Thin layers are features with an accumulation of plankton or particles on a vertical scale from centimeters to a few meters (DONAGHAY; RINES; SIEBURTH, 1992), often extending horizontally for kilometers (COWLES; DESIDERIO; CARR, 1998) and persisting for hours to several days. Fine-scale aggregations of phytoplankton are common features and can be found in a wide variety of environments, being recurrent in stratified coastal and ocean waters (SULLIVAN; DONAGHAY; RINES, 2010).

Marine phytoplankton influence the abundance and diversity of organisms, stimulate the functioning of the marine ecosystem, and determine the maximum limits for fishery production (CHASSOT et al., 2010), in addition to exerting a strong influence on climatic processes and biogeochemical cycles (ROEMMICH; MCGOWAN, 1995; SABINE et al., 2004). Previous research has pointed out important implications of thin layers of phytoplankton for trophic dynamics (BENOIT-BIRD; COWLES; WINGARD, 2009), carbon fluxes in the ocean (BOCHDANSKY et al., 2010), and harmful algal blooms (MCMANUS et al., 2008). Thin layers represent an important source of food restricted vertically in the water column, being important in determining the nutrition and survival of grazers (MULLIN; BROOKS, 1976). The presence of thin layers likely alters local concentrations of nutrients, toxins, and organisms, playing an important role in biological processes in coastal environments (COWLES; DESIDERIO; CARR, 1998).

In view of their role in planktonic ecosystems, it is essential to determine what controls the formation of thin plankton layers. Thin layers can be generated by a variety of biological and physical mechanisms, including cell behavior, morphology, population dynamics, fluid stratification, and vertical current shear (DURHAM; STOCKER, 2012). Studies have documented the processes involved in the formation and persistence of thin layers in coastal regions (BARNETT et al., 2019; MCMANUS et al., 2012) and in frontal and coastal upwelling zones (DE VERNEIL; FRANKS; OHMAN, 2019; VELO-SUÁREZ et al., 2010).

Dekshenieks et al. (2001) provided one of the first quantitative studies of thin layers and the associated physical processes, in a Northern Pacific fjord, and emphasized the importance of

studying local circulation patterns and regional physical forcing in understanding the dynamics of these features. Cheriton et al. (2007) studied the occurrence of thin layers along the west coast of the U.S., noting that a change in regional wind patterns precipitated a change in physical structure of the water column, leading to the absence of thin layers of zooplankton. Stacey et al., (2007) point out that the turbulent diffusion caused by regional winds, convective processes and action of internal waves act as divergent or dissipating processes of layers, while the vertical current shear, the passive deposition of phytoplankton on a density surface and the phytoplankton mobility act as convergent, layer-forming processes.

Thin layers are often related to the thermocline, halocline or pycnocline (DEKSHENIEKS et al., 2001; RINES et al., 2002; STEINBUCK et al., 2009) and have been reported in environments with both low shear and turbulent mixing. Shroyer et al. (2014) identified thin biological layers in regions where intense mixing events were rare, within the pycnocline (close to maximum stratification) and at the base of the pycnocline. Talapatra et al. (2013) found several peaks of *Chaetoceros socialis* colonies, non-motile diatoms, near the pycnocline, in a region of almost zero shear, low rates of dissipation, and high stratification. Onitsuka et al. (2018) observed the temporal evolution of a diatom-rich layer formed just below the pycnocline, where the turbulent mixture was weak, in a stratified bay in Japan.

Studies on fine-scale plankton structures have been highly dependent on available technology and sampling methodologies (MCMANUS et al., 2012). Effective measurement methods comprise profiling with high vertical resolution (order of centimeters), typically from sensors with slow deployment speeds through the water column and/or high sampling rates. In addition, the decrease in the effects of the vessel's movement during profiling must be considered, using free-fall sensors or from platforms decoupled from the vessel (SULLIVAN et al., 2010).

In this study, optical and acoustic sensors and a high-resolution imaging system were combined to investigate the occurrence, persistence, and dissipation of fine-scale phytoplankton aggregations and to study the influence of these structures on zooplankton distributions. Thin layers of phytoplankton were observed in the coastal waters of Ubatuba, southeastern Brazil, in February 2019 during the summer, when vertical stratification associated with bottom intrusions of cold and nutrient-rich water occur.

Motivated by the hypothesis that physical constraints provide an appropriate environment for the formation of thin layers in the study area and that their presence has important ecological

implications for this meso-oligotrophic environment, this work investigates the short-term temporal changes in phytoplankton vertical distribution and its relationship with physical and biological processes and represents the first study on thin layers in the southwestern Atlantic Ocean.

2.3. Materials and Methods

Sampling – fixed stations

A fixed oceanographic station was occupied in two consecutive 12-hour intervals from 8:00 to 20:00 on February 20 and 21, 2019, aboard the 14 m research boat *Veliger II* of the Oceanographic Institute of the University of São Paulo (IOUSP), at the study site (Fig. 2.1; 45°5.533' W, 23°35.318' S). During these intervals, profiles were collected roughly every 30-min, resulting in a total of 48 profiles over two days. The RINKO-profiler and a plankton imaging system were attached to the same frame for simultaneous profiling. The sinking speed (~0.27 m s^{-1}) and buoyancy of the instrumentation packaged were controlled by adding floats to the frame to reduce turbulence during lowering.

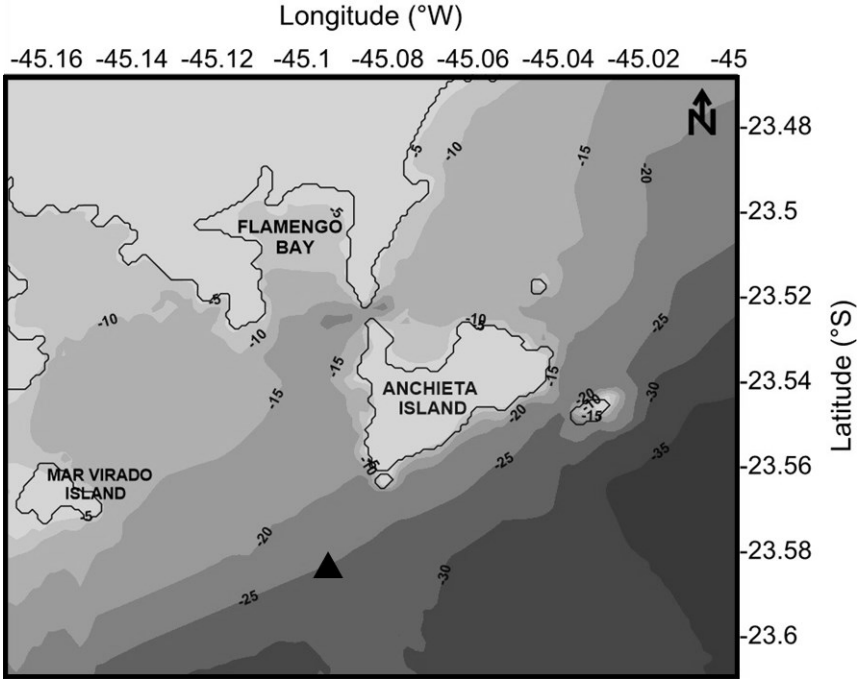

Fig. 2.1. Map of the study area on the inner shelf off Ubatuba. The location of the fixed-point sampling station is indicated by the closed black triangle (25 m isobath). Bathymetric contours are in 5-m increments, where dark grey represents deeper depths.

A high-resolution multiparameter ***RINKO-profiler*** (JFE Advantech Co.) was used to obtain fine-scale profiles of water temperature, salinity, chlorophyll-a fluorescence (Chl-Flu), and turbidity (optical backscatter intensity) at 0.1 m intervals (depth trigger mode) at each station (Fig. 2.2B). Table 2.1 shows the specifications of the sensors used.

Table 2.1. RINKO-profiler sensor specifications.

Sensor	**Type**	**Resolution**	**Accuracy**
Depth	Pressure sensor	0.01 m	±0.3% FS
Temperature	Thermistor	0.001 °C	±0.01 °C (0 to 35 °C)
Salinity	Practical salinity	0.001	----------
Turbidity	Backscattered light	0.03 FTU	±0.3 FTU or ±2% of measured value
Chlorophyll	Fluorometric	0.01 ppb	±1% FS (0 to 200 ppb)

A plankton imaging system was used to obtain qualitative and quantitative plankton data (Fig. 2.2A). The system, based on shadowgraphic imaging, is a prototype developed by IOUSP (MEDEIROS, 2017). Consisting of a collimated infrared LED beam and a high-resolution camera (4MP) with a frame rate ranging between 6 and 15 frames per second, pixel size of 5.5 µm, and a volume of 4.5×10^{-6} m³ per image. Computer vision processing tools developed at the Laboratory of Plankton Systems (LAPS-IOUSP) allowed for the characterization and classification of organisms down to taxonomic groups, using the Random Forest algorithm. The system captures particles above 5.5 µm, but only particles above 100 µm can be reliably identified in the taxonomic classification step.

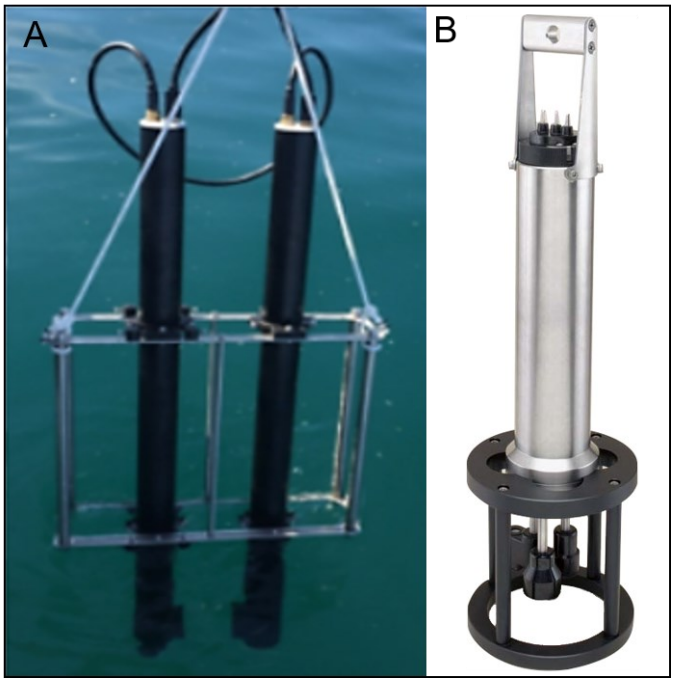

Fig. 2.2. (A) Shadowgraphic imaging system consisting of two cylindrical tubes, both 1.12 m long and 9.5 cm wide. (B) Rinko-profiler, 49.1 cm long and 13.6 cm wide. The RINKO-profiler was coupled to the imaging system frame for simultaneous profiling.

For analysis of the chlorophyll-a (Chl-*a*) and nutrient concentrations, water was collected with a go-flo bottle every 4 hours at various depth levels along the water column: surface (0 m), mixing layer (~5 m), top of the thermocline (~10 m), vicinity of the fluorescence peaks (~15 m to ~21 m, at 2 m intervals) and bottom (~23 m). The water samples were filtered through a 25 mm GF/F filter immediately after collection and the filters were stored in an ultra-freezer (-80 °C) until the extraction of Chl-*a* in the laboratory. Aliquots of the filtered water were separated and frozen (-20 °C) for analysis of dissolved inorganic nutrients (nitrite, nitrate, phosphate, and silicate). The nutrients were determined in the laboratory using a flow injection auto-analyzer (AutoAnalyzer 3 HR, SEAL Analytical Inc.). Chl-*a* concentrations were measured using a fluorometer (10-AU, Turner designs Inc.) according to the method proposed by Welschmeyer (1994). The correlation coefficient between the Chl-Flu and the extracted Chl-*a* concentration was 0.89 (n = 50).

To obtain velocity data throughout the water column, a vessel-mounted downward-looking Sontek 500-kHz ADCP was used. The vessel-mounted ADCP made measurements from near-surface (~3 m) to near-bottom with 1.0 m vertical resolution, during the 12-h observations, on both days. The tidal level was predicted by harmonic analysis (HARARI; MESQUITA, 2003). The

hourly sea level data were provided by the Copernicus Marine Environment Monitoring Service (CMEMS). Wind data were obtained from the Climate Forecast System Version 2 (CFSv2), produced by the NOAA National Centers for Environmental Prediction (NCEP).

Calculation of physical variables

Stratification in the water column was estimated by calculating the Brunt-Väisälä Frequency (N^2; in s^{-2}). This parameter is related to both the stability of the water column and the vertical density gradient, and was calculated from:

$$N^2 = -\frac{g}{\rho_0}\left(\frac{\partial \rho}{\partial z}\right) \tag{1}$$

where g is the acceleration of gravity, z is the depth, ρ is the seawater density and ρ_0 is the average density (POND; PICKARD, 1983). High N^2 values indicate a stratified portion of the water column, while low values are found in vertically homogeneous regions. The quantification of vertical shear (S^2) was determined by:

$$S^2 = \left(\frac{\partial U}{\partial z}\right)^2 + \left(\frac{\partial V}{\partial z}\right)^2 \tag{2}$$

where U and V are, respectively, the zonal and meridional components of the currents (ITSWEIRE; OSBORN; STANTON, 1989).

The Richardson number (*Ri*) defines the relative importance of stabilization due to vertical density stratification *versus* destabilization due to vertical velocity shear, and was calculated by the following equation:

$$Ri = \frac{N^2}{S^2} \tag{3}$$

To analyze the effects of the wind forcing at the surface, a simplification of the Ekman transport (U_e), east-southeastward, considering the shoreline orientation, was estimated as:

$$U_e = \frac{\tau_y}{\rho_0 f} \tag{4}$$

where τ_y is the wind stress on the sea surface, obtained using the bulk formula (STEWART, 2008), ρ_0 is the density of sea water (ρ_0 = 1025 kg/m³), and f is the Coriolis parameter.

Estimation of the mean volume backscatter strength

The Sontek 500 kHz ADCP was initially deployed to measure water velocity, however, it was also used to estimate the volume backscattering strength from the ADCP signal strength data (echo level). To estimate the volume backscattering strength, a rearrangement of the sonar equation was used (DEINES, 1999; SONTEK-YSI INC., 1997):

$$MVBS = C + 10log_{10}[(T_x + 273.16)R^2] - L_{DBM} - P_{DBM} + 2\alpha R + K_c(E - E_r) \quad (5)$$

where *MVBS* is the mean volume backscattering strength (dB); *C* is a constant factor specific to the instrument used (dB); T_x is the temperature detected at the transducer (°C); *R* is the slant rage (m); L_{DBM} is the $10\log_{10}$ of the transmit pulse length (1 m); P_{DBM} is the $10\log_{10}$ of the transmit power, specific for the instrument; α is the frequency-specific absorption coefficient in seawater (0.14 dB/m at 500 kHz); K_c is an instrument-specific constant that converts counts in decibels (in this case K_c = 0.43; Sontek-YSI Inc. 1997); *E* is echo level or signal strength (counts); E_r is the noise level. Because *C* and P_{DBM} could not be accurately measured during sampling, they were set to zero. These missing parameters do not affect the objectives of the application of the acoustic data in this study. However, in this contribution, the MVBS was considered an indirect and qualitative proxy for relative zooplanktonic biomass, representing *relative volume backscatter* - RVBS.

Thin Layer identification

During the evolution of research on thin layers, the criteria for their identification have been customized for different environments. There is no standard for thin layer characterization in the literature, but there are some criteria to be followed for identification, which vary depending on the instruments to be used, the type of organisms in the layer, and the region of study in the ocean (DEKSHENIEKS et al., 2001; SULLIVAN et al., 2010).

For this work, three specific criteria were established to define a thin layer structure. (1) The fluorescence peak must be present in two or more subsequent profiles; this helps eliminate ephemeral structures. (2) The layer must be ≤ 3.61 m thick at half maximum intensity; this value

was chosen based on previous studies (DEKSHENIEKS et al., 2001; MCMANUS et al., 2012; RYAN et al., 2008). (3) The intensity of the fluorescence peak must be at least 1.3 times the background levels, a signal intensity previously considered for oligotrophic or mesotrophic waters with low plankton biomass (BENOIT-BIRD et al., 2010; MCMANUS et al., 2012).

2.4. Results

Meteorological and oceanographic conditions

On Feb 20th, 2019, winds were predominantly from the northwest and the northeast with speeds from 3.60-5.70 m s^{-1} and 2.10-3.60 m s^{-1}, respectively (Fig. 2.3D). On Feb 21st winds were predominantly from the southwest and southeast at speeds between 2.10 and 3.60 m s^{-1}, and from the east with speeds between 3.60 and 5.70 m s^{-1} (Fig. 2.3E). The wind fields for Feb 20th and 21st are illustrated in Fig. 2.3A. The ocean currents in this region have a predominant flow to the southwest, however, when cold fronts pass through the area from the southwest, the current direction is known to reverse and flow to the northeast (CASTRO et al., 2006).

The general shoreline orientation of the southeastern Brazilian coast, approximately southwest-northeast, and the shallow shelf with isobaths parallel to the coast, provides conditions for raising or lowering sea level by Ekman transport, due to the action of winds along the coast from southwest or northeast, respectively (TRUCCOLO, 2011). Over the study days, there was an increase in sea surface height (Fig. 2.3B, solid line), of about +0.1 m, while the Ekman transport (Fig. 2.3B, dashed line) changed direction from offshore (to east, positive signal) to onshore (to west, negative signal). This was most likely due to the relaxation of the winds from north-northeast (weak winds < 3 m s^{-1}) and an increase in winds from southwest-southeast.

The study took place during a spring tide. The tides in this region are semi-diurnal with diurnal inequality (MESQUITA; HARARI, 1983). On Feb 20th, the tide flooded from 09:49 h to 14:32 h, with a range of 0.80 m, and ebbed from 14:32 h to 22:13 h, with a range of 1.20 m. On Feb 21st, the tide flooded from 10:24 h to 15:00 h, with a range of 0.90 m, and ebbed from 15:00 h to 23:00 h, again with a range of 1.20 m (Fig. 2.3C).

On Feb 20th, during the flood tide, the currents flowed to east/northeast in the subsurface (3-5 m) and, predominantly, to west between 7-18 m, and northwest near the bottom, between 19-

25 m (Fig. 2.4 A1). During the ebb tide, the current direction was reversed to east/southeast (Fig. 2.4 A2). On Feb 21st, during the flood tide, currents flowed to the east/northeast between the surface (3 m) and 15 m depth, while from 16 m to the bottom the currents underwent anticyclonic rotation, flowing to the west/northwest (Fig. 2.4 B1). On ebb tide, the predominant flow throughout the water column was to the east, except for a rotation in current to the north between 18 m and 21 m (Fig. 2.4 B2).

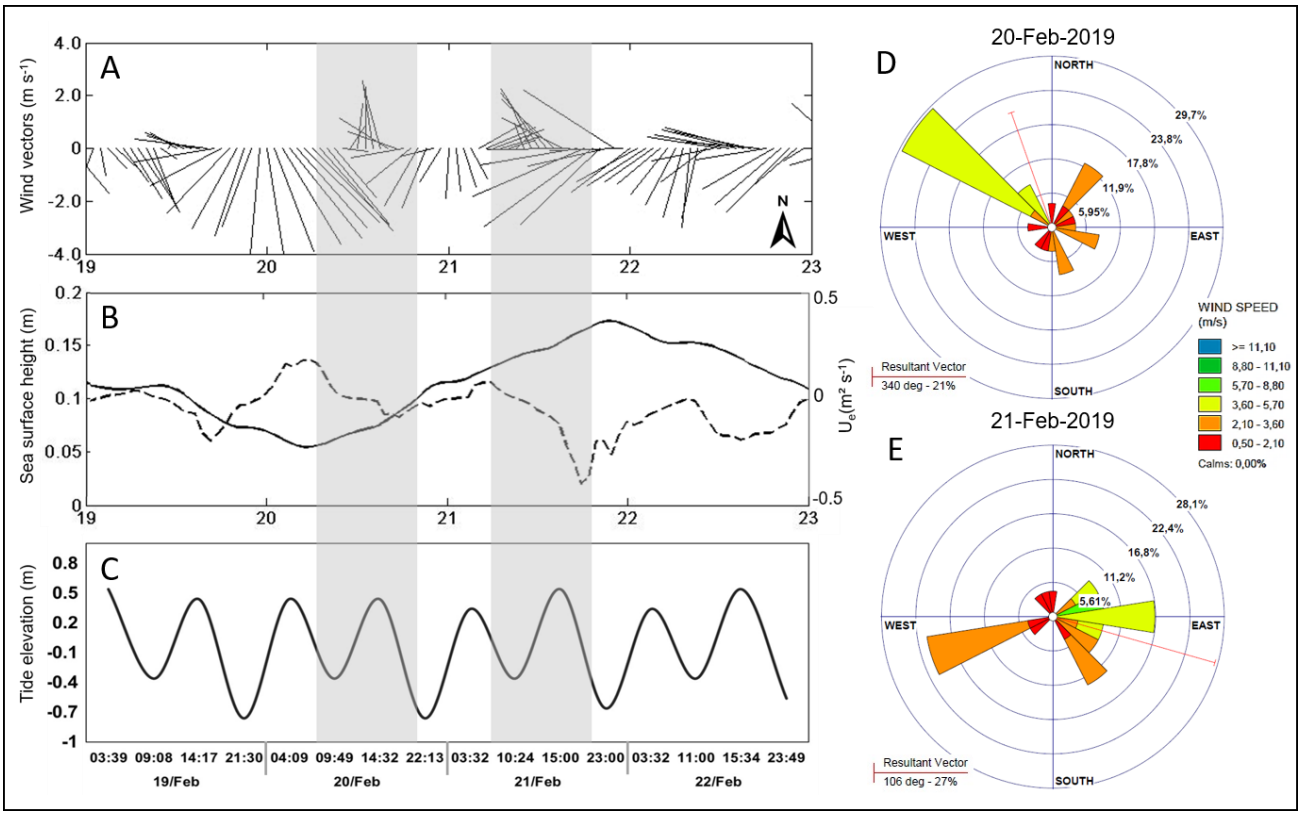

Fig. 2.3. Wind and ocean conditions between Feb 19 and 23, 2019. (A) Stick plots showing the direction the wind is "going to" and the magnitude of the wind speed (data from CFSv2/NCEP). (B) Sea surface height (m; left axis) (solid line) (provided by CMEMS). Ekman transport, Ue (m^2 s^{-1}; right axis), in the surface layer (dashed line). (C) Predicted tidal curve (m) with the times of occurrence of high and low tide levels. The shadows display the fixed-stations periods on Feb 20th and 21st. (D) wind rose for Feb 20th, (E) wind rose for Feb 21st. Wind rose (direction frequency) indicates the direction the wind is coming from. The red lines in (D) and (E) are the resultant vector derived from the wind direction data. Wind speed range is indicated on the color bar (red: 0.50-2.10 m s^{-1}; orange: 2.10-3.60 m s^{-1}; yellow: 3.60-5.70 m s^{-1}; light green: 5.70-8.80 m s^{-1}; dark green: 8.80-11.10 m s^{-1}; blue: ≥ 11.10 m s^{-1}).

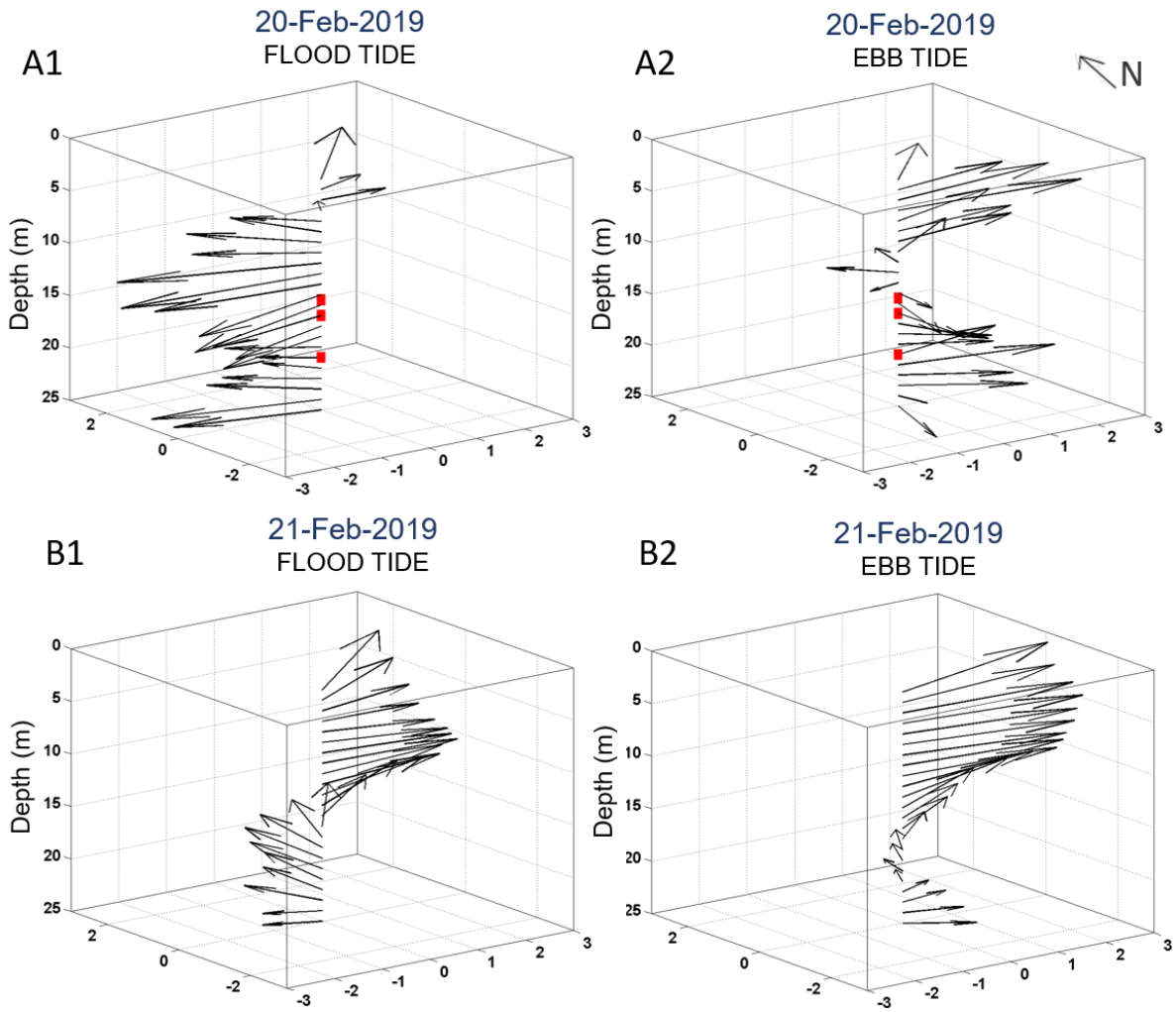

Fig. 2.4. (A) ADCP measured currents (m s^{-1}) from near-surface to near bottom on Feb 20th: (A1) Average of the current vectors during the flood tide; (A2) Average of the current vectors during the ebb tide. The red markings indicate the medium depths where thin layers were observed (at ~14.5 m, ~16 m, and ~20 m). (B) ADCP measured currents (m s-1) from near-surface to near bottom on Feb 21st. (B1) Average of the current vectors during the flood tide; (B2) average of current vectors during the ebb tide.

Thin layer observations

Three thin layers were observed on Feb 20th (Fig. 2.5A). In the 24 profiles on Feb 20th, 50 fluorometric chlorophyll (Chl-Flu) peaks were detected, among which 45 (90%) were considered discrete observations of the 3 thin layers. Sixty percent of these observations were within the pycnocline, while 40% were below the pycnocline. The average Chl-Flu intensity in the thin layer depths inside the pycnocline was 2.12 μg L^{-1}, and the thickness averaged 0.85 m. The Chl-Flu

intensity in the layer depths below the pycnocline averaged 3.62 µg L^{-1}, and the thickness averaged 2.27 m.

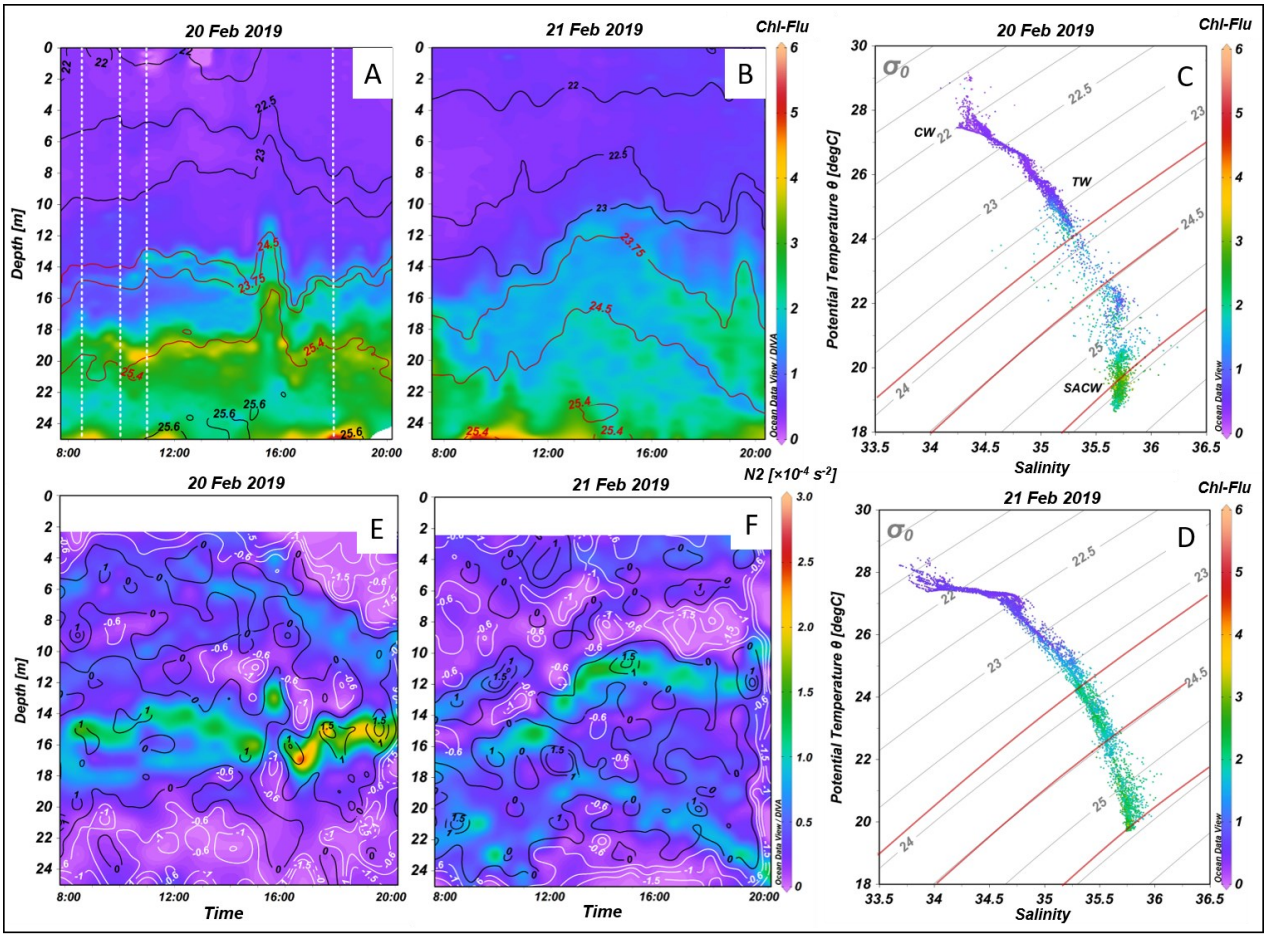

Fig. 2.5. (A) Vertical distributions of chlorophyll-a fluorescence (Chl-Flu) with isopycnal contours (σt black contours) over the day of Feb 20th; the dotted blank lines indicate the times when the profiles in the Fig. 2.8 were collected. (B) Vertical distributions of Chl-Flu with isopycnal contours on Feb 21st. (C) TS-Chl-Flu diagram with isopycnals indicating water bodies on Feb 20th (CW = Coastal water; TW = Tropical water; SACW = South Atlantic central water). The red contours represent the 25.4, 23.75, and 24.5 isopycnals in the A and B panels, and in the T-S diagrams. (D) TS-Chl-Flu diagram on Feb 21st. (E) and (F) illustrate the vertical distributions of N^2 ($\times 10^{-4}$ s^{-2}) with log10Ri contoured, on Feb 20th, and Feb 21st, respectively; white contours represent log10Ri < -0.60 (equivalent to Ri < 0.25).

The vertical distribution of Chl-Flu and density indicated that thin layers closely followed the 25.4, 23.75, and 24.5 isopycnals (Fig. 2.5A). The TS-Chl-Flu diagram confirmed the presence of SACW (T < 20 °C and S < 36.40; Miranda and Katsuragawa, 1991) associated with higher Chl-Flu intensity (Fig. 2.5C). The water column was strongly stratified, with temperatures that ranged from 29 °C in the surface and 18.6 °C near the bottom, and salinities that varied from 34.0, at the

surface, to 36.5, near the bottom. The average concentrations of dissolved nutrients at the surface were: 0.08 μM for nitrite, 0.60 μM for nitrate, 0.18 μM for phosphate, and 5.44 μM for silicate. Near the bottom, the average nutrient concentrations were: 0.93 μM for nitrite, 3.16 μM for nitrate, 0.64 μM for phosphate, and 10.00 μM for silicate. These high concentrations of nutrients at the bottom corroborate the presence of SACW in this zone.

The overall vertical distribution of particles (Fig. 2.6) captured by the imaging system reveals higher particle concentration at the surface (0-5 m; ~200 $\times 10^3$ Particles L^{-1}), near the thin layers (13-16 m, ~10 $\times 10^3$ Particles L^{-1}; and 19-21 m, ~50 $\times 10^3$ Particles L^{-1}), and a particle aggregation near the bottom (> 23m, ~170 $\times 10^3$ Particles L^{-1}), presumably because of bottom sediment resuspension (after Ryan et al. 2014) caused by the increase in the current shear close to the bottom (Fig. 2.5E). Full-frame images provided an overall assessment of particle occurrence in different layers (Fig. 2.6 A1 to D1).

The water in the layer regions ~20 m (Fig. 2.6 C1) and near the bottom (Fig. 2.6 D1) visually appeared to be more turbid. The shadowgraphic system captured small disturbances in a thin fluid layer on the top of the pycnocline (~15 m) with a “mixing appearance” seen in the images in Fig. 2.6 B1. This appearance is likely due to small turbulence induced by diffusive convection in the presence of small density inversions. According to Yoshida (1987), even with very small density differences between fluids double diffusive effects can produce inhomogeneity of density and induce currents (shear).

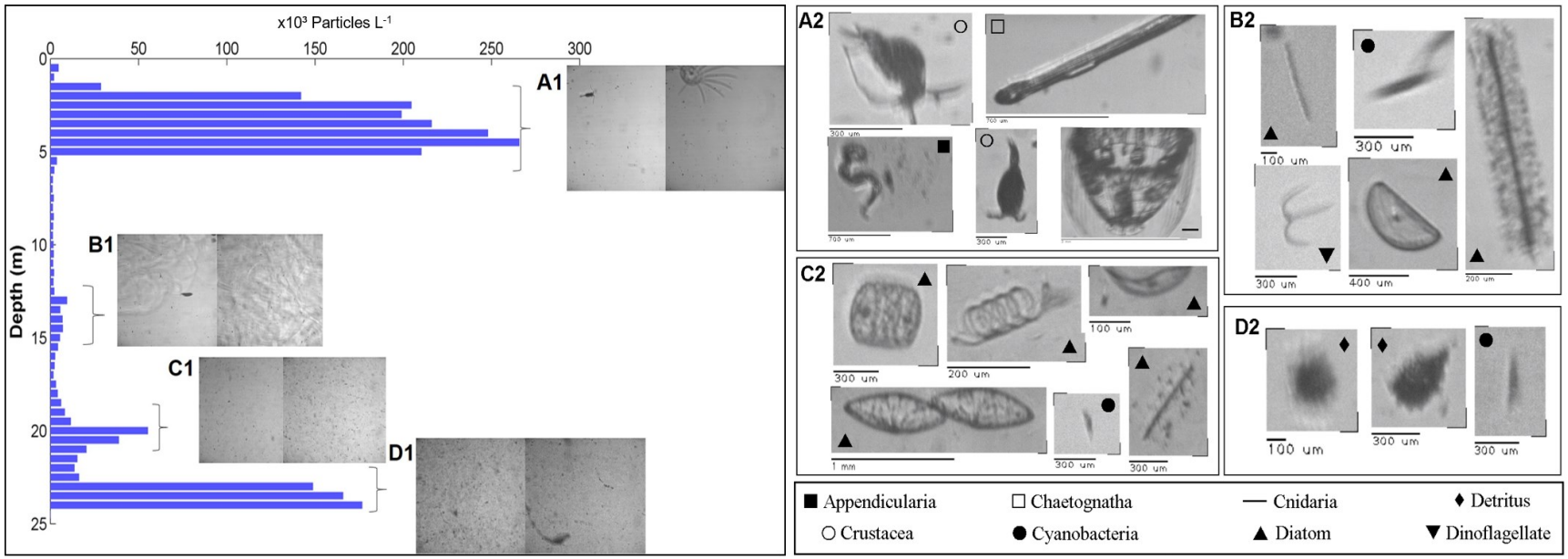

Fig. 2.6. Vertical distribution of the average particle concentration (x10^3 Particles L^{-1}) captured by the imaging system on Feb 20th. (A1) to (D1) are full frames obtained by the system. (A2) to (D2) are examples of organisms from each corresponding region (A1 to D1), obtained after the image segmentation and classification process. The classification according to the organism group is indicated by the symbols (open square: chaetognath; black square: appendicularia; black line: cnidaria; open dot: crustacea; black dot: cyanobacteria, black triangle: diatom, upside-down triangle: dinoflagellate; diamond: detritus).

The classification results for Feb 20th showed mesozooplankton (appendicularians, cnidarians, chaetognaths, cladocerans, and copepods) peaks between 0-5 m (Fig. 2.6A2). There were higher concentrations of appendicularians (~50 Ind L^{-1}) and cnidarians (~20 Ind L^{-1}) near the surface (0-3 m) and in the mixed layer (~5 m, and 9-10 m), respectively, while the concentrations of crustaceans were higher between 15 m and 24 m, reaching a maximum of ~80 Ind L^{-1} (Fig. 2.7 A).

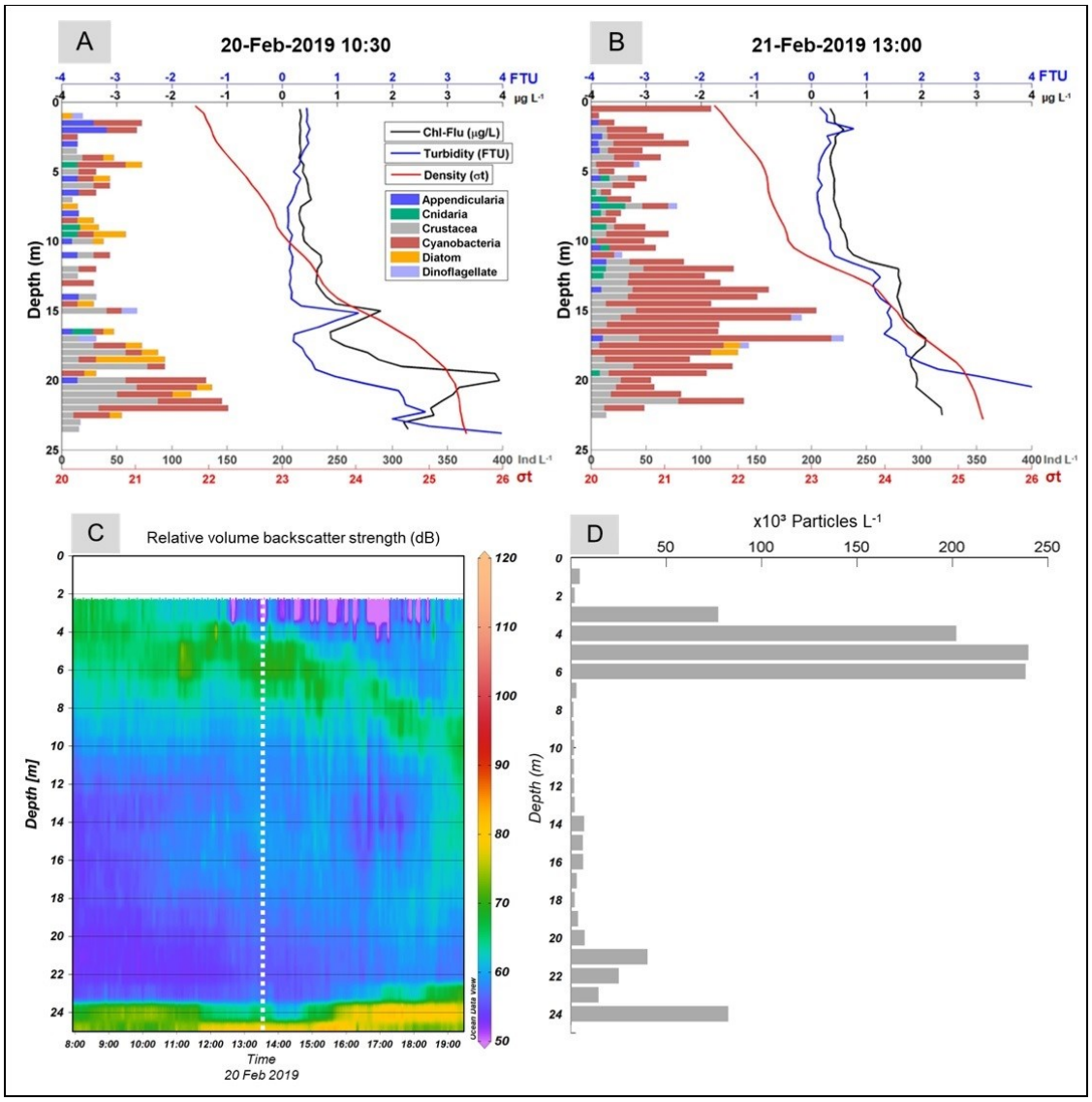

Fig. 2.7. (A) Vertical distribution of individuals per liter of the main taxonomic groups found (bars; bottom-axis) and vertical profiles of Chl-Flu (black line; top-axis), turbidity (blue line; top-axis), and density (red line; bottom-axis), on Feb 20th at 10:30 h. (B) vertical distribution of individuals per liter (bars; bottom-axis) and vertical profiles of Chl-Flu (black line; top-axis), turbidity (blue line; top-axis), and density (red line; bottom-axis), on Feb 21st at 13:00 h. (C) Time distribution of the relative volume backscatter strength (RVBS, in dB); the dotted blank line indicates the time when the profile in panel D was collected. (D) the particle distribution profile corresponding to time 13:30, on Feb 20th.

In the region between 18-22 m cyanobacteria and diatoms were observed most frequently. The regions above and below the pycnocline (~15 m and ~20 m, respectively) showed corresponding turbidity (optical backscattering) and Chl-Flu peaks (Fig. 2.7 A). Within the pycnocline diatoms, dinoflagellates and cyanobacteria were identified (Fig. 2.6 B2). Below the pycnocline, there was a noticeable increase in cyanobacterial concentration (~80 Ind L^{-1}), but many diatom species were also identified in the thin layer region (Fig. 2.6 C2).

On Feb 21st, there was an enhancement in the cyanobacterial population between 11 m and 20 m depth compared to the previous day, reaching a maximum of ~150 Ind L^{-1}. This enhancement was accompanied by an increase in crustacean concentration and Chl-Flu and turbidity signals (Fig. 2.7 B).

The relative volume backscatter strength (RVBS, in dB), obtained from ADCP acoustic backscatter data, is a measure that can be used to estimate the relative amount of particles suspended in the water (such as sediments, organisms, or bubbles) (Guerra et al. 2019). On Feb 20th, the RVBS distribution revealed higher values (> 65 dB) in the upper mixed layer (~3-6 m) and near-bottom (24-25 m; Fig. 2.7 C). This result shows relationships to the particle concentration profile obtained by the imaging system (Fig. 2.7 D), indicating a peak of particles at the surface and another peak at the bottom.

Thin layer formation

Thin layers within the pycnocline were associated with median values of $N^2 = 0.89\times10^{-4}\ s^{-2}$ and $S^2 = 0.37\times10^{-4} s^{-2}$. The thin layers below the pycnocline were associated with lower stratification, $N^2 = 0.12\times10^{-4}\ s^{-2}$ (median value), and with higher current shear, $S^2 = 0.89\times10^{-4}\ s^{-2}$ (Table 2.2). The Richardson number, Ri, was used to assess water column stability due to stratification, and instability due to shear in the regions where thin layers were observed. Higher Ri values occurred in regions with higher N^2. The critical value Ri = 0.25 (equivalent to $\log_{10}Ri = -0.6$) is related to regions with high mixing potential due to shear instabilities. The $\log_{10}Ri$ had an average of 0.57 within the pycnocline, and 0.01 below the pycnocline (Table 2.2).

Table 2.2. Average and median values for intensity, layer thickness, Brünt-Vaisala frequency N^2, shear S^2, and Richardson number (log10 Ri) related to the thin layer depths for the three observed thin layers within and below the pycnocline on Feb 20th. The corresponding minimum (maximum) values are in parentheses, above (below) the average values.

Layer location	**Intensity**		**Layer thickness (m)**		**N^2 ($\times 10^{-4}$ s^{-2})**		**S^2 ($\times 10^{-4}$ s^{-2})**		**Log_{10} Ri**	
	Average	Median	Average	Median	Average	Median	Average	Median	Average	Median
Within the pycnocline (*n=27*)	(1.12) 2.12 (3.52)	2.12	(0.40) 0.85 (3.00)	1.00	(-0.13) 0.96 (1.85)	0.89	(0.07) 0.46 (1.93)	0.37	(-1.42) 0.57 (1.17)	0.40
Below the pycnocline (*n=18*)	(2.39) 3.62 (4.32)	3.62	(0.80) 2.27 (3.40)	2.40	(-0.04) 0.14 (0.92)	0.12	(0.02) 0.34 (1.49)	0.89	(-2.40) 0.01 (0.83)	-0.29

In Fig. 2.5 (E and F panels) the temporal distributions of N^2 are illustrated, with contours indicating the $log_{10}Ri$ values, highlighting critical values ($log_{10}Ri \leq -0.6$), to indicate the regions with intense mixing processes. On Feb 20th (Fig. 2.5E) higher values of $log_{10}Ri$, between 1-1.5, occurred in the pycnocline region, where the N^2 values were higher. From the pycnocline, the $log_{10}Ri$ decreased towards the surface and the bottom. Negative values of $log_{10}Ri$ probably occurred due to the influence of high shear near the surface, due to wind-driven mixing, and below 20 m depth, due to bottom friction. From 17:00 h, approximately, mixing processes along the water column intensified, as indicated by values less than -0.6.

Consecutive profiles of Chl-Flu and Ri (in terms of $log_{10}Ri$) obtained between 08:30-11:00 h on Feb 20th (Fig. 2.8 A to 8C) showed that an initial Chl-Flu patch, between 19-21 m depth, increased in intensity and thinned as the Ri approached the critical value ($log_{10}Ri = -0.6$). This indicates that the mechanism leading to thin layer formation in the region below the pycnocline was most likely related to shear. Around 15-16 m depth, Chl-Flu peaks were associated with $log_{10}Ri > 1$, showing the strong influence of stratification within the pycnocline. In this case, the observed thin layers were likely associated with both density stratification and current shear processes.

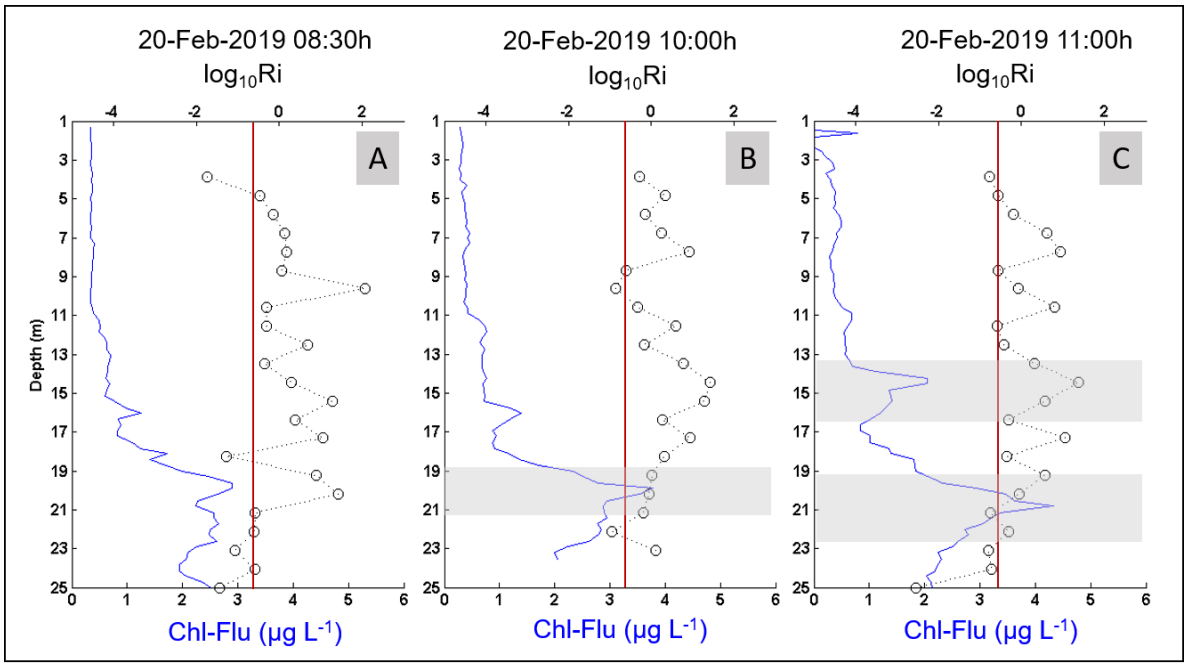

Fig. 2.8. Chl-Flu (solid blue line) and log10Ri (dotted line with open circles) profiles, obtained at the fixed-station point on Feb 20th at (A) 08:30 h, (B) 10:00 h, and (C) 11:00 h. The gray bars indicate the portions of the profile that met the criteria defining thin layers. The solid red lines indicate the critical value of log10Ri = -0.60 (log10Ri < -0.60 is equivalent to Ri < 0.25).

Thin layer dissipation

From 17:00 on Feb 20th, the thin layers started to increase in the vertical dimension (Fig. 2.5A), and on Feb 21st they had completely dissipated (Fig. 2.5B). Differences in weather and oceanographic conditions between February 20-21, 2019, are likely causes of the disappearance of the thin layers. The T-S diagram does not indicate the presence of SACW (Fig. 2.5D) on Feb 21st. The temperature ranged between 28.5 °C, at the surface, and 19.8 °C, near the bottom, and the salinity varied from 33.8, at the surface, to 36.0 near the bottom. In addition, the distribution of the $\log_{10}$Ri contours indicated high mixing potential throughout most of the water column (Fig. 2.5F). The average speed, V (cm s^{-1}), throughout the water column was 1.13 cm s^{-1} on Feb 20th, and 1.92 cm s^{-1} on Feb 21st (Table 2.3).

Table 2.3. Average speed and average shear through the water column (3-25 m), mixed layer (3-11 m), through the pycnocline (12-18 m), and below the pycnocline to the bottom (19-25 m) for the flood and ebb tide periods, on February 20 and 21, 2019.

				S^2 ($\times 10^{-4}$ s^{-2})			
		V (cm s^{-1})		Flood tide		Ebb tide	
	Depth (m)	**20/Feb**	**21/Feb**	**20/Feb**	**21/Feb**	**20/Feb**	**21/Feb**
Mixed layer	3-11	1.18	2.10	0.57	0.59	0.65	0.54
Pycnocline	12-18	1.14	2.08	0.33	0.49	0.36	0.44
Below pycnocline	19-25	1.07	1.50	0.61	0.56	0.66	0.59
Water column	3-25	1.13	1.92	0.51	0.55	0.56	0.53

On Feb 20th, the current shear increased during the ebb tide. The shear through the entire water column averaged 0.51×10^{-4} s^{-2} during the flood tide and 0.56×10^{-4} s^{-2} during the ebb tide. Below the pycnocline (near the bottom), in general, there was an increase in the current shear in relation to the upper levels (within the pycnocline and in the mixed layer; Table 2.3). A small increase in current intensities and shear close to the bottom is shown in the vertical profiles of current vectors (Fig. 2.4).

The relaxation of the winds observed from the end of the day on Feb 20th (Fig. 2.3A), and the change in wind direction on Feb 21st, caused an increase in the sea surface height by Ekman transport (Fig. 2.3B), and, consequently, the offshore advection of the SACW. Moreover, on Feb 21st there was an increase in current speed and shear, likely caused by the variability in the winds (Table 2.3). Thus, changes in the winds ultimately dissipated the thin layers observed on Feb 20th by driving the downwelling and the offshore advection of the nutrient-rich water mass, forcing changes in the vertical current distribution, and increasing the turbulent processes through the water column.

2.5. Discussion and conclusion

Meteorological and oceanographic forcings and biological responses

Horizontal (or lateral) transport mediated by meso- and submesoscale processes is a major player in the dynamics of plankton populations, providing the basic mechanism for patchiness in the plankton distribution (MARTIN, 2003). On the SBCS, the hydrodynamics are controlled primarily by winds, especially on the inner shelf, limited by the coast and by the 40-50 m isobaths. The South Atlantic Subtropical Anticyclone, the main feature of the atmospheric circulation over the South Atlantic Ocean, favors upwelling conditions on the SBCS during spring and summer months via Ekman transport, due to the predominant winds from the northeast (CASTRO et al., 2006). These meteorological and oceanographic conditions led to the presence of the SACW, a relatively cold (< 20°C) and nutrient-rich water body, close to the bottom, below 19.5 m depth (25 m total depth), on Feb 20th, 2019. Thin layers of phytoplankton with a Chl-Flu intensity ~2 times the background formed just below the pycnocline, coinciding with the upper limit of the SACW advection zone (Fig. 2.5A).

As SACW flows towards the coast in contact with the bottom layer, it is enriched with inorganic nutrients from the microbial mineralization of organic matter in the water column and the sediments, acquiring high levels of nutrients, mainly nitrate (BRAGA; MÜLLER, 1998). The marine environment of the study area is meso-oligotrophic (SASSI; KUTNER, 1982). In such areas, primary productivity is strongly dependent on nutrients regenerated in the water and sediment, discharged by runoff from land or transported with oceanic water to the coast during upwelling events (TEIXEIRA, 1973).

Upon reaching the euphotic zone on the inner shelf, SACW often triggers phytoplankton blooms due to its enhanced nutrient levels (AIDAR et al., 1993; BRANDINI, 2006). For subtropical ecosystems of the southwestern Atlantic, the responses of the planktonic community to the enrichment of nutrients are well known, both for phytoplankton (GAETA et al., 1999; METZLER et al., 1997; SALDANHA-CORRÊA; GIANESELLA, 2004), and for zooplankton (LOPES et al., 2006; MARCOLIN; LOPES; JACKSON, 2015; MELO JÚNIOR et al., 2016). However, until this contribution, the action of both physical and biological mechanisms on the formation of fine-scale phytoplankton aggregations had not been well documented.

Despite the quasi-synoptic sampling of this study (2 days), the mechanism that led to the formation of the phytoplankton-rich layer can be placed within a larger temporal context. We assume that the wind-driven meso- and submesoscale (1-500 km) processes allowed SACW to approach the coast, reaching the euphotic zone, and the phytoplankton responded to the availability of nutrients with *in situ* growth. The presence of SACW on the coast has a seasonal time scale, being more frequent from late spring to early autumn.

Regional meteorological and oceanographic conditions also acted in the dissipation of the phytoplankton layers. Between 08:00 h on Feb 20th and 20:00 h on Feb 21st, there was a relaxation in the upwelling winds (north-northeast winds < 3 m s^{-1}), and a subsequent increase in the winds from the southwest and southeast. These meteorological variations caused rapid changes in the water column, the sea surface height increased and favored coastal surface water downwelling, resulting in the SACW moving away from the coast. On Feb 21st, Chl-Flu was more evenly distributed and thin layers were absent.

Mechanisms of thin layer formation and dissipation

Several mechanisms have been posed leading to the formation of thin layers. In this work, the physical mechanisms of stratification and vertical current shear will be specifically discussed. Fluid stratification can cause organisms and biogenic materials (e.g., marine snow) to establish at certain depths based on density gradients (ALLDREDGE et al., 2002; PRAIRIE; WHITE, 2017). Large plankton patches can become thinner by vertical shear due to current jets, internal waves, and horizontal intrusion (DURHAM; STOCKER, 2012; ECKART, 1948; RYAN et al., 2008). Phytoplankton motility can also act to form thin layers (DURHAM; STOCKER, 2012; STACEY; MCMANUS; STEINBUCK, 2007).

Strong vertical density stratification was established on Feb 20th, with density (σ_t) ranging from 21.8 at the surface to 25.6 at the bottom. Thin phytoplankton layers were observed at different depths in the water column. Sixty percent of the recorded chlorophyll peaks were associated with high stability within the pycnocline (~14.5-16.0 m depth) with average $N^2 = 0.96\times10^{-4}$ s^{-2}. Forty percent of the chlorophyll-a peaks formed below the pycnocline (~19-21 m depth), in a relatively cold water zone (~19°C), with an average $N^2 = 0.14$ x10^{-4} s^{-2} (Table 2.2).

Although with low values, the vertical current shear was present in the depths of the thin layers on Feb 20th. Vertical profiles of horizontal currents indicate vertical shear at medium depths

(~14.5, 16, and 20 m) where thin layers were observed (Fig. 2.4 A1). However, no thin layers were observed in regions with values of Ri < 0.25 – a critical value that signals regions with high turbulent processes due to shear. Dekshenieks et al. (2001) found no thin layers when Ri < 0.23, which was probably due to the dissipation caused by the turbulence.

Consecutive profiles, obtained between 8:00 h and 11:00 h on Feb 20th, allowed us to observe that as the $\log_{10}Ri$ approached critical values (-0.6, i.e., Ri = 0.25), a Chl-Flu patch located below the pycnocline (~ 19-21 m) decreased in the vertical scale (thickness) and increased in intensity (Fig. 2.8 A to 8C). This suggests that the increase in current shear resulted in the phytoplankton layer thinning at this depth, a mechanism known as *straining* (Durham and Stocker 2012). Ryan et al. (2008) indicated shear as a convergent process (forming thin layers) in a coastal upwelling system (Monterey Bay), in 2003, where 92% of the thin layers recorded were associated with shear peaks.

Over this same sequence of profiles (Fig. 2.8 A to 8C), for thin layers located in the pycnocline (~14.5-16.0 m), the $\log_{10}Ri$ values remained greater than 1, while the Chl-Flu peak increased, indicating a greater influence of the stratification in this region. The thin layers that had formed within the pycnocline followed two isopycnals (σ_t = 24.5 and σ_t = 23.75), suggesting that the phytoplankton could be composed of motile cells in these layers (DURHAM; STOCKER, 2012; RYAN; MCMANUS; SULLIVAN, 2010). The results of the imaging system indicate the presence of motile dinoflagellate cells of the genus *Tripos (*formerly known as *Ceratium*) and colonies of *Chaetoceros coarctatus* with their motile *Vorticella* epibionts in this region (around 15 m) (Fig. 2.6 B2). Stratification may have driven the establishment of phytoplankton in a specific density gradient according to cell buoyancy. The shear probably acted to form thin layers at this depth, by interrupting the vertical movement of cells through the fluid, trapping them in the form of thin layers, the mechanism known as *gyrotactic trapping* (HOECKER-MARTÍNEZ; SMYTH, 2012). The thin layers below the pycnocline followed a single isopycnal (σ_t = 25.4) during the study period, indicating that the cells did not move vertically. Image classification results revealed filamentous cyanobacteria and many species of diatoms in this depth (19-21 m) (Fig. 2.6 C2). Although some C*haetoceros coarctatus* were found in this layer depth, most diatoms were non-motile cells.

Mechanisms of thin layer formation triggered by shear have been pointed out in several studies (DEKSHENIEKS et al., 2001; HOECKER-MARTÍNEZ; SMYTH, 2012; STACEY;

MCMANUS; STEINBUCK, 2007). Even though the shear values were underestimated by Ryan et al. (2008) by the coarse sampling scale (meter-scale), it was possible to identify shear as the main mechanism for the formation of thin layers observed in their study. The results of our study imply that differencing levels of shear acted both as a convergent process in the formation of thin layers, and as a divergent process leading to the dissipation of thin layers at the end of Feb 20th and throughout Feb 21st.

On Feb 21st, the average current speed almost doubled in value through the pycnocline between 12-18 m (2.08 cm s^{-1}) compared to the previous day (1.14 cm s^{-1}) (Table 2.3). Higher shear values were obtained in both flood and ebb tide periods through the water column ($S^2 = 0.55\times10^{-4}\ s^{-2}$ and $S^2 = 0.53\ \times10^{-4}\ s^{-2}$, respectively). In addition, a water column with a higher mixing potential was evidenced by the more widespread distribution of critical values ($Ri < 0.25$). No thin layers were observed under these conditions, probably due to decreased stability. According to Dekshenieks et al. (2001), persistent thin layers are not expected in regions under tidal mixing, nor in surface layers subject to wind stress. That is, in regions of instability and active mixing, the maintenance of these structures is impaired and there is a greater tendency to dissipate.

The current speed had intensities in the order of centimeters per second, which is consistent with the typical tidal currents (supra-inertial) on the continental shelf of the study region (ALVES, 1992). Although tidal regimes in coastal and shallow areas can act strongly in the mixing of the water column, the tide is not considered the most energetic forcing in this region, but the wind is. The ocean circulation response to the wind field variability, in the inner and mid-shelf regions, can occur practically in phase with the wind, as the local forcing is dominant in highly frictional regimes (CSANADY, 1978).

Vertical distribution of particles and plankton

Studying the distribution of plankton organisms in their natural environment and their behavior in relation to the thin layers is of crucial importance to assess the ecological importance of these structures. Imaging systems have been used to document the relationships between thin layers of phytoplankton and higher trophic levels (MÖLLER et al., 2012; NAYAK et al., 2018; TALAPATRA et al., 2013). Here images were used quantitatively and qualitatively to analyze the distribution of micro- and meso-plankton, generating an overview of the main classes occurring in the vicinity of the phytoplankton layers and through the water column.

In the images collected in the location of the thin layers, on Feb 20th, dinoflagellates, diatoms, and cyanobacteria were identified. In the depths between 13-16 m, within the pycnocline, dinoflagellate species of the genus *Tripos* were found (Fig. 2.6 B2). Species of *Tripos* are mixotrophic, i.e., they are both photosynthetic and heterotrophic, feeding on other plankton (FENSOME, 1993). They belong to the microplankton (20-200 µm), but some species can reach more than 200 µm in length. Most dinoflagellates are motile cells during their planktonic stage and can migrate vertically (BAEK et al., 2009). This may explain why the thin layers found in this depth range appeared to move vertically between two isopycnals.

Some species of large diatoms (> 200 µm) were identified in the depths between 19-21 m, mostly non-motile species, and many filaments of the cyanobacteria *Trichodesmium erythraeum* (Fig. 2.6 C2). Although *Trichodesmium* and the large diatoms contribute to Chl-a fluorescence, the Chl-Flu peaks may also had been composed mainly of phytoplankton less than 100 µm in length, which were not considered in the image classification stage. In addition, small diatoms and dinoflagellates from the pico- and nano-phytoplankton (< 20 µm fractions) make up a large part of the plankton in the study area (VILLAC; CABRAL-NORONHA; PINTO, 2008) and could not be identified using the imaging system. The organisms in the fraction > 20 µm were estimated in the general particle count, which indicated aggregations of particles at depths coinciding with the locations of the thin layers.

A higher abundance of crustaceans was found in the vicinity of Chl-Flu peaks on Feb 20th. A major representative of crustaceans in the region are copepods (MELO JÚNIOR et al., 2016), which feed on phytoplankton but are mostly omnivorous (TURNER, 2004). Marcolin et al. (2015) employed a Laser Optical Particle Counter (LOPC) to study the distribution of marine particles and mesozooplankton, on the Brazilian coast, finding positive correlations between chlorophyll fluorescence and particle aggregates, and between Brunt-Väisälä frequency and particle aggregates; peaks of zooplankton and aggregate concentration usually coincided with each other and with the pycnocline.

Appendicularians and cnidarians were found in greater quantities close to the surface (0-3 m) and subsurface (3-10 m) on both days. The presence of these two groups was also verified close to the Chl-Flu peaks (between 14.5-16 m and 19-21 m) on Feb 20th (Fig. 2.7 A). Large concentrations of appendicularians close to the surface have been reported previously in the region. Marcolin et al. (2015) found appendicularians peaks near the surface and below 20 m on the inner

shelf off Ubatuba, in 5-year time series data, from 2007 to 2012. In this same region, (Miyashita and Lopes (2011) found the most abundant appendicularian species above the thermocline and in surface layers, where high temperatures and low Chl-a prevailed. Appendicularians are free-swimming, solitary, herbivorous tunicates, feeding primarily on nanoplankton-sized particles using a "house" secreted by the glandular epithelium. The images indicated that several appendicularians were without their mucus houses, probably due to the sensitivity of these structures to the increased turbulence and friction of the currents in the mixed layer. Appendicularians are an important link between pico-nanoplankton and higher trophic levels since they are part of the diet of fish, cnidarians, ctenophores, and chaetognaths (URBAN-RICH; FERNÁNDEZ; ACUÑA, 2006). Cnidarians are free-living carnivorous that feed on various species, from microscopic zooplankton to small fish. Feeding behavior is regulated by chemosensors, and they move through the water column in search of food (MIGLIETTA et al., 2000). The presence of cnidarians in the mixed layer and close to the peaks of Chl-Flu can be related to the presence of appendicularians and crustaceans.

On Feb 21st, there was a significant increase in the density of cyanobacteria through the water column, especially in mid-water (11-20 m), accompanying the increase in Chl-Flu (Fig. 2.7 B). Cyanobacteria of the genus *Trichodesmium* commonly bloom in calm tropical and subtropical waters (VILLAREAL; CARPENTER, 1990). Previous studies have reported blooms of *Trichodesmium* spp. on the southeastern coast of Brazil (CARVALHO; GIANESELLA; SALDANHA-CORRÊA, 2008; DETONI et al., 2016). The maximum *Trichodesmium* abundances were associated in previous studies with local enrichments of phosphate, iron, or both (DETONI et al., 2016; FERNÁNDEZ et al., 2010), high surface temperatures (CARVALHO; GIANESELLA; SALDANHA-CORRÊA, 2008) and salinity range between 33 and 37 (FU; BELL, 2003). In situations where there is a strong thermal stratification and a shallow mixed layer, phytoplankton groups that demonstrate rapid growth under conditions of abundant nutrients (mainly phosphate and iron) can be overcome by *Trichodesmium* (CHEN et al., 2008). On the days leading up to the *Trichodesmium* bloom on Feb 21st, the weather conditions were stable, with a calm sea and a smooth water surface, weak winds (<11 m s^{-1}), and partly cloudy skies. Thermal stratification of the water column was observed on Feb 20th, with the temperature ranging from 29 °C at the surface to 18.6 °C in the bottom layer, and the salinity ranging from 34 to 36.5. These characteristics, together with the high relative concentration of phosphate (> 0.12 μM) likely triggered the population growth of *Trichodesmium erythraeum.*

Based on the hypothesis that particles are transported passively by water bodies and move together at the same speed, ADCPs use the backscattered sound by particles suspended in water to measure the velocity of currents. From the measurements of vertical velocity and echo intensity (signal strength), ADCPs have been used in the investigation of zooplanktonic biomass (COMFORT et al., 2017; GUERRA et al., 2019; SEVADJIAN; MCMANUS; PAWLAK, 2010). The ADCP signal strength was used to estimate the number of particles suspended from the relative volume backscatter strength (RVBS) calculation. Because acoustic waves are reflected by all objects greater than ¼ of the pulse wavelength, it is not possible to determine exactly how much of the reflected signal is due to zooplankton (THOMSON; EMERY., 2014). In our case, the wavelength of the sound pulses is about 0.3 cm (considering the sound speed in seawater of 1475 m s^{-1} and the ADCP frequency of 500 kHz), meaning that, in general, particles larger than 750 µm in diameter reflect the sound, and the smaller than 750 µm scatter the sound. However, the signal strength is proportional to the aggregation of the organisms. Organisms that are aggregated into patches have a greater volume scattering strength than uniform distributions of the same zooplankton organisms (THOMSON; EMERY., 2014).

The RVBS distribution graph suggests a patch of particles in the subsurface layer (~ 3-6 m) (Fig. 2.7 C). As zooplankton swarms tend to aggregate at specific depths (BASEDOW et al., 2019), the higher intensity of RVBS may indicate the detection of a zooplankton layer in this region. Mesozooplankton organisms such as appendicularians, cnidarians, and chaetognaths, were detected by the imaging system in this depth range. In addition, the particle counts from the imaging system also revealed a higher particle concentration in the subsurface layer (Fig. 2.7 D).

Concluding remarks

This contribution describes coupled biological-physical processes leading to the presence of thin layers in the coastal region of Ubatuba, Brazil. We demonstrated that the occurrence and persistence of thin layers were conditioned by the variability of hydrographic conditions through the water column. The dynamic processes in the quasi-synoptic scale influenced the fine-scale physical processes of stratification and current shear, which influenced biological processes, such as the accumulation of phytoplankton biomass. Although the observation of the phenomenon was local, the entire region of the SBCS has its circulation controlled by the same meteorological conditions on a synoptic scale, according to Castro et al. (1987). The thin layers observed are associated with meso- and submesoscale flows, related to Ekman transport and the advection of water bodies in the coastal zone. Thus, the observed changes are likely to occur at the regional level and are representative of similar coastal ecosystems.

The higher concentration of organisms found in the thin layer depths, compared to the environment above and below the layers, indicates that thin phytoplankton layers are likely attractive food sources for grazers. The importance of thin phytoplankton layers as enhanced feeding grounds for consumers that migrate to the vicinity of the layers has been well documented (BENOIT-BIRD et al., 2010; GREER et al., 2013; HOLLIDAY; GREENLAW; DONAGHAY, 2010). As trophic hotspots, thin layers of phytoplankton can mediate the survival and reproduction rates of organisms belonging to higher trophic levels (DURHAM; STOCKER, 2012).

We conclude that thin layers on the inner shelf of Ubatuba have a transitory nature, influenced by regional winds and intermittent SACW intrusions from the outer shelf, and their occurrence contributes to the ecological function of this ecosystem. Future research projects would require sampling strategies targeting fine-resolution spatial and temporal scales, with improved multifrequency acoustic and direct sampling methods. Studies on thin biological layers in the South Atlantic are still incipient and there are many questions to be answered, such as the influence of nonlinear internal waves on the occurrence of thin layers, and the role of thin layers in fish and zooplankton feeding processes. Future studies that quantify the phytoplankton taxa and size classes exploited by zooplankton in thin layers will help to better assess the ecological role that these structures play in meso-oligotrophic coastal environments.

3. Chapter III - Short-term variability in plankton abundance on the inner shelf off Ubatuba, Brazil.

3.1. Abstract

The interaction between seasonal and short-term physical processes affects plankton distribution and composition variability, with consequences for the entire ecosystem. Aspects of the plankton distribution at smaller scales have been understudied, mainly in coastal regions where highly variable conditions promote variations in the biophysical environment. This work aimed to investigate the seasonal and short-term variations in the distribution of plankton along the inner shelf off Ubatuba, Brazil. We quantified the abundance and diversity of the main planktonic taxa (>100 µm) and their spatiotemporal distribution in winter 2018 and summer 2019 using high-resolution sensors and a shadowgraphic imaging system at cross-shore and fixed stations (12 and 24 hours). Seasonal variability (summer-winter contrast) was evident in the water column stability. In the summer, higher values of plankton abundance and diversity were obtained. Our results suggested that spatiotemporal variations related to wind-induced mixing and water mass intrusions lead to variabilities in plankton populations on a time scale of a few hours, vertically between depth layers, and at spatial scales less than 2 km. This study contributes to the knowledge of the mechanisms of biophysical interactions and their spatiotemporal variation, which is crucial for assessing the effects of climate variability on plankton-mediated ecosystem services.

This chapter was submitted to the *Journal of Plankton Research.*

Keywords: plankton distribution, spatiotemporal variability, plankton imaging, South Atlantic Central Water, southwestern Atlantic Ocean.

3.2.Introduction

There is growing evidence that submesoscale features shape marine life by acting on the vertical and lateral transport of nutrients (HOSEGOOD et al., 2017; LÉVY; FRANKS; SMITH, 2018). Phytoplankton productivity may be influenced by these changes in light and nutrient availability caused by submesoscale processes as the spatiotemporal scales at which biological processes occur are comparable to the submesoscale ranges (0.1-10 km; 1-10 days) (HERNÁNDEZ-HERNÁNDEZ et al., 2021). Ocean fronts, boundary zones between water bodies characterized by horizontal gradients in oceanographic properties (e.g., salinity, temperature, density), are (sub)mesoscale structures known to have high biodiversity in pelagic habitats (WHITT; TAYLOR; LÉVY, 2017). Positive correlations between ocean fronts, chlorophyll concentration, and species recruitment have been documented (HERNÁNDEZ-HERNÁNDEZ et al., 2021; WOODSON et al., 2012). Coastal upwellings are also associated with submesoscale fronts and play an important role in transporting nutrients from the bottom to the euphotic zone (HOSEGOOD et al., 2017; LÉVY; FRANKS; SMITH, 2018).

Tides and internal waves, which occur on much shorter time scales than mesoscale features (MAHADEVAN, 2016), are also important physical phenomena in coastal zones and are related to mechanisms that contribute to phytoplankton productivity (WOODSON et al., 2011; YANG; YE; WANG, 2010). Biological responses to rapid changes in physicochemical conditions can occur at intervals of a few hours, or within a few days in community structure (PANNARD et al., 2008). Short-term variations may be greater than seasonal changes, especially in coastal regions, where highly variable hydrodynamic conditions have been correlated with strong spatiotemporal variations in nutrient concentration, phytoplankton biomass, and dominant species concentration (NOGUEIRA; BRANDINI, 2018; YIN et al., 2004). Despite this, little attention has been given to the short-term dynamics (hours, days, weeks) of phytoplankton communities in coastal ecosystems (PANNARD et al., 2008).

This study aimed to investigate seasonal and short-term (hours) variations in plankton distribution in the coastal zone of Ubatuba, Brazil, where transient meteorological and oceanographic phenomena drive changes in water column stability and distribution of physicochemical variables throughout the year. Many studies, mostly descriptive, have analysed the spatiotemporal distribution of phytoplankton (GAETA et al., 1995; SASSI; KUTNER, 1982)

and zooplankton (LOPES; BRANDINI; GAETA, 1999; MELO JÚNIOR et al., 2016; MIYASHITA et al., 2010) in the oligo-mesotrophic waters in the coastal ecosystem of Ubatuba. However, some aspects of the spatial distribution of plankton at smaller scales, on the inner shelf, have been little explored so far, mainly regarding the mechanisms of interaction between physical and biological processes (LOPES, 2007).

We quantified the abundance of the main plankton taxa and their vertical (meter scale) and cross-shore (few kilometres scale) distributions along the inner shelf, investigating interactions with physical processes in two different scenarios: winter/18 and summer/2019. The methodology used in this study is in line with efforts to incorporate *in situ* imaging technologies into plankton distribution studies. Observational data were obtained from fixed and spatial stations using high-resolution *in situ* techniques, such as optical plankton imaging, environmental sensors, acoustic current profiling, and remote sensing satellite data.

Given the full range of physical and biological processes in the coastal zone, observing and understanding how the plankton community responds to different environmental scenarios is critical to accurately predict its behaviour in a climate change context. In addition to increasing our knowledge of the spatial and temporal patterns of plankton distribution in the Ubatuba coastal region, focusing on the interactive dynamics between small and submesoscale oceanographic processes and plankton distribution, this work also advances our current understanding of the main drivers that regulate planktonic community structure in oligo-mesotrophic coastal marine systems. Furthermore, the study of how the physical environment affects plankton dynamics may help future research at high trophic levels, including fish production.

3.3.Materials and methods

Sampling

Water sampling and profiling with high-resolution sensors were carried out aboard the 14 m research vessel *Veliger II* of the Oceanographic Institute of the University of São Paulo (IOUSP), in the inner shelf off Ubatuba-SP, Brazil, between latitudes 23.45°S-23.65°S and longitudes 45.20°W-45.00°W (Fig. 3.1A). The campaigns were conducted in the winter, from July 19 to 25, 2018, and in the summer, from January 09 to 14, 2019. Fixed oceanographic stations to monitor the temporal variation in environmental parameters were conducted in the study area from 19 July 2018, 11:00 h (GMT-3) to 20 July 2018, 11:00 h (totaling 24 hours), and on 09 January 2019 and 14 January 2019, from 07:00 h to 19:00 h on both days. Cross-shore transects to study the spatial variation in environmental parameters were conducted along the inner shelf at 9 sites on 25 July 2018 (Fig. 3.1B) and at 7 sites on 11 January 2019 (Fig. 3.1C). The collection sites were set less than 2 km apart from each other.

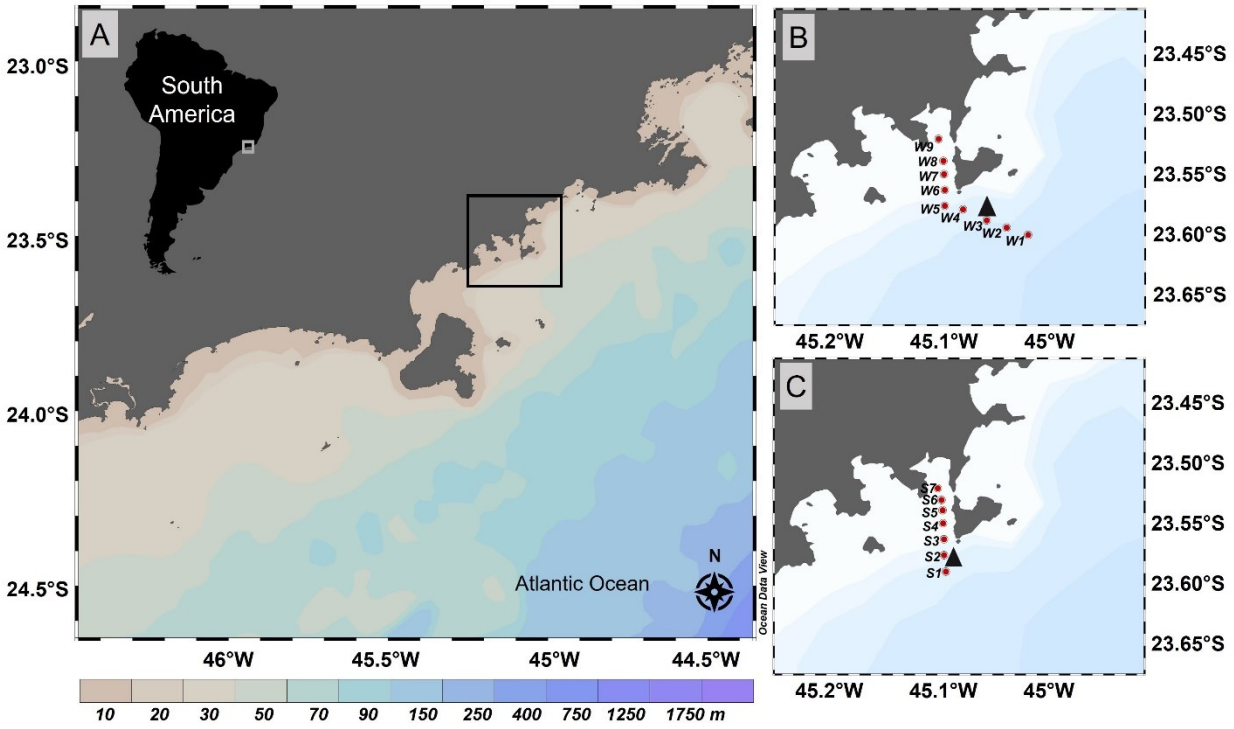

Fig. 3.1 (A) Bathymetric map of the study area on the inner shelf in Ubatuba, Brazil, with the location of the sampling stations along the onshore transects carried out in the (B) winter campaign in July 2018 (red dots; W1 to W9) and (C) summer campaign in January 2019 (red dots; S1 to S9). The locations of the fixed stations are represented by the black triangles in the B and C maps.

Pressure, temperature (T), conductivity, dissolved oxygen (DO), and chlorophyll-a (Chl-a) fluorescence were measured with a multiparameter RINKO-Profiler (JFE Advantech) continuously from surface to bottom at 0.1 m intervals. A shadowgraphic imaging system was used to obtain quantitative and qualitative data on vertical plankton distribution. This system, developed by the Laboratory of Plankton Systems, University of São Paulo (LAPS-IOUSP), consists of a collimated infrared LED beam and a high-resolution camera (4 MP) with a capture rate ranging between 6 and 15 frames per second, pixel size of 5.5 µm and a volume of 4.5×10^{-6} m³ per image (MEDEIROS, 2017). The plankton imaging system and the RINKO-profiler were coupled in the same frame for simultaneous casts. The buoyancy and decay speed (~0.27 m s^{-1}) of the system were controlled with the addition of buoys to its frame to minimize turbulence. The casts were performed at each station of the transects and during the fixed stations regularly every 30 min on average.

Flow characteristics related to the current velocity field were measured by a vessel-mounted downwards-looking Sontek 500-kHz ADCP. The ADCP made measurements from the near-surface (~3 m) to the bottom with a 1.0 m vertical resolution during the fixed stations.

Analysis of chlorophyll-a concentration and nutrients

Water sampling for the analysis of inorganic nutrients and Chl-a concentrations was performed using Niskin bottles from the surface to near-bottom at certain levels chosen according to the depth of the thermocline and the Chl-a maximum. To analyse the Chl-a concentration in µg L^{-1}, the samples were filtered on board in a GF/F 25 mm filter immediately after collection using a vacuum pump, and the filters were kept in an ultrafreezer (-80 °C) until extraction of Chl-a in the laboratory. Aliquots of 50 mL of the filtered content were separated and refrigerated (-20 °C) for the analysis of dissolved organic nutrients (nitrite, nitrate, phosphate, and silicate).

The concentration of nutrients, in µM, was determined in the laboratory using a flow injection autoanalyzer (AutoAnalyzer 3 HR, SEAL Analytical Inc.). The Chl-a concentration was determined using a fluorimeter (10-AU, Turner designs Inc. according to the nonacidified fluorometric method described in Welschmeyer (1994). The results of the Chl-a extraction were used to obtain a calibration curve for the Chl-a fluorescence data from the RINKO-Profiler. The correlation coefficient between the Chl-a fluorescence and the extracted Chl-a concentration was 0.94 (n = 38).

Satellite data - winds, geostrophic circulation field, sea surface height, and temperature

Hourly wind fields, sea surface velocity, sea surface height (SSH), and seawater temperature were obtained from satellite remote sensing products for the period of the study provided by the Copernicus Marine Environment Monitoring Service (CMEMS; http://marine.copernicus.eu; accessed 2021/11/01).

Wind speeds, provided by CMEMS, were obtained from Advanced Scatterometer (ASCAT MetOp-A) with a spatial resolution of 0.125° (~12.5 km). Daily mean data for sea surface velocity, SSH, and seawater temperature were obtained from a CMEMS global ocean reanalysis product (GLORYS12V1) with a spatial resolution of 1/12° (~8 km). Reanalysis models assimilate altimetry data and are built in a way to produce more realistic results, i.e., the closest to observations.

Estimation of stratification and stability

To estimate the stratification in the water column, the Brunt-Väisälä frequency (*N*), or buoyancy frequency, was calculated by:

$$N = \sqrt{-\frac{g}{\rho_0}\left(\frac{\partial \sigma_t}{\partial z}\right)} \qquad (1)$$

where g is the acceleration due to gravity, z is the depth (positive upwards), ρ_0 is the mean density, and $\sigma_t = \rho(s, t, p = 0) - 1{,}000$ (POND; PICKARD, 1983). *N* values were expressed in cycles per hour (cycles h^{-1}). The *N* was calculated every 1-m depth. High values of *N* indicate a stratified portion of the water column, while low values are found in vertically homogeneous regions.

The Richardson number (*Ri*), an index of stability, defines the relative importance of stabilization due to vertical density stratification *versus* destabilization due to vertical shear and is determined by:

$$Ri = \frac{N^2}{\left(\frac{\partial U}{\partial z}\right)^2 + \left(\frac{\partial V}{\partial z}\right)^2} \qquad (2)$$

where *U* and *V* are the zonal and meridional components of the currents measured by the Sontek 500-kHz ADCP, respectively, and *N* is the buoyancy frequency. A threshold value of *Ri* = 0.25 is

generally assumed to be the transition between regions of active mixing ($Ri < 0.25$) and regions where the effects of stratification act to inhibit mixing (Ri > 0.25) (POND; PICKARD, 1983).

Plankton data - enumeration and taxonomic classification

Computational image processing tools developed at the LAPS-IOUSP, using the random forest algorithm, allowed for the particle enumeration and characterization and classification of organisms in high-rank taxonomic groups. After *in situ* imaging, images captured by the LAPS Camera Recorder (LCR) were processed by LAPS Plankton Detector (LPD) software, where full frames representing particles were selected and segmented according to specific characteristics (size and texture, for example). After the image segmentation process, the classification of particles and organisms (>100 µm in size) was carried out using the LAPS Learning Set (LLS) software based on taxonomic classes available in the LAPS libraries.

The abundance of organisms was quantified in individuals per liter (Ind. L^{-1}), with phytoplankton chains being quantified as a single individual. The validation of the taxonomic classification was performed manually in a final step within the LLS software based on taxonomic information available in the literature in the World Register of Marine Species (WoRMS Editorial Board, 2021) and the algae database provided by Guiry & Guiry (2021).

Ecological indices

After identification and counting of taxa (abundance), communities along the transects were evaluated by ecological indices. The Shannon diversity index is widely used in the study of communities and reflects the diversity of species in a given environment and time. The higher the index value, the greater the number of species found at a given point (SHANNON, 1948). The Shannon index (H') is determined by:

$$H' = -\sum \frac{n_i}{n} ln\left(\frac{n_i}{n}\right) \qquad (3)$$

where ln = natural logarithm (e); n_i = number of individuals sampled for species i; and n = total number of individuals sampled.

Simpson's dominance index measures the probability that two randomly selected individuals in the sample are of the same species (SOMERFIELD; CLARKE; WARWICK, 2008).

Its value ranges from 0 to 1, and the higher it is, the more likely individuals are to belong to the same species. Thus, the greater the dominance, the lower the species diversity. Simpson's dominance index (D) considers the proportion of occurrence of each species and is calculated by:

$$D = \sum \left(\frac{n_i}{n}\right)^2 \qquad (4)$$

where n_i represents the number of individuals sampled for species *i*, and *n* is the total number of individuals sampled.

The Margalef richness index, also known as the Margalef biodiversity index, is based on the number of species as a function of the total number of individuals in the community in question, giving the weight equally between rare and abundant species. The Margalef index (α) is obtained by:

$$\alpha = \frac{S - 1}{ln\,(n)} \qquad (5)$$

where *S* is the number of species/taxa sampled, *ln* = natural logarithm, and *n* = total number of individuals sampled.

The Pielou equitability index is derived from the Shannon diversity index and allows representing the uniformity of distribution of individuals among existing species (PIELOU, 1966). Its value ranges from 0 (minimum uniformity) to 1 (maximum uniformity). Equitability will be maximum in communities where all species have the same representation. Pielou's equitability index (*J*) is determined by:

$$J = \frac{H'}{ln\,S} \qquad (6)$$

where: H' = Shannon index; ln = natural logarithm; *S* = number of species/taxa sampled.

Statistical analyses

Variability in the abundance of planktonic organisms over a short period – 12 hours or 24 hours – and between depth layers was evaluated using data from the fixed stations. Statistical analyses to determine sample differences in protozooplankton, phytoplankton, and metazooplankton abundances between periods of the day and depth layers were performed using

the nonparametric Kruskal–Wallis test ($p < 0.05$) followed by Dunn's post-hoc test. The Kruskal–Wallis statistical test was used to compare three or more independent groups to assess quantitative variables that did not comply with normality parameters or ordinal qualitative variables. Dunn's post-hoc test was used to make a pairwise comparison to verify the differences between the groups, with a significance level of 5%. Four groups of samples were selected according to the time of collection: morning, afternoon, evening, and night; and three groups of samples were adopted according to the depth of collection: surface, midwater, and bottom.

Additionally, descriptive statistics using box plots were made to better visualize and analyse the behaviour of phytoplankton populations and the distribution of physical parameters over time and depth layers. The statistical analyses were performed using the software PAST version 4.02.

3.4. Results

Meteorological and oceanographic conditions

Winter 2018 fieldwork:

Surface currents flowed predominantly to the southwest during the fixed station on July 19-10, 2018 (Fig. 3.2A), and to the north–northeast on July 25, during the onshore transect stations. The reversal of the current direction to the north–northeast was evidenced by the intensification of the meridional component of velocity (v) to the north (positive values; Fig. 3.2B) and accompanied by an increase in sea surface height of +0.13 m (Fig. 3.2C). During the fieldwork days in July, the surface and bottom seawater temperatures averaged 21.46 °C and 21.32 °C, respectively (Fig. 3.2D).

The mean wind fields obtained by satellite for the southeast continental shelf region (Fig. 3.3) indicated prevailing winds from the north–northeast with speeds between 3 and 6 m s^{-1} for July 19-20. On July 21-22, south of 24°S, an inversion in the wind direction was observed, blowing from the south and southwest with intensities above 9 m s^{-1}, indicating the approach of a frontal system in the continental shelf region off Ubatuba. It was not possible to obtain the wind field for July 25 due to cloud cover.

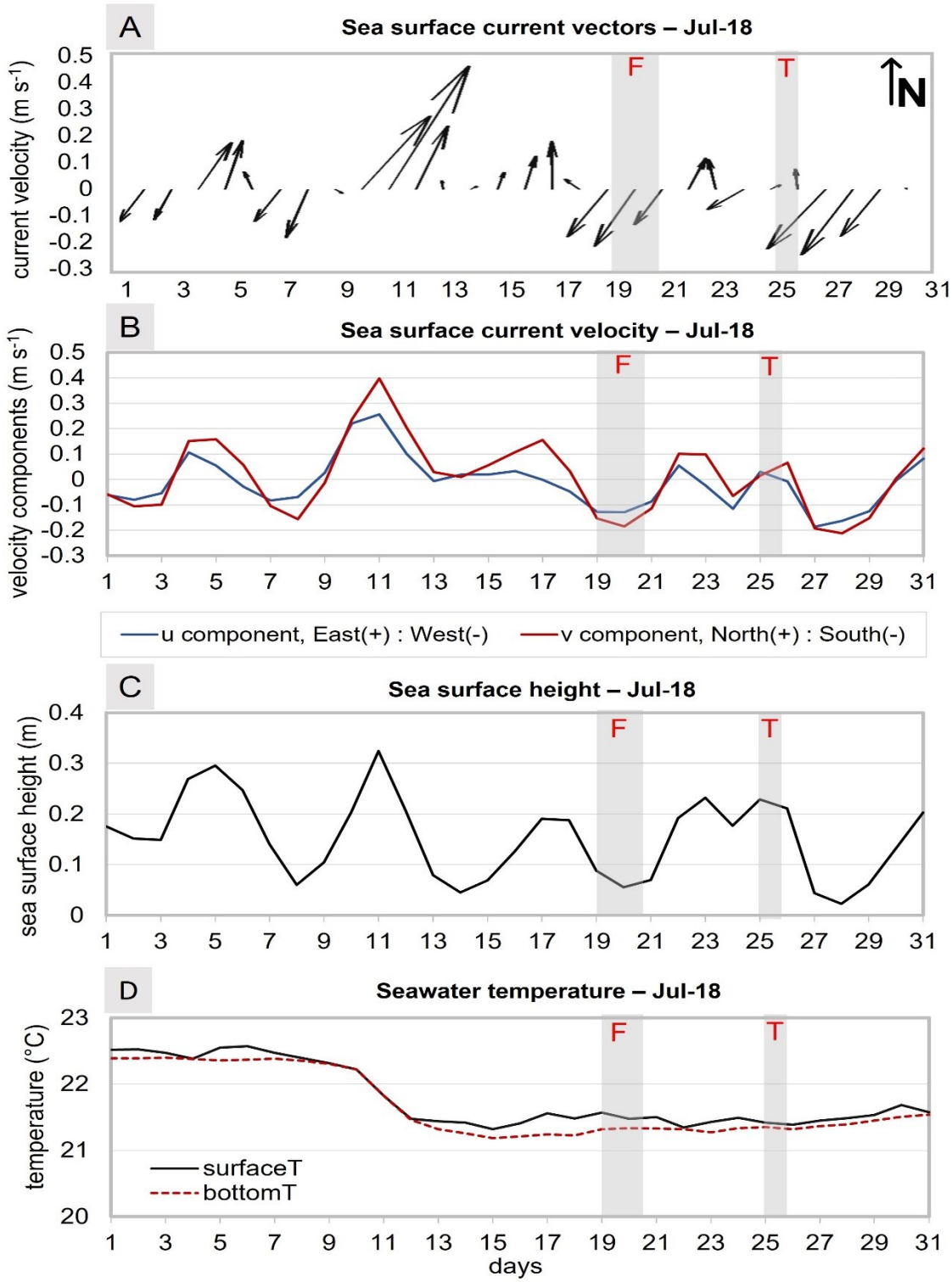

Fig. 3.2. Oceanographic data for July 2018: (A) velocity vectors of surface currents, (B) sea surface velocity components (m s^{-1}), (C) sea surface height (m), and (D) seawater temperature (in degrees Celsius). The shadings show the (T) transect station period and (F) fixed-station period. Data provided by the Copernicus Marine Environment Monitoring Service (CMEMS).

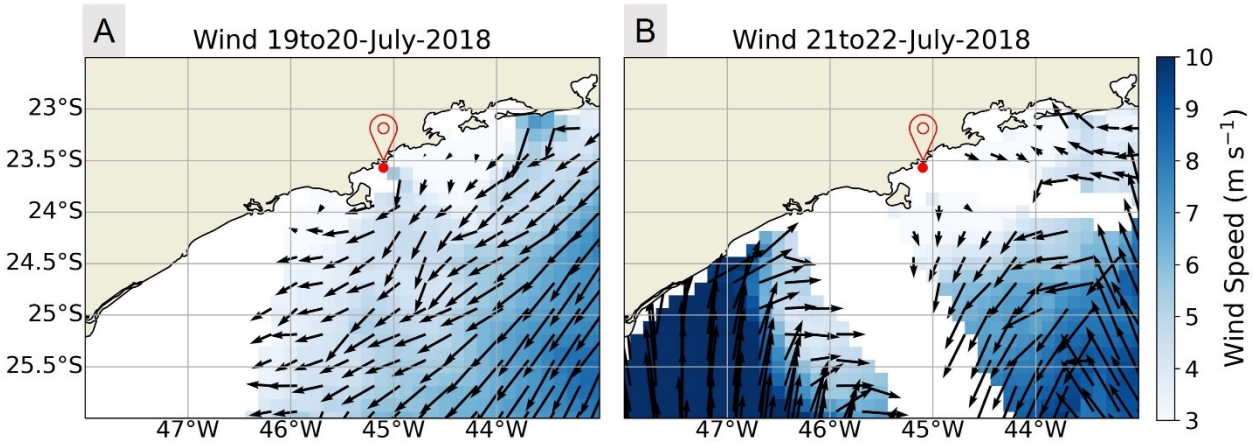

Fig. 3.3. Average wind speeds (in m s^{-1}) in the continental shelf region off Ubatuba for (A) 19-20 July 2018 and (B) 21-22 July 2018. Data are from satellite images provided by CMEMS.

Summer 2019 fieldwork:

During the summer campaign, carried out from January 9 to January 14, 2019, surface currents flowed predominantly to the southwest (Fig. 3.4A), with a northeast reversal event between Days 12 and 13, when there was no collection. On the fieldwork days (9, 11, and 14 January), the meridional (v) and zonal (u) components of the velocity vector had negative values (i.e., to the south and west, respectively; Fig. 3.4B), and there was no significant sea surface height increase (average 0.04 m; Fig. 3.4C). The surface and bottom seawater temperatures averaged 28.5 °C and 19.2 °C, respectively (Fig. 3.4D). The mean wind field for the summer fieldwork period indicated stronger winds (~7-10 m s^{-1}) blowing from the east and northeast in the continental shelf region of Ubatuba (Fig. 3.5).

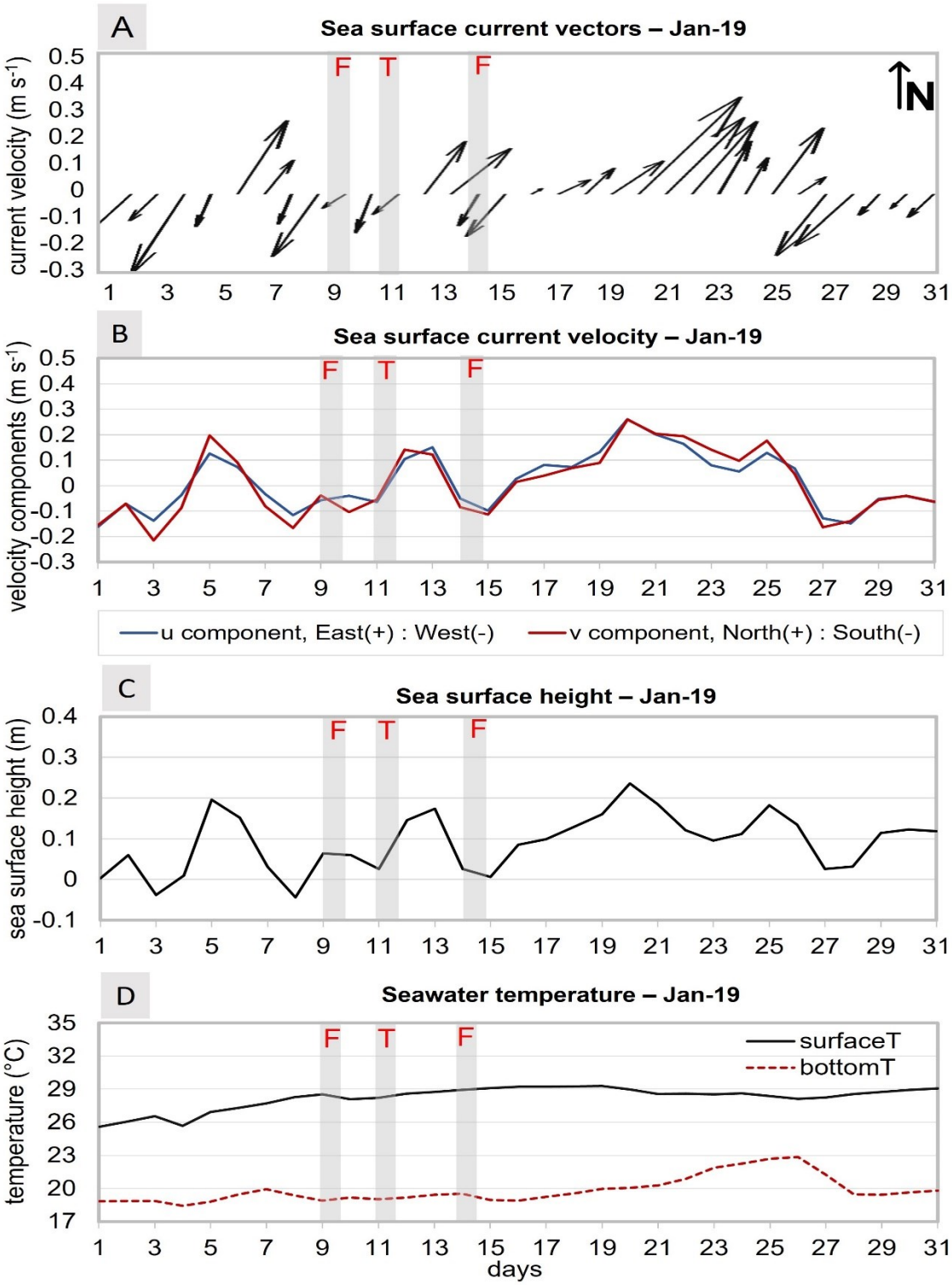

Fig. 3.4. Oceanographic data for January 2019: (A) velocity vectors of surface currents, (B) sea surface velocity components (m s^{-1}), (C) sea surface height (m), and (D) seawater temperature (in degrees Celsius). The shadings show the (T) transect station period and (F) fixed-station period. Data provided by CMEMS.

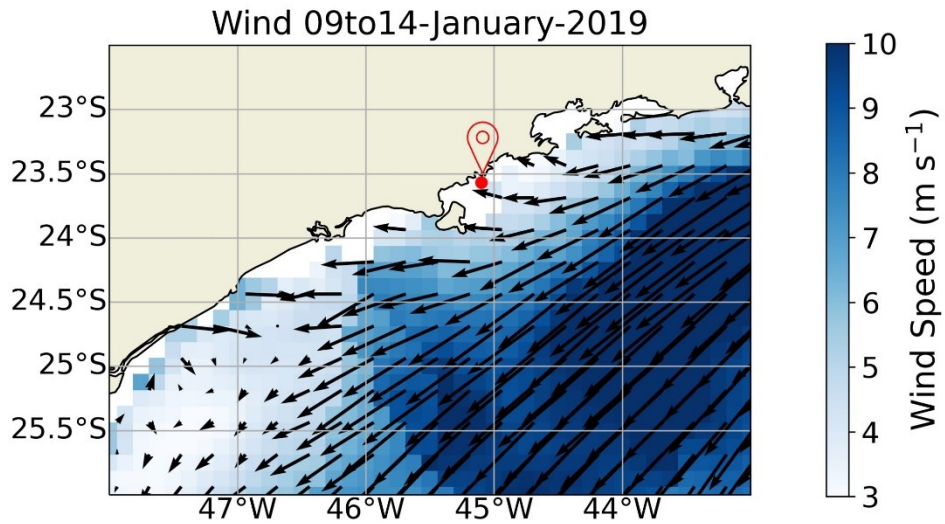

Fig. 3.5. Average wind speeds (in m s^{-1}) in the continental shelf region off Ubatuba for 9-14 January 2019. Data are from satellite images provided by CMEMS.

Hydrological and environmental conditions - Fixed Stations

Winter 2018 fieldwork:

During the fixed station held on July 19-20, there was very low thermal stratification, with no thermocline formation throughout the study period (24 hours). The homogeneity of the water column is corroborated by the low values of the buoyancy frequency (N≤5 cycles h^{-1}), mainly in midwater (Fig. 3.6C). The temperature had a maximum of 23 °C at the surface and a minimum of 21 °C at the bottom (Fig. 3.6A). The salinity ranged from 34.8 at the surface to 35.2 at the bottom.

There was a formation of Chl-a patchiness from 13:00 h onwards at midwater (~15-25 m) with a maximum concentration of 2 µg L^{-1}. The patchiness dissipated over time (Fig. 3.6B). Surface Chl-a was very low, close to zero. At the bottom, below 25 m, there was an increase in Chl-a concentration from 21:00 h on July 19, reaching an average of 1.5 µg L^{-1}. Nutrient concentrations, mainly nitrite and nitrate, also increased in the bottom layer from 21:00 h on July 19, reaching higher averages on July 20 (Table I).

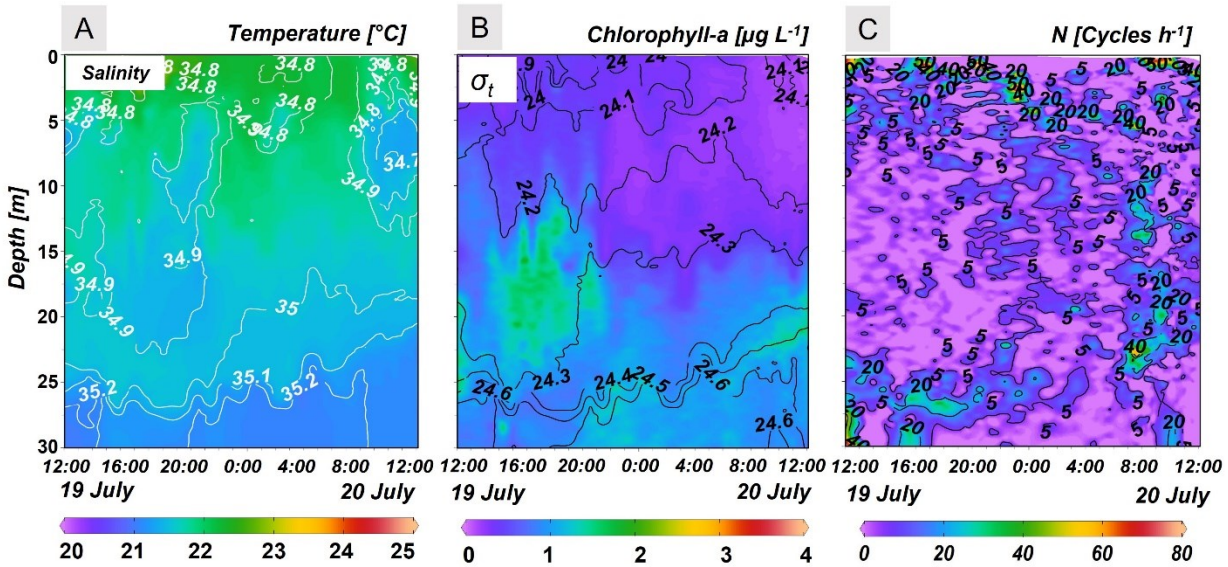

Fig. 3.6. Temporal distribution of environmental data obtained at the fixed station on 19-20 July 2018: (A) Temperature, in °C, with isohalines; (B) Chlorophyll-a concentration, in µg L^{-1}, with isopycnals; (C) Contour plot of Brunt-Väisälä frequency (N), in cycles h^{-1}.

Table 3.1. Mean concentration (± standard deviation) of inorganic nutrients (nitrite, nitrate, phosphate, and silicate; in µM) in the surface and bottom layers on July 19 and 20, 2018, and January 9 and 14, 2019.

[µM]	Layer	Jul 19	Jul 20	Jan 09	Jan 14
Nitrite	Surface	0.11 ± 0.07	0.15 ± 0.03	0.03 ± 0.01	0.05 ± 0.07
	Bottom	0.13 ± 0.18	0.54 ± 0.13	0.03 ± 0.02	0.16 ± 0.06
Nitrate	Surface	0.35 ± 0.52	0.87 ± 1.06	0.20 ± 0.16	0.13 ± 0.13
	Bottom	0.28 ± 0.49	0.79 ± 0.47	0.07 ± 0.04	1.03 ± 0.66
Phosphate	Surface	0.34 ± 0.07	0.38 ± 0.14	0.11 ± 0.03	0.13 ± 0.02
	Bottom	0.37 ± 0.08	0.55 ± 0.21	0.17 ± 0.03	0.35 ± 0.07
Silicate	Surface	9.97 ± 0.95	9.32 ± 2.79	2.77 ± 0.78	2.15 ± 0.89
	Bottom	8.55 ± 1.24	8.46 ± 1.40	2.15 ± 0.39	3.46 ± 0.55

Summer 2019 fieldwork:

Data from fixed stations carried out on January 9 and 14, 2019, indicate the occurrence of natural phenomena of stratification and water mass intrusions in the region. In the surface waters, the temperature had a maximum between 29 and 30 °C, and the salinity reached approximately 34.9-35.0 on both days. On January 9, at the bottom, the temperature and salinity were approximately 20 °C and 35.5, respectively (Fig. 3.7 A1). On January 14, the temperature was approximately 18-19 °C, and the salinity was 35.7 at the bottom (Fig. 3.7 A2). The Chl-a

concentration on both days was greater near the bottom, reaching a maximum of 10 µg L^{-1} (Fig. 3.7 B2). On January 14, the nitrate concentrations at the bottom were higher, reaching 1 µM on average (see Table I).

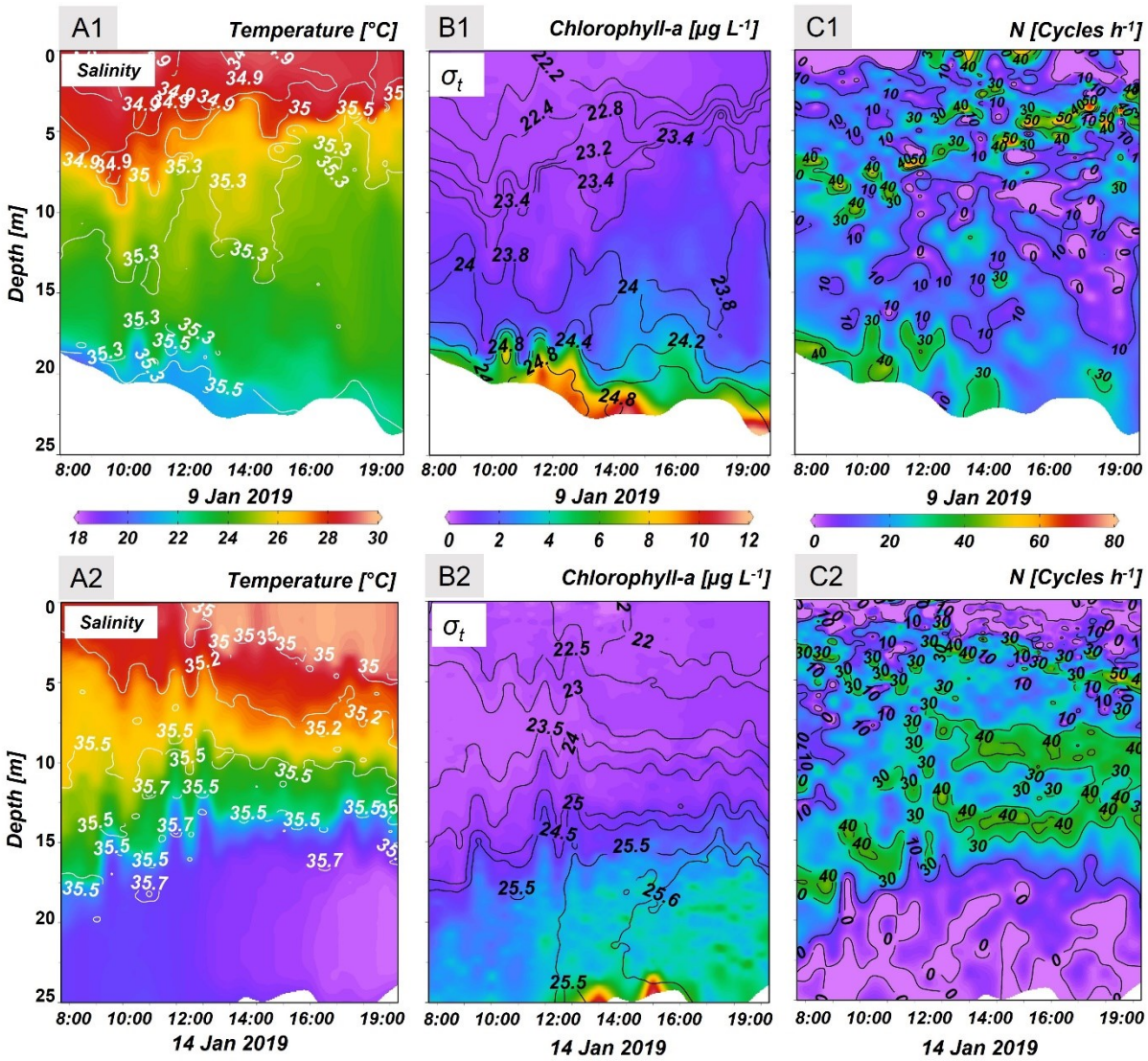

Fig. 3.7. Temporal distribution of environmental data obtained at the fixed station on 9 January 2019 (A1-C1) and 14 January 2019 (A2-C2): (A) temperature, in °C, with isohalines; (B) chlorophyll-a concentration, in µg L^{-1}, with isopycnals; (C) contour plot of Brunt-Väisälä frequency (N), in cycles h^{-1}.

The vertical distribution of the buoyancy frequency, N, allows us to estimate the spatial extent of the thermocline throughout the observation periods. On January 9, the N values were higher at the surface (3-6 m) and below 17 m, reaching approximately 40 cycles h^{-1}, indicating a

greater density gradient in these zones during the entire observation period. In midwater, in the zone between 6 and 16 m, there was a decrease in stratification during the day. The N values for January 14 indicated greater stratification in the zone between 7 and 17 m, the thermocline, reaching frequencies above 20 cycles h^{-1} (Fig. 3.7 C2). The maximum N was approximately 40 cycles h^{-1} at higher density gradients. According to the distribution of N values, the water column stratification remained high at midwater throughout the sampling period on January 14.

Plankton temporal variability

Winter 2018 fieldwork:

The temporal distribution of the mean abundance of the main plankton groups during the fixed station held on July 19-20, 2018, was analysed by layers, considering the lack of density stratification and the maximum depth of the sampling station (~30 m depth): surface layer (0-10 m), midwater layer (10-20 m), and bottom layer (over 20 m), as illustrated in Fig. 3.8.

Surface layer: In the surface layer, diatoms had the highest mean abundance (24.6 Ind. L^{-1}), followed by dinoflagellates (8.7 Ind. L^{-1} on average), ciliates (6.6 Ind. L^{-1} on average), larvaceans (5.5 Ind. L^{-1} on average), and crustaceans (3.8 Ind. L^{-1} on average). The mean diatom abundance fluctuated over time, being smaller in the period between 16:00 h and 00:20 h and on the second day of observations from 7:00 h on. Crustaceans decreased in abundance from 23:00 h (19 July) to 11:00 (20 July). Ciliate and larvacean abundances were greater at the beginning of the observations, decreasing over time. Dinoflagellates had an almost homogeneous distribution over time (Fig. 3.8A).

***Midwater layer*:** In the intermediate layer of the water column, the mean diatom abundance was approximately 36.2 Ind. L^{-1}. Crustaceans reached 7.5 Ind. L^{-1} on average, followed by dinoflagellates (8.0 Ind. L^{-1} on average), ciliates (7.8 Ind. L^{-1} on average), and larvaceans (5.0 Ind. L^{-1} on average). Dinoflagellates, larvaceans, and ciliates were more abundant in the first hours of observation (11:00-16:00 h on July 19). Diatom and crustacean abundances were relatively constant most of the time, decreasing at the end of the collection, between 7:40 h and 11:35 h (Fig. 3.8B).

***Bottom layer*:** Diatoms and ciliates were more abundant in this region of the water column, reaching 54.8 Ind. L^{-1} and 18.4 Ind. L^{-1} on average, respectively. The mean crustacean, larvacean, and dinoflagellate abundances were 7.4 Ind. L^{-1}, 3.9 Ind. L^{-1}, and 3.6 Ind. L^{-1}, respectively. The

diatoms and crustaceans at the bottom grew in abundance considerably in the period between 22:20 h and 07:40 h. Dinoflagellates and ciliates also grew in abundance during the dark period from 18:00 h onwards (Fig. 3.8C).

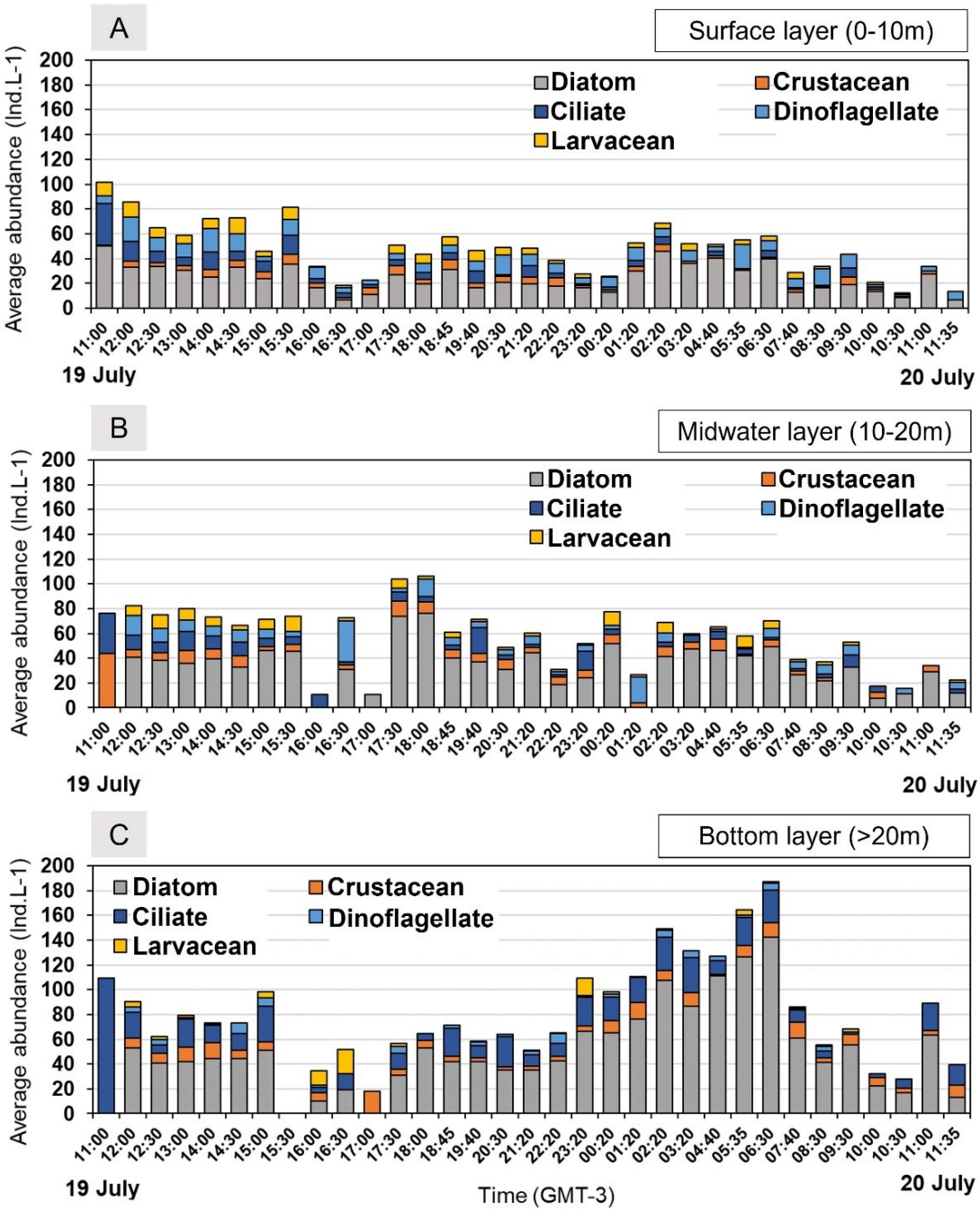

3.8. Temporal distribution of the abundance (Ind. L^{-1}) of the main plankton groups (ciliate, crustacean, cyanobacteria, diatom, dinoflagellate, and larvacean) on July 19-20, 2018, in the (A) surface layer (0-10 m); (B) midwater layer (10-20 m); and (C) bottom layer (>20 m).

Summer 2019 fieldwork:

The temporal distribution of the mean abundance of the main plankton groups during the fixed stations carried out on January 9 and 14, 2019, was analysed by layers defined according to the thickness of the mixing layer, thermocline, and the maximum depth of the sampling station (~25 m): surface layer (0-5 m), midwater layer (5-15 m), and bottom layer (> 15 m), as seen in Fig. 3.9.

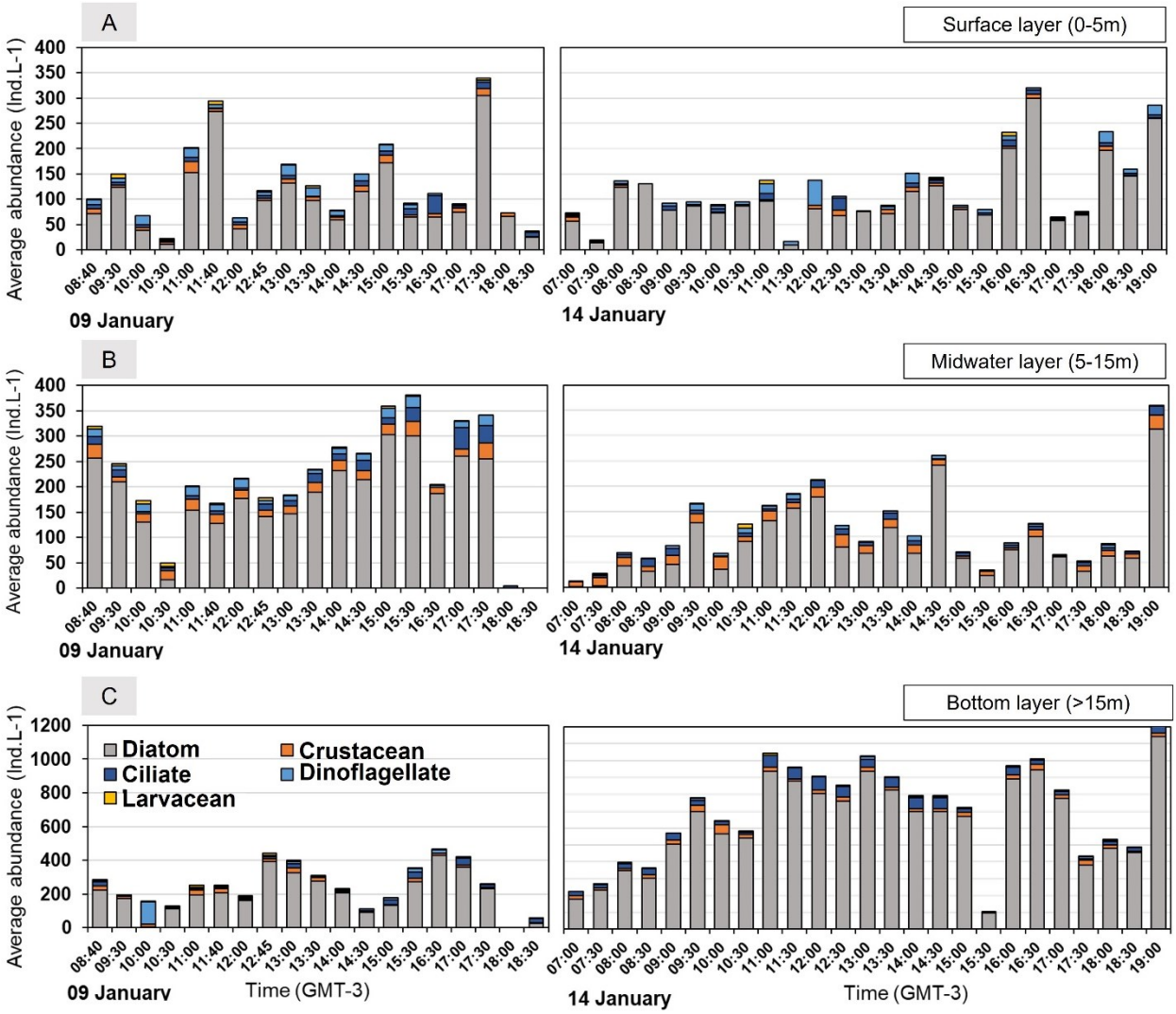

Fig. 3.9. Temporal distribution of the abundance (Ind. L^{-1}) of the main plankton groups (ciliate, crustacean, cyanobacteria, diatom, dinoflagellate, and larvacean) on January 9 and 14, 2019, in the (A) surface layer (0-5 m); (B) midwater layer (5-15 m); and (C) bottom layer (>15 m).

Surface layer: On January 9, diatoms were the most abundant group, with an average of 104.5 Ind. L^{-1} (Fig. 3.9A). Dinoflagellates were the second largest group, reaching approximately 9.5 Ind. L^{-1} on average. Crustaceans and ciliates were homogeneously distributed over time, both with an average of 8.0 Ind. L^{-1}. Larvaceans were more abundant in the morning and early afternoon (2.5 Ind. L^{-1} on average).

On January 14, the mean diatom abundance was 106.8 Ind. L^{-1} throughout the entire observation period, reaching peaks between 16:30 h and 19:00 h with maximum values between 200.0 and 300.0 Ind. L^{-1}. Dinoflagellates reached 9.9 Ind. L^{-1} on average, with higher abundances between 11:00 h and 12:00 h and between 18:00 h and 19:00 h. Dinoflagellates, crustaceans, and ciliates were distributed homogeneously, with means of 5.1 Ind. L^{-1} and 6.1 Ind. L^{-1}, respectively (Fig. 3.9A).

***Midwater layer*:** On January 9, the diatom abundance was greater in midwater than at the surface and increased over time, with higher values between 15:00 h and 17:30 h (194.0 Ind. L^{-1} on average) (Fig. 3.9B). Ciliates had a small growth throughout the day, with 14.8 Ind. L^{-1} on average. Dinoflagellates and crustaceans were distributed almost homogeneously over time, reaching mean abundances of approximately 12.0 Ind. L^{-1} and 18.0 Ind. L^{-1}, respectively. Larvaceans were present at the beginning of the observations with low abundance (3.3 Ind. L^{-1} on average).

On January 14, diatom abundances increased between 7:00 h and 12:00 h, with a peak of 180.0 Ind. L^{-1} at noon and a drop between 15:00 h and 18:30 h. The mean abundance of diatoms throughout the entire period was 88.3 Ind. L^{-1}. Crustaceans and ciliates were homogeneously distributed over time, with mean abundances of 13.5 Ind. L^{-1} and 7.0 Ind. L^{-1}, respectively. Dinoflagellates grew in abundance between 9:30 h and 14:30 h, reaching 5.0 Ind. L^{-1} on average. Larvaceans appeared with low abundance (2.2 Ind. L^{-1} on average) (Fig. 3.9B).

***Bottom layer*:** On January 9, in the bottom layer, the mean abundances of diatoms and dinoflagellates were higher compared to the other layer depths (Fig. 3.9C). All plankton groups, in general, had an increase from the beginning of the observations (8:40 h) until the beginning of the afternoon (13:00 h), with a decline between 14:00 h and 15:00 h, and they grew again until 18:00 h. Diatoms and dinoflagellates had mean abundances of 212.0 Ind. L^{-1} and 8.4 Ind. L^{-1}, respectively. Ciliates, crustaceans, and larvaceans had mean abundances of 16.0 Ind. L^{-1}, 14.8 Ind. L^{-1}, and 5.0 Ind. L^{-1}, respectively.

On January 14, the diatom group was most abundant at the bottom (630.0 Ind. L^{-1} on average), where the abundance increased over time and decreased towards the end of the observations (17:30-18:30 h) (Fig. 3.9C). Ciliates formed the second most abundant group (70.0 Ind. L^{-1} on average), reaching higher values between 11:00 h and 14:30 h and decaying at the end of the observations. Dinoflagellates and crustaceans were distributed almost homogeneously throughout the observation period, with mean abundances of 6.2 Ind. L^{-1} and 21.8 Ind. L^{-1}, respectively. Larvaceans reached 3.3 Ind. L^{-1} on average with low variation over time.

Analysis of variance using Kruskal–Wallis and Dunn`s post-hoc tests indicated significant differences (p value<0.05) in phytoplankton abundances between morning and night periods and between afternoon, evening, and night in the data referring to the 24-hour fixed station in July 2018. Metazooplankton abundances differed significantly between the morning-afternoon, morning-evening, and morning-night periods. Along the water column, significant differences occurred in phytoplankton and protozooplankton abundances between the surface-bottom and midwater-bottom (Table II).

Table 3.2. The results for Kruskal–Wallis and Dunn's post-hoc tests with Bonferroni correction for phytoplankton, protozooplankton, and metazooplankton abundances between the depth layers and the periods along the fixed station on July 19-20, 2018. Values in bold are significantly different between the sites (p<0.05).

	Phytoplankton	**Protozooplankton**	**Metazooplankton**
Between periods of the day			
Kruskal-Wallis	**1.83E-06**	1.24E-01	**3.37E-06**
Chi-square	28.47	3.96	24.17
Dunn's post hoc test periods			
morning-afternoon	9.00E-01	8.25E-02	**4.53E-07**
morning-evening	9.76E-01	**2.77E-02**	**1.08E-04**
morning-night	**5.65E-06**	4.59E-01	**4.94E-03**
afternoon-evening	8.80E-01	5.84E-01	3.43E-01
afternoon-night	**2.90E-06**	3.74E-01	5.47E-02
evening-night	**1.39E-05**	1.72E-01	3.42E-01
Between layers			
Kruskal-Wallis	**1.28E-12**	**6.90E-10**	5.70E-01
Chi-square	53.02	28.98	0.97
Dunn's post hoc test layers			
surface-midwater	6.68E-02	9.25E-01	3.69E-01
surface-bottom	**7.72E-12**	**1.43E-07**	9.31E-01
midwater-bottom	**3.63E-08**	**1.11E-08**	3.60E-01

The analysis of variance in the data referring to the 12-hour fixed stations on January 9 and 14, 2019, had significant variability in the abundances of phytoplankton, protozooplankton, and metazooplankton throughout the day (morning, afternoon, and evening). There were significant differences in the abundances between the surface-bottom and midwater-bottom (Table III).

Table 3.3. The results for Kruskal–Wallis and Dunn's post-hoc tests with Bonferroni correction for phytoplankton, protozooplankton, and metazooplankton abundances between the depth layers and the periods along the fixed station on January 9 and 14, 2019. Values in bold are significantly different between the sites ($p<0.05$).

	Phytoplankton	**Protozooplankton**	**Metazooplankton**
Between periods of the day			
Kruskal-Wallis	**1.13E-10**	**9.93E-04**	**1.82E-05**
Chi-square	45.47	10.64	18.53
Dunn's post hoc test periods			
morning-afternoon	**2.43E-06**	**4.26E-03**	**1.58E-02**
morning-evening	**6.54E-03**	2.61E-01	**3.92E-06**
afternoon-evening	**2.62E-09**	**2.18E-03**	**1.40E-03**
Between layers			
Kruskal-Wallis	**1.21E-33**	**1.76E-10**	**1.82E-05**
Chi-square	150.50	34.57	18.53
Dunn's post hoc test layers			
surface-midwater	6.54E-01	9.99E-01	**1.58E-02**
surface-bottom	**7.38E-12**	**8.58E-05**	**3.92E-06**
midwater-bottom	**5.10E-33**	**1.08E-10**	**1.40E-03**

In January 2019 (Fig. 3.10B), the Ri values had greater dispersion (variability) and higher median and maximum values than those in July 2018 (Fig. 3.10A). In both months, there was a significant difference between the groups regarding the Ri value, especially between midwater and bottom, as indicated by the p value ($p<0.01$). Diatom abundance was greater in summer (Fig. 3.10D) than in winter (Fig. 3.10C) and, in both scenarios, had significant differences between midwater-bottom and surface-bottom ($p<0.001$).

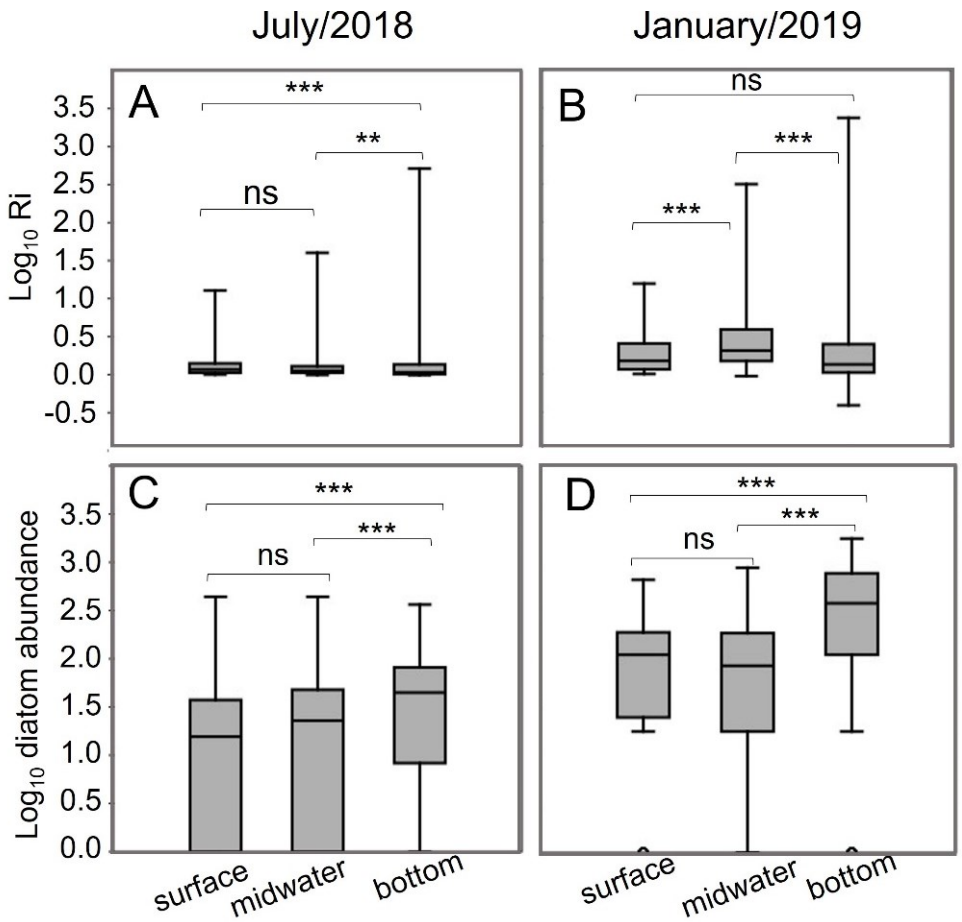

Fig. 3.10. Boxplots of the Richardson number (Log_{10} Ri) for (A) July 2018 and (B) January 2019. Boxplots of diatom abundance (Log_{10}) for (C) July 2018 and (D) January 2019. Data are grouped according to depth layers (surface, midwater, and bottom). The p values of pairwise comparisons between the groups are summarized with asterisks (** = $p \leq 0.01$; *** = $p \leq 0.001$; ns = $p > 0.05$). The boxes display (from lower to upper limit) the first, second (median), and third quartiles; the lower whiskers extend from the first quartile to the minimum value, and the upper whiskers extend from the third quartile to the maximum value. The outliers (if any) are represented with circles.

Hydrological and environmental conditions - Spatial stations

Winter 2018 fieldwork:

The water column had vertical homogeneity in environmental parameters. The vertical temperature profile had low stratification, averaging 21.5 °C. However, horizontally, there was a slight decrease in the average seawater temperature by 1 °C offshore (Fig. 3.11 A1). Salinity ranged from 34.3 in the superficial layers to 34.7 in the deeper layers. The Chl-a concentration was very low in the surface layer (<0.5 µg L^{-1}), showing a small increase towards the bottom and close to

the shore (average of 1.5 µg L^{-1}) (Fig. 3.11 A2). Density (sigma-t) ranged from 23.9 (surface) to 24.3 (bottom), with a strong isopycnal slope (Fig. 3.11 A2). The dissolved oxygen (DO) had a mean value of approximately 7.5 mg L^{-1} throughout the water column (Fig. 3.11 A3). Low buoyancy frequency values were predominant at the surface and in midwater.

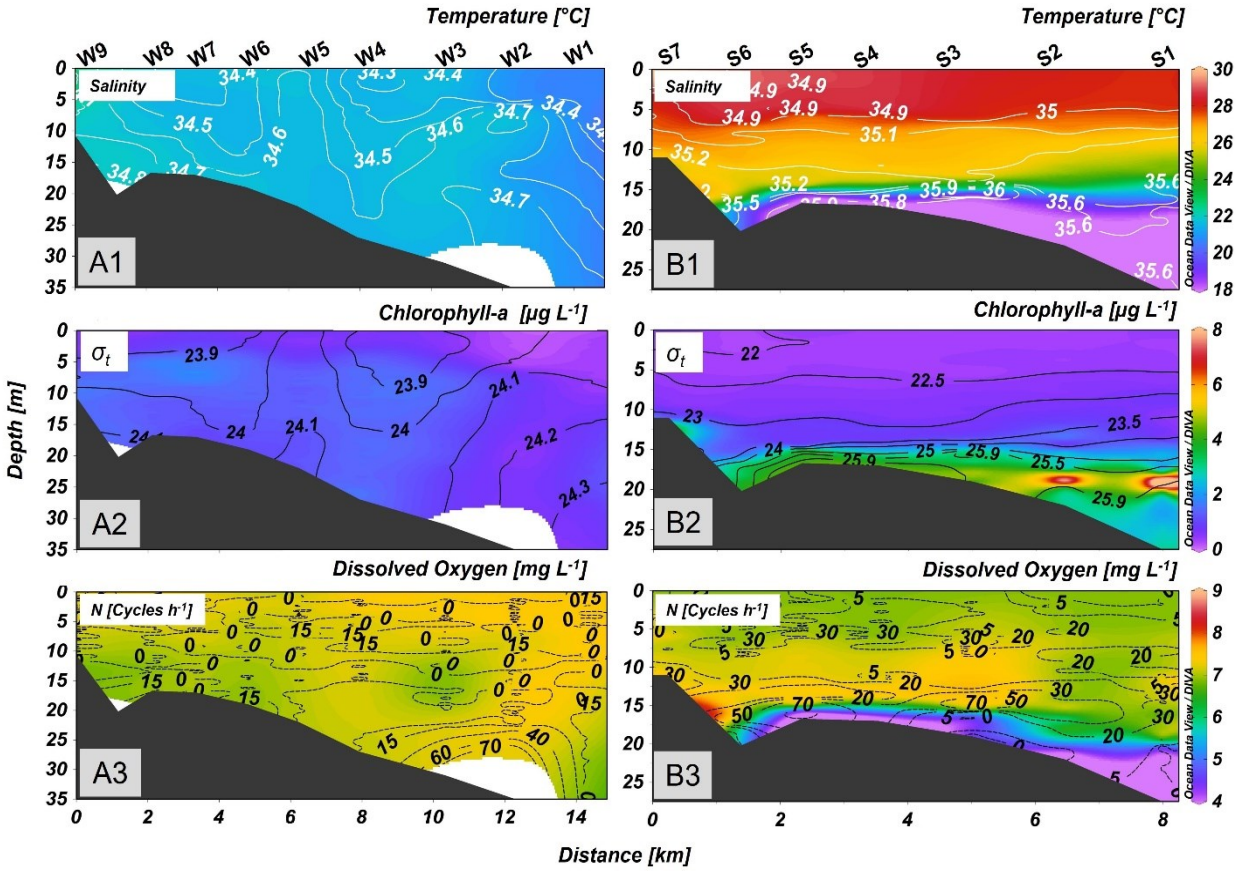

Fig. 3.11. Spatial distribution of environmental parameters over the transect performed on 25 July 2018 (left; A1-3) and on 11 January 2019 (right; B1-3): (A1-B1) temperature (°C) with salinity contours (isohalines); (A2-B2) chlorophyll-a concentration (µg L^{-1}) with isopycnals σ_t (black continuous lines); and (A3-B3) dissolved oxygen (mg L^{-1}), with N contours (in cycles h^{-1}, black dashed lines).

Summer 2019 fieldwork:

The water column had strong thermal stratification, with a maximum temperature of ~30 °C at the surface and a minimum of 18 °C at the bottom (Fig. 3.11 B1). Salinity ranged from 34.9 in the more superficial layers to 35.6 in the deeper layers. The presence of South Atlantic Central Water (SACW) occurred below a depth of 17 m (T<19 °C; S<36.4), as evidenced by an increase in the inorganic nutrient concentrations. Below 17 m depth, Chl-a peaks were found, reaching

intensities between 4 and 8 µg L^{-1} (Fig. 3.11 B2). The density (sigma-t) ranged from 22 at the surface layer to 25.9 at the bottom. DO had minimum values of approximately 3.5 mg L^{-1} at the bottom and maximum values of 7.5 mg L^{-1} at the surface (Fig. 3.11 B3). The distribution of buoyancy frequency isolines indicated a stratified and stable environment, with N>20 cycles h^{-1} in midwater.

Spatial and vertical distribution of plankton

Winter 2018 fieldwork:

Phytoplankton organisms, mainly diatoms, had a quasi-homogeneous vertical distribution from the surface to the bottom, except for Station W3, where there was a clear increase towards the bottom, and Station W2, where phytoplankton abundance (Log_{10} Ind. L^{-1}) was greatest near the surface (Fig. 3.12). Metazooplankton abundance, represented mainly by crustaceans and larvaceans, was homogeneously distributed throughout the water column. Ciliate abundance was greater towards the bottom and at the two stations closest to the coast (W8 and W9).

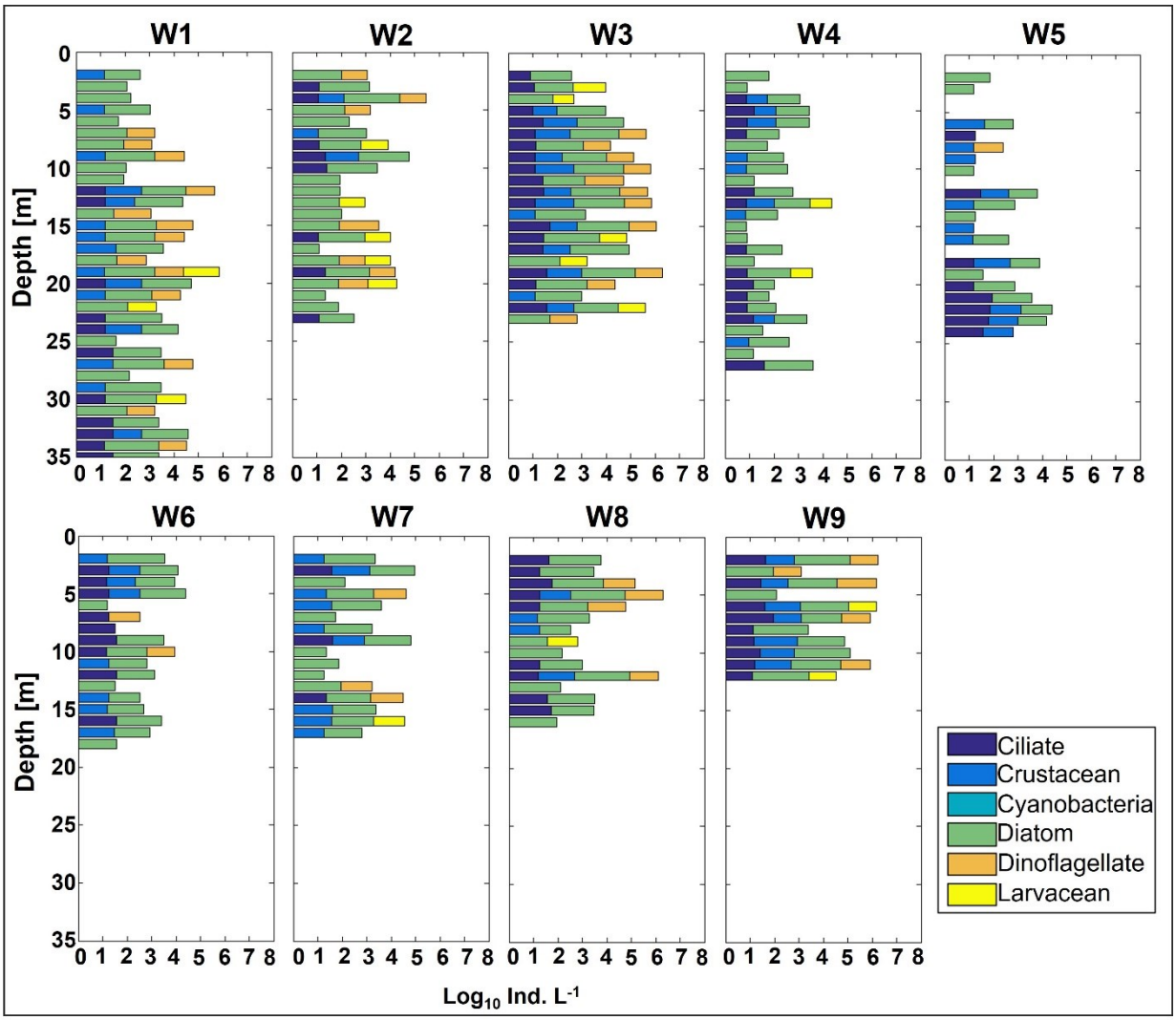

Fig. 3.12. Vertical distribution of the abundance (Log_{10} Ind. L^{-1}) of the main plankton groups (ciliate, crustacean, cyanobacteria, diatom, dinoflagellate, and larvacean) for each station of the transect carried out in the winter on July 25, 2018.

The distribution of the relative abundance (%) of the main groups at each sampling station in the winter campaign revealed a decrease in diatom abundance from the outermost station towards the mid-Station W5 and an increase from this station towards the shallower Station W9 (Fig. 3.13A). Crustaceans and ciliates had an opposite spatial distribution pattern: they increased from the outermost station towards mid-Station W5 and decreased from this station towards the coast (Station W1). Larvaceans had greater relative abundance at the outermost Stations W2 to W4. Dinoflagellates had greater relative abundance at Stations W1 to W3 and near the coast at Stations W8 and W9.

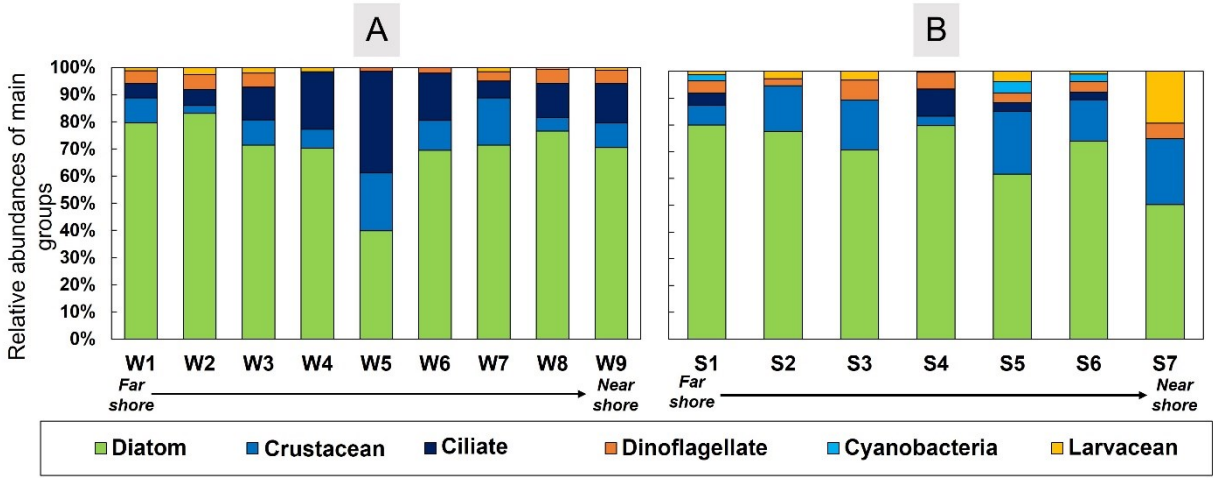

Fig. 3.13. Spatial distribution of the relative abundance (%) of the main groups (ciliate, crustacean, cyanobacteria, diatom, dinoflagellate, and larvacean) along the cross-shore transect stations carried out on 25 July 2018 (A) and 11 January 2019 (B). Stations W3 to W9 in winter fieldwork correspond to Stations S1 to S7 in summer fieldwork.

Summer 2019 fieldwork:

The analysis of the relative abundance of the main groups at each station indicated a decreasing trend in the relative diatom abundance from the outermost Station S1 towards the innermost Station S7. Crustacean and ciliate abundance had a slight increase towards the coast, and the relative larvacean abundance was greatest at coastal Station S7 (Fig. 3.13B).

The vertical abundance distribution of organisms (in Log_{10} Ind. L^{-1}) showed that diatom abundance increased with depth, peaking near the bottom in the colder water intrusion depth of the SACW (Fig. 3.14). Dinoflagellates have been found near the surface and in midwater. Cyanobacteria were observed more abundantly in midwater and near the bottom, with a higher abundance in summer than in winter. Crustaceans were homogeneously distributed from the surface to the bottom. Larvaceans, or appendicularians, had a heterogeneous vertical distribution, being observed with greater abundance between the surface and midwater. Analysis of variance for the main plankton groups between the transect sites can be found in the APPENDIX B.

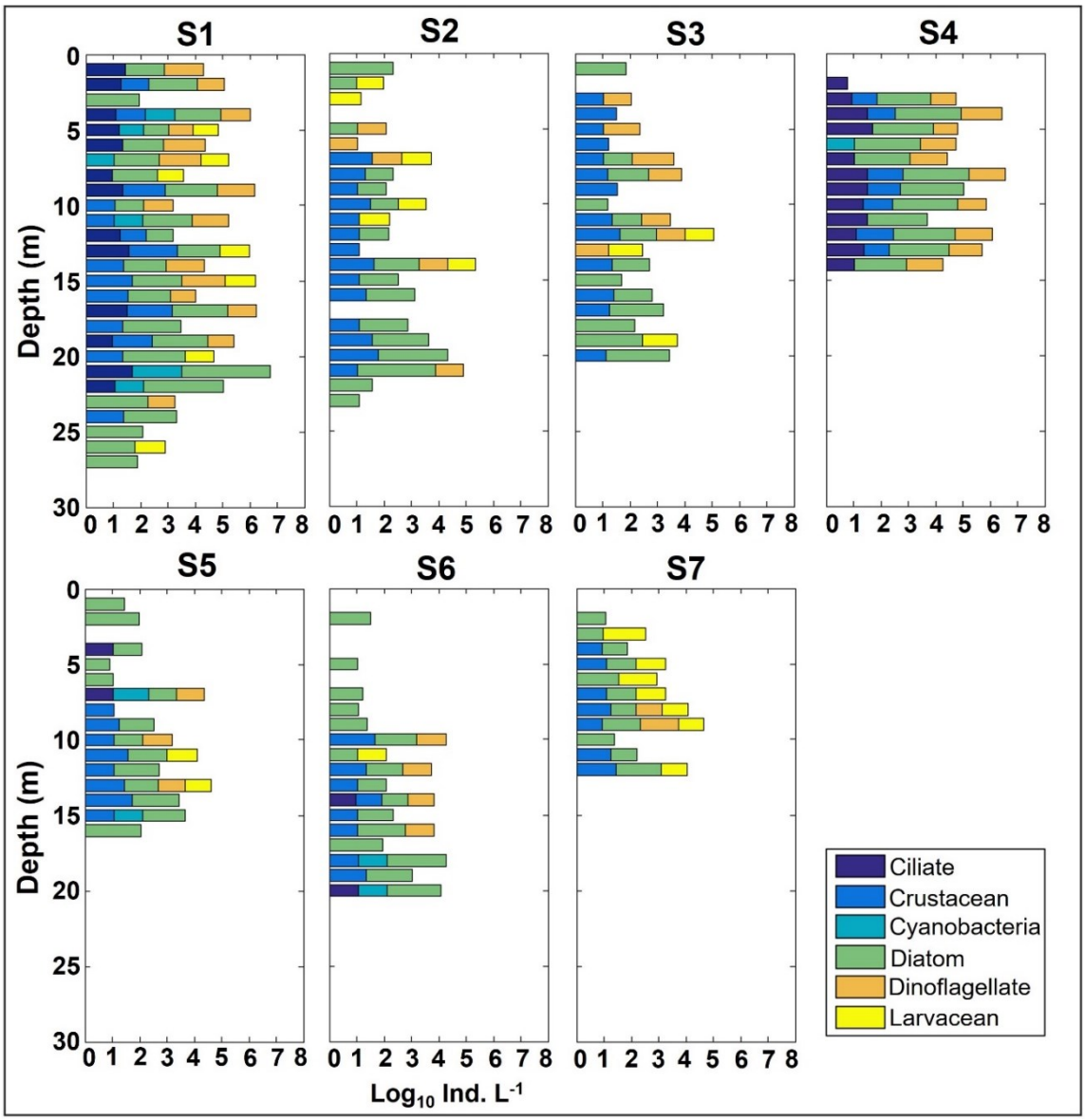

Fig. 3.14. Vertical distribution of the abundance (Log_{10} Ind. L^{-1}) of the main plankton groups (ciliate, crustacean, cyanobacteria, diatom, dinoflagellate, and larvacean) for each station of the transect carried out in the summer on January 11, 2019.

Ecological indices

For the analysis of ecological indices, data from specimens classified into the categories of genus or species within the group of diatoms, dinoflagellates, and cyanobacteria were used. We identified 22 genera of diatoms (Bacillariophyceae), seven genera of dinoflagellates (Dinophyceae), and a genus of cyanobacteria (Cyanophyceae). The complete list of the identified specimens used in the ecological index calculation can be found in the APPENDIX B.

The highest values for specific richness, expressed by the Margalef index, and for diversity, expressed by the Shannon index, were observed at the furthest stations from the coast, W1-W2 and S1-S2, in winter and summer fieldwork, respectively (Fig. 3.15 A-D). In general, the distribution of diversity and richness indices tended to decrease from deeper to shallower waters. The diversity index ranged between 1.09 and 2.52 in winter and between 1.07 and 2.89 in summer. The richness index ranged between 1.14 and 5.16 in winter and between 1.08 and 5.06 in summer. Simpson's dominance index was lower at the furthest transect stations in winter, W1-W2 (0.12 and 0.18), and in summer, S1-S2 (0.08 and 0.12); the highest values for dominance were at Stations W3 (0.43) and S7 (0.44) (Fig. 3.15 A-B). Pielou's equitability had an opposite trend to Simpson's dominance, reaching higher values at the furthest stations of the transects. The equitability index ranged between 0.57 (W3) and 0.79 (W1) in winter (Fig. 3.15C) and between 0.58 (S4) and 0.86 (S1) in summer (Fig. 3.15D).

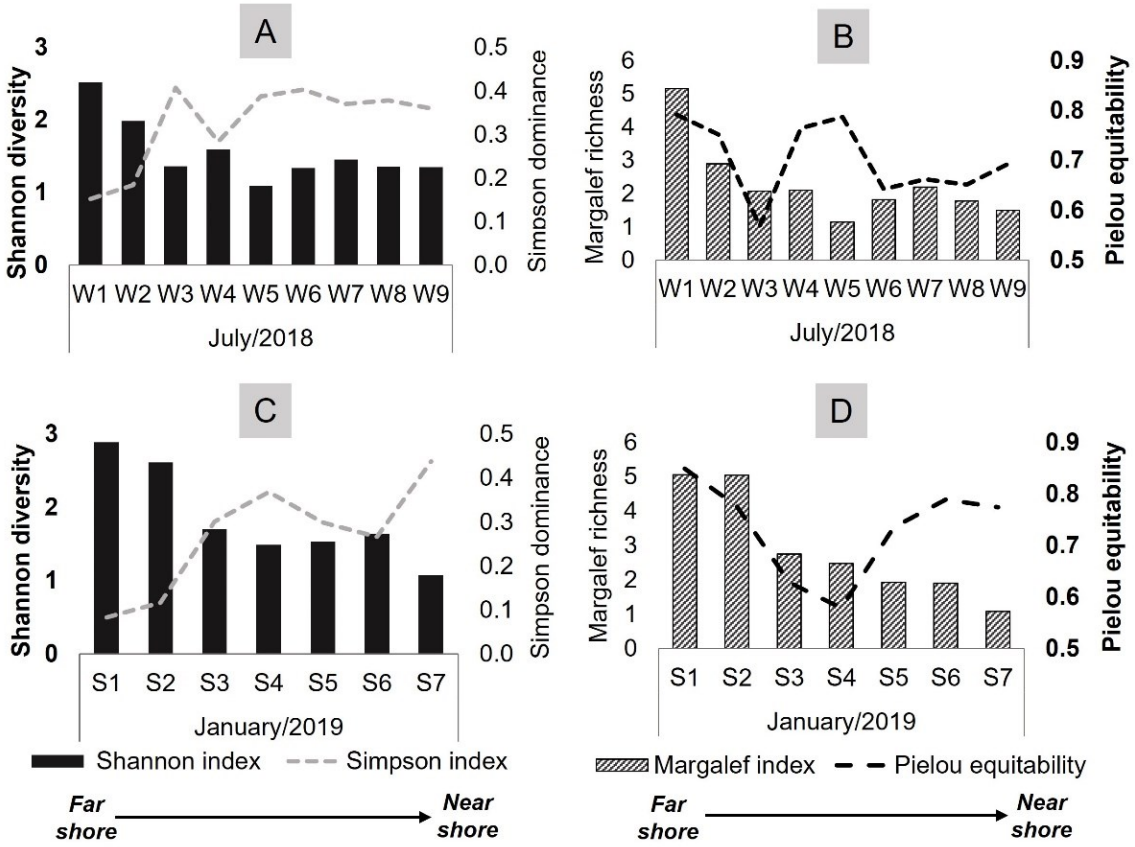

Fig. 3.15. Shannon diversity index (bars) and Simpson dominance index (dashed line) on (A) 25 July 2018 and (B) 11 January 2019. Margalef richness index (bars) and Pielou equitability (dashed line) on (C) 25 July 2018 and (D) 11 January 2019. Stations W3 to W9 in the winter fieldwork correspond to Stations S1 to S7 in the summer fieldwork.

3.5. Discussion and conclusion

Meteorological and oceanographic conditions

The inner portion of the SBS is influenced by small and submesoscale processes associated with the action of winds. Both local and remote winds can force subinertial oceanic reactions over the continental shelf (DAVIS; BOGDEN, 1989). The general pattern of ocean circulation on the continental shelf off Ubatuba includes surface currents flowing southwest influenced by the South Atlantic Subtropical Anticyclone. The latter leads to the dominance of northeasterly winds between 20°S and 30°S, with higher intensity averages in summer (CASTRO et al., 2006; REBOITA et al., 2019). On the inner shelf off Ubatuba, winds prevail over tidal action, determining the direction and magnitude of currents (DOTTORI; CASTRO, 2018). The direct effect of wind shear stress on circulation is felt at the surface within the Ekman layer and extends to tens of metres deep.

The coastline orientation in the SBS (SW–NE direction) and the shallow shelf with isobaths parallel to the coast, provide conditions for the sea surface height to increase or decrease due to the action of the prevailing SW or NE winds, respectively. Changes in local wind direction from N–E to SE–SW are promoted by frontal systems (cold fronts), which run along the coast of South America with a SW-NE trajectory and occur throughout the year (CERDA; CASTRO, 2014; RODRIGUES; FRANCO; SUGAHARA, 2004). The prevailing current flow to the SW with inversion events to the NE due to the passage of cold frontal systems on the inner shelf off Ubatuba was recorded by Castro (1997) during the winter in three consecutive years. In this work, we verified that during the winter fieldwork in July 2018, surface currents flowed predominantly to SW on July 19-20, with a change in direction to N–NE on July 25. Sea surface height increased by approximately 0.13 m from July 21 to July 26 (Fig. 3.2). Wind field data showed the arrival of a cold front on July 21 with stronger winds blowing from S–SW (Fig. 3.3).

During the summer fieldwork from 9 to 14 January 2019, currents flowed predominantly to the SW, with a current reversal event to the NE and a sea surface elevation of approximately +0.1 m between 12 and 13 January. However, the average winds for the observation period indicated a predominance of northeasterly winds, with greater intensities than those observed in winter. This wind pattern, acting parallel to the shoreline, favours coastal upwelling phenomena that lead to the subsurface intrusion of the cold, nutrient-rich waters of SACW onto the Ubatuba

inner shelf (BRAGA; MÜLLER, 1998; PENNINCK et al., 2021), as observed during the study period (Fig. 3.4 D).

Temporal plankton distribution - Short-term variability

As discussed by Teixeira & Gaeta (1991), temporal variability in the distribution of plankton populations may result from the diel periodicity of phytoplankton and environmental conditions, and biological rhythms (biochemical, physiological, and behavioural events). During the 24-h fixed station on July 19-20, 2018, conditions favoured greater temperature homogeneity in the water column (Fig. 3.6). The increase in Chl-a concentration and diatom abundance verified in the deep layer was probably due to turbulent processes and tidal currents that favor sediment resuspension, promoting nutrient release accumulated by regeneration and leading to an increase in phytoplanktonic production and biomass (AIDAR et al., 1993; REYNOLDS, 2006).

Although the Chl-a concentration remained very low at the surface, Chl-a aggregation in midwater occurred in the first hours of observation on July 19, with an intensity 2 times greater than the background. This patch started to disperse when a strong vertical inclination of isopycnal 24.3 was also observed, with an upwards displacement of approximately 10 m (at ~19:00 h, Fig. 3.6). This isopycnal slope may be associated with advective flows or the passage of internal waves, generating instabilities that lead to the dissipation of layers and patches of plankton (STACEY; MCMANUS; STEINBUCK, 2007). In the early hours of July 20, the variability in the stability of the water column led to variability in the plankton populations, especially in the increase in diatom abundance in the bottom layer (Fig. 3.8).

The analysis of variance in the winter data confirmed the observed variability, indicating significant differences in phytoplankton and protozooplankton abundances between the surface and the bottom, where they had higher medians. Most likely due to the increase in mixing processes throughout the day, phytoplankton abundances were significantly different between the morning-night and afternoon-night periods, with higher abundances at night. This process likely influenced the variability of the metazooplankton population, which also had higher abundances in the afternoon and night periods (Table 3.1).

During the 12-hour fixed stations held on January 9 and 14, 2019, there was, in general, thermal stratification in the water column (Fig. 3.7). However, the isopycnal and buoyancy frequency (N) distributions for January 9 indicated a less stable environment compared to January

14, when a more strongly established seasonal thermocline was observed and the presence of the SACW was more evident near the bottom. The increased penetration of SACW on January 14 led to an increase in diatom abundance towards the bottom, representing an enhancement of food for zooplankton populations (HUNT; HOSIE, 2005; LONGHURST; HARRISON, 1989), which had their increase represented in the crustacean abundances (Fig. 3.9).

There were significant differences in the abundance of the main plankton groups throughout the day, with the highest abundances being observed in the afternoon and the lowest in the evening (Table 3.2). Plankton abundance and water column stability varied between depth layers. In terms of stability (Ri number), there were significant differences between the midwater layer and the bottom of the water column, with the bottom being the most unstable layer (Fig. 3.10). The increase in current shear in the bottom layer, due to tidal flow and SACW intrusion, may be related to the increase in the diatom population in this layer during the summer. SACW onshore intrusions have been related to current shear (PENNINCK et al., 2021), the transport of diatoms in resting stages to coastal areas (BRANDINI et al., 2014), and the resuspension of nutrients accumulated in the sediment (AIDAR et al., 1993; BRAGA; MÜLLER, 1998), contributing to the variability in plankton abundance and diversity.

Many works have addressed the influence of physical conditions on plankton distribution (FRANKS; WALSTAD, 1997; MACÍAS et al., 2013; PRAIRIE et al., 2012). Pannard et al. (2008) associated mixing and water advection events with fluctuations in total phytoplankton biomass and the concentration of dominant species in the English Channel; according to the authors, the phytoplankton response to physical changes in the environment can occur in a few hours in terms of photosynthetic production and a few days in the composition of the community. Our results suggested significant changes in short periods of 12 hours and 24 hours mainly in diatom abundance related to mixing processes and water intrusions.

Spatial distribution of plankton

In the winter cross-shore transect on July 25, 2018, the water column along the transect was almost homogeneous, but the analysis of the isopycnal allowed the observation of horizontal density gradients (Fig. 3.11 A2). The density distribution (σ_t) in the surface layer showed that the isopycnals 23.9 and 24 sloped strongly downwards, and the isopycnals 24.1 and 24.2 sloped upwards at the outermost stations. Tilted isopycnals may be associated with advective flows

intensified by submesoscale dynamics (MAHADEVAN, 2016). The passage of a cold frontal system from July 21, building up surface waters along the coast and, consequently, causing downwards movements, may explain this highly dynamic scenario.

The influence of the cold front and the turbulent processes involved were probably felt in the plankton population. The physical disturbance caused by transient atmospheric events associated with S–SE winds in a nonupwelling scenario has been related to an increased abundance of benthic macrofauna (QUINTANA et al., 2015) and changes in phytoplankton structure (GAETA et al., 1999) in the coastal system of Ubatuba. Our results showed a greater abundance of organisms at the outermost stations (W1 to W3), with a predominance of diatoms and dinoflagellates, and a lower abundance at the intermediate stations (W4 to W6), with a decrease in phytoplankton and an increase in ciliates and crustaceans (Fig. 3.12). The spatiotemporal variability of plankton related to submesoscale processes was studied by authors such as Hernández-Hernández et al. (2021), who observed significant differences between picoplankton populations at stations less than 5 km away and between periods shorter than 24 hours, relating that to the high physical spatiotemporal variability. In this study, we observed significant differences in plankton distribution between transect sites less than 2 km away, both in the winter and summer transects.

On the summer transect on January 11, 2019, the data indicated a vertically stratified and stable water column between depths of 5 and 20 m (Fig. 3.11 B1-3). The SACW was below ~18 m, where the subsurface chlorophyll maximum (SCM) was observed. Diatom abundance had an increase near the SCM, where an increase in the number of crustaceans was also observed (Fig. 3.14). Phytoplankton and metazooplankton abundances were higher along the summer transect, corroborating previous studies in the Ubatuba region, which indicate that the abundance of these organisms is generally higher in the warm seasons due to the increase in food availability caused by SACW onshore intrusions, sustaining a local increase in phytoplankton biomass (MELO JÚNIOR et al., 2016; MIYASHITA et al., 2010; TEIXEIRA; GAETA, 1991) and governing temporal variability in zooplankton vertical distribution (MARCOLIN; GAETA; LOPES, 2015).

There were opposite trends in the spatial distribution of the abundance of diatoms, crustaceans, and ciliates (Fig. 3.12 to Fig 3.14). Lower crustacean and ciliate abundances at the outermost stations are likely to occur due to the establishment of outer-shelf conditions forced by the upwelling of the oceanic SACW, leading to a decrease in the abundance of coastal metazooplankton species (NAGATA et al., 2014). Miyashita et al. (2009) studied the vertical and

spatial distribution of copepod abundance during the summer along the inner shelf off Santos (SE Brazil) and observed a decrease in the total metazooplankton abundance from the coast to the open sea. Nogueira Jr et al. (2014) observed an increase in the number of species (richness) of siphonophores from the coast to the open ocean off the coast of Santa Catarina (South Brazilian Bight), concluding that the abundance and distribution of jellyfish and siphonophores were strongly influenced by SACW intrusions, which favoured the development of species with more offshore affinities on the shelf and simultaneously reduced the abundance and geographic range of coastal species.

In addition to abundance, our results showed that phytoplankton diversity was also higher in the summer fieldwork (Fig. 3.15). In general, species richness was higher at the outermost stations, with greater uniformity in the distribution of organisms between species (equitability), in summer and winter. This suggested that the nutrient enhancement driven by submesoscale processes, SACW intrusion in summer and vertical mixing in winter, may have increased local productivity at the outermost stations, increasing resource availability and decreasing competition and predation due to greater availability of niches and less intraspecific pressure, leading to an increase in species diversity and richness (PIANKA, 2011).

It is important to emphasize that the ecological indices reported in this work were calculated based on the relative abundance of phytoplankton above 100 µm in size, which corresponds to a small fraction of the total phytoplankton in the study area (FRAZÃO, 2001). This may limit the ecological indices analysis and our assessment of the impact of increasing phytoplankton abundance at higher trophic levels, as much of the trophic web in meso- and oligotrophic environments is supported by pico-nanoplankton and the smaller fractions of microphytoplankton, in addition to many species of zooplankton being selective in terms of prey size.

Studies involving physical-biological coupling models indicate that marine plankton may respond strongly to climate variability through changes in their biological parameters, such as growth, grazing, and mortality (LI; GARGETT; DENMAN, 2000; PEÑA; MASSON; CALLENDAR, 2016). Benedetti et al. (2021) projected a scenario until the end of this century under conditions of high emissions of greenhouse gases, in which there is a decrease in zooplankton richness in the tropics and an increase in temperate to subpolar latitudes, where approximately 40% of phytoplankton and zooplankton assemblages are replaced by species that move to the poles driven by ocean warming.

Since plankton are highly sensitive to hydrographic conditions and nutrient dynamics (RICHARDSON, 2009), observations of plankton distribution driven by variabilities in environmental conditions can help us to understand likely scenarios of climate change. Alterations in ocean circulation, stratification, and upwelling intensity are examples of climate-induced changes that have been pointed out by studies involving models and *in situ* observations (Cooley et al., 2022). Studies on the spatial variability of marine plankton in response to changes in the physical structure of the environment are, therefore, fundamental, supporting model results and contributing to the projection of future marine environmental conditions.

Concluding remarks

The Ubatuba shelf region has highly variable hydrodynamic conditions, where submesoscale oceanographic processes, associated with the action of local and remote winds, influence the environmental and biological processes. It was observed that variations in the regional wind regime, associated with a cold frontal system during the winter fieldwork, led to rapid changes in the physicochemical conditions and water column stability. Short-term observations indicated that the intensification of mixing processes led to an increase in Chl-a concentration and diatom abundance. In summer, vertical stratification and SACW cross-shore advection were probably the main factors influencing the vertical distribution of plankton. Therefore, the diurnal variation observed in the plankton distribution was not only due to diel cycles but also to wind-driven mixing and water mass advection.

Seasonal variability, with emphasis on the summer-winter contrast, was evident regarding water column stratification and stability. Differences were also observed regarding the abundance and diversity of the main plankton groups, which were higher in summer. Wind-driven SACW intrusion is the most relevant (sub)mesoscale phenomenon in this region (CERDA; CASTRO, 2014), affecting the dynamics of the entire ecosystem. Upon reaching the inner shelf, SACW stimulates phytoplankton growth, favouring metazooplankton populations and increasing the abundance and diversity of plankton. Therefore, our results suggested that seasonal phenomena or transient states can induce mixing processes that result in spatiotemporal physical variability leading to significant variability in plankton populations on a time scale of a few hours, vertically between depth layers (a few metres), and at spatial scales less than 2 km along the inner shelf.

By evaluating how plankton distribution responds to variability in seasonal and short-term conditions (hours), this study contributes to current knowledge and future projections on the plankton behaviour in the face of changes in the physicochemical properties of water masses and ocean circulation caused by climate change, which can alter the functioning of the marine ecosystem with threats to ecosystem services mediated by plankton. In addition, understanding the distribution of autotrophic and heterotrophic organisms and their interactions with the physicochemical conditions in the coastal ecosystem of Ubatuba can help in the sustainable exploitation of fisheries resources and serve as a database for future monitoring.

4. Chapter IV – Influence of environmental conditions on the pico-nanophytoplankton distribution on the inner shelf off Ubatuba, Brazil.

4.1. Abstract

Changes in physicochemical properties caused by wind dynamics are linked to changes in the biological components of marine ecosystems. The influence of physical conditions on plankton distribution has been analyzed in different marine environments, however, the distribution of pico-nanoplankton in coastal areas in the Southwest Atlantic Ocean, and its interaction with submesoscale processes, have been relatively poorly studied. In this work, we aimed to evaluate the influence of the wind-driven environmental conditions on the distribution of pico- and nanoplankton (<20 µm) populations along the inner shelf off Ubatuba. Data collection campaigns were conducted in December/2018 and January/2019. Profilings with high-resolution environmental sensors and discrete water sampling were carried out at seven spatial stations (roughly at 1.5 km intervals). Variations in meteorological conditions led to two distinct scenarios, allowing the observation of the biological variables' response to different stratification conditions and nutrient availability. The observed relationships between the environmental conditions and the distribution of *Synechococcus*, *Prochlorococcus*, picoeukaryotes, and nanoeukaryotes suggest that wind-driven physical processes influenced the plankton abundance distribution by controlling the water column stability and the nutrient-rich South Atlantic Central Water (SACW) intrusion onto the inner shelf. Pico- and nanophytoplankton distributions were likely affected by vertical mixing and lower nutrient concentrations in December/2018. The greater stability and availability of nutrients favored populations in January/2019, with an increase in biomass in the subsurface chlorophyll maximum formed by the stronger SACW intrusion.

Keywords: Biophysical interactions, Picophytoplankton, Nanoeukaryotes, Picocyanobacteria, South Atlantic Central Water, Ubatuba inner shelf.

4.2.Introduction

Current concern about the role of the oceans in climate change has increased interest in better understanding the physical-biological interactions in the marine planktonic ecosystem. Many works have addressed how physical and chemical factors can drive plankton distribution patterns (BASTERRETXEA; FONT-MUÑOZ; TUVAL, 2020; VILLAMAÑA et al., 2019) and described the structure of microbial communities in certain regions of the Atlantic Ocean (FERREIRA et al., 2022; PÉREZ et al., 2005; TARRAN; HEYWOOD; ZUBKOV, 2006). However, the vertical and spatial distribution of pico-nanoplankton in coastal areas in the Southwestern Atlantic Ocean and its interaction with submesoscale processes have been relatively poorly studied (BERGO et al., 2017; FRAZÃO et al., 2021; RIBEIRO et al., 2016).

Meso- and submesoscale processes can drive mixing and diapycnal nutrient fluxes that stimulate phytoplankton growth in coastal areas (CORREDOR-ACOSTA et al., 2020). Margalef (1978) explained the relationship between the distribution of marine microorganisms and the physical environment through a conceptual model that separates groups of phytoplankton according to turbulence and nutrient availability. Although the Margalef model focuses on large phytoplankton, the distribution of smaller organisms in the pico- and nanoplankton groups can also be explained by physical forcing (LEE et al., 2016; SCHMOKER; HERNÁNDEZ-LEÓN, 2013; SILOVIC et al., 2018). Photosynthetic microorganisms have developed adaptive, physiological, and behavioral strategies to deal with adverse conditions (WHEELER et al., 2019), such as buoyancy and adaptation of chlorophyll and lipid content, and modulation of vertical migration in response to environmental conditions (SENGUPTA; CARRARA; STOCKER, 2017).

Picophytoplankton is represented by the marine cyanobacteria *Synechococcus* and *Prochlorococcus*, and by eukaryotic picoplankton (picoeukaryotes). *Prochlorococcus* and *Synechococcus* dominate the picoplankton and represent approximately 60% of all autotrophic biomass in the oceans (MANN; LAZIER, 2006). In addition, picoplankton are important carbon exporting agents, via both aggregate formation and consumption by organisms of higher trophic levels (BUITENHUIS et al., 2012). Photosynthetic pico- and nanoeukaryotes groups are generally less abundant; however, they contribute significantly to the biomass of the epipelagic community due to their larger cell sizes compared to prokaryotes (RIBEIRO et al., 2016; TARRAN; HEYWOOD; ZUBKOV, 2006).

This work aimed to study the influence of the wind-driven environmental conditions on the spatial distribution of planktonic autotrophic microorganisms belonging to picoplankton (0.2-2.0 µm) and nanoplankton (2-20 µm) along the inner shelf of Ubatuba, southeastern Brazil. For this, the vertical and spatial distribution (horizontal scales of about 1.5 km) of pico- and nanoplankton abundances and their relationship with environmental conditions were analyzed in two campaigns carried out in late spring and summer (December/2018 and January/2019), when scenarios with different stability conditions and nutrient concentration were observed.

Phytoplankton abundance on the continental shelf off Ubatuba is influenced by mixing processes (GAETA et al., 1999) and by the intrusion of the oceanic and nutrient-rich South Atlantic Central Water (SACW), regulated by meteorological and oceanographic processes throughout the year (BRANDINI, 2006). The intermittent coastal upwelling events in the Southwestern Atlantic Ocean affect the pico- and nanoplanktonic communities (BERGO et al., 2017) and favor the formation of subsurface chlorophyll maxima (SCMs) (BRANDINI et al., 2014) and plankton aggregates (MARCOLIN; LOPES; JACKSON, 2015). These features play a crucial role in ocean carbon fluxes, fish and zooplankton feeding processes, optical and acoustic attenuation, and remote sensing reflectance (MCFARLAND et al., 2015; SULLIVAN et al., 2010).

In addition to increasing our knowledge about pico- and nanoplankton distribution patterns on the inner shelf of Ubatuba, focusing on the dynamics between physical-chemical processes and plankton distribution, this study also advances our current understanding of the main factors that regulate the structure of the microbial community in coastal meso-oligotrophic marine systems. Studying how the plankton populations respond to different environmental scenarios is essential to predict their response to climate change that may force changes in the physical environment and, consequently, impact the structure and functioning of marine ecosystems.

4.3.Materials and methods

Sampling

Profilings with high-resolution environmental sensors and water samplings were carried out at seven oceanographic stations along a cross-shore transect on the inner shelf off Ubatuba on 04 December 2018 and 08 January 2019 (Fig. 4.1). Discrete water samplings with go-flo bottles to determine physicochemical and biological variables were performed at 4 or 5 depth levels along the water column: in the surface layer, in the thermocline or midwater, in the vicinity of the subsurface chlorophyll maximum (SCM), and in the bottom layer. Sampling depths varied according to the maximum depth of the collection site.

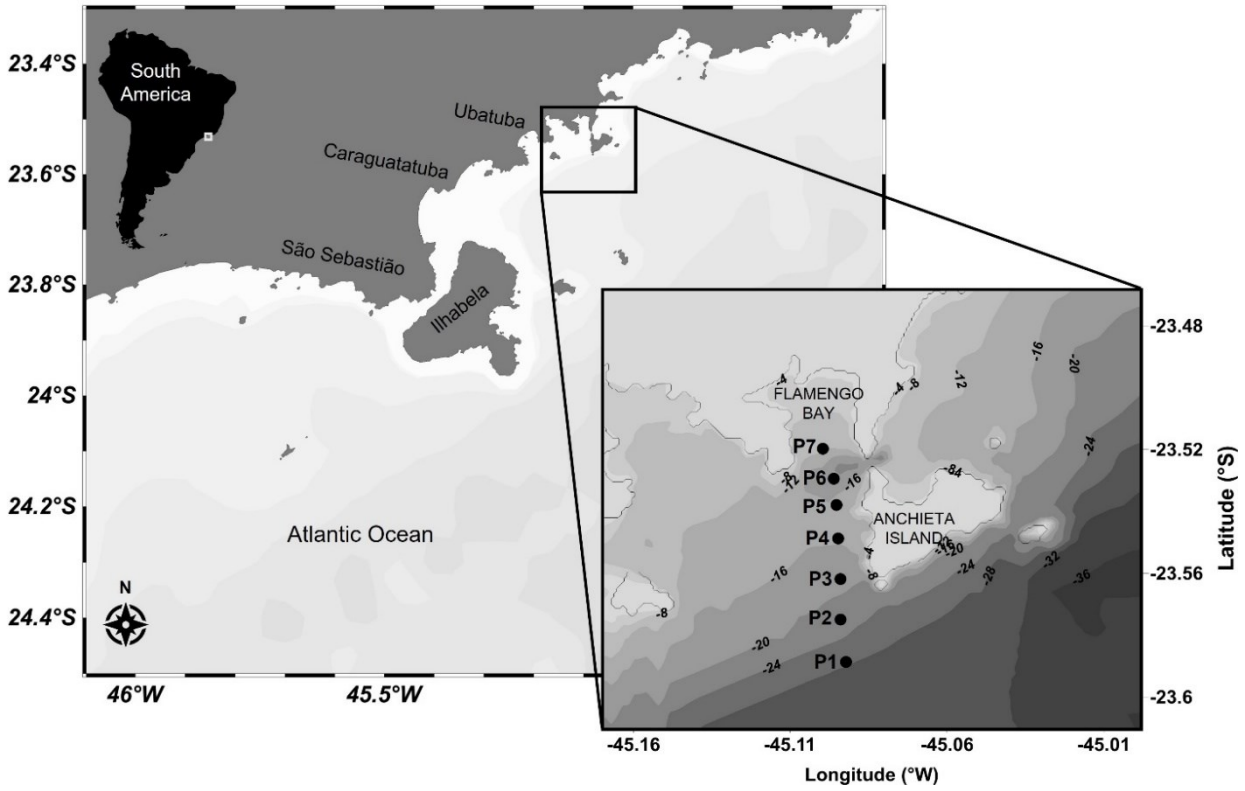

Fig. 4.1. Map of the study area with the location of the cross-shore stations (P1 to P7) on the inner shelf off Ubatuba, southeastern Brazil. Bathymetric curves in meters.

Meteorological and oceanographic data

Wind data were obtained from the Climate Forecast System Version 2 (CFSv2), produced by the NOAA National Centers for Environmental Prediction (NCEP). A multiparameter probe, RINKO-Profiler (JFE Advantech), was used to acquire temperature and salinity data, through continuous measurement through the water column, at 0.1 m intervals. The probe data were used to obtain density profiles and to estimate stratification in the water column by calculating the Brunt-Väisälä frequency (N). This parameter is related to both the stability of the water column and the vertical density gradient, and is calculated from equation 1:

$$N = \sqrt{-\frac{g}{\rho_0}\left(\frac{\partial \sigma_t}{\partial z}\right)} \tag{1}$$

where g is the acceleration of gravity, z is the depth (positive upwards), ρ_0 is the average density and $\sigma_t = \rho(s, t, p = 0) - 1{,}000$ (POND; PICKARD, 1983). The N values were expressed in cycles per hour (cycles h^{-1}). High N values indicate a stratified portion of the water column, while low values are found in vertically homogeneous regions.

Chemical and biological variables

Vertical profiles of dissolved oxygen (DO, in mg L^{-1}), turbidity (in FTU), and chlorophyll-a (Chl-a) fluorescence (ppb) were obtained by the RINKO-Profiler. The DO concentration was estimated by the Weiss equation (WEISS, 1970). The apparent oxygen utilization (AOU, in µmol Kg^{-1}), determined by the difference between the oxygen concentration at saturation and the DO in seawater, was calculated in the Ocean Data View (ODV) software (SCHLITZER, 2021). The turbidity sensor is integrated with the Chl-a fluorescence sensor. Particles suspended in water are irradiated with infrared light at 880 nm, so the intensity of the reflected/scattered light is measured by the light receiver, that is, the sensor uses backscatter light to measure turbidity.

To obtain a calibration curve for Chl-a concentrations, estimated by the fluorescence sensor, water samples were collected for analysis of the actual Chl-a concentration, in µg L^{-1}. The samples were filtered on board in a GF/F 25mm filter immediately after collection and the filters were kept in an ultra-freezer (-80°C) until the extraction of Chl-a in the laboratory. The Chl-a concentration was determined using a fluorimeter (10-AU, Turner designs Inc.), according to the non-acidified

fluorometric method described in Welschmeyer (1994). The correlation coefficient between the Chl-a fluorescence and the extracted Chl-a concentration was 0.80 (n = 20) for December 2018, and 0.94 for January 2019 (n = 40) (calibration curve in APPENDIX C). For analysis of dissolved inorganic nutrients (nitrite, nitrate, phosphate, and silicate), 50 mL aliquots of water samples filtered through GF/F 25mm filters were separated and refrigerated (-20°C) until laboratory analysis by a flow injection autoanalyzer (AutoAnalyzer 3 HR, SEAL Analytical Inc.). The euphotic zone (Zeu), the depth where 1% of the photosynthetically active radiation remains (400-700 nm), was estimated by multiplying the Secchi depth (m) measured in the field by the conversion coefficients proposed by Luhtala & Tolvanen (2013) for coastal waters.

Flow cytometer analysis

Flow cytometry was used to determine the pico- and nanophytoplankton abundance (in cells mL^{-1}), following the method proposed by Marie et al. (2005). Water sample aliquots were separated (1.5 mL), preserved on board with glutaraldehyde (0.2%), frozen in liquid nitrogen, and stored in an ultra-freezer (-80Cº) until analysis. The samples were analyzed using an Attune® NxT flow cytometer (Thermo Fisher-Scientific).

The populations of *Synechococcus* (Syne), *Prochlorococcus* (Pro), picoeukaryotes (PicoEuk), and nanoeukaryotes (NanoEuk) were discriminated by the autofluorescence of the chlorophyll (red fluorescence, BL3, > 650 nm) or the phycoerythrin content (orange fluorescence, BL2, 585 nm), and by the cells' forward angle light scatter (FSC), which is proportional to cell size. Flow cytometry data were analyzed in the FlowJo v10 software.

From the abundance data, the biomass (in µg C L^{-1}) was estimated for picophytoplankton through cell-to-carbon conversion factors according to Buitenhuis et al. (2012): 36 fg C $cell^{-1}$ for *Prochlorococcus*; 255 fg C $cell^{-1}$ for *Synechococcus*; and 2,590 fg C $cell^{-1}$ for picoeukaryotes. Currently, there is no consensus on a consistent conversion factor for nanophytoplankton (BERGO et al., 2017; BUITENHUIS et al., 2012).

Statistical analyses

Logarithmic transformation was applied ($\log_{10}X+1$) to the environmental and biological data to equalize the order of magnitude of the different variables (standardization) and for the calculation of robust principal components. Principal component analysis (PCA) was applied to

environmental data to summarize the physicochemical conditions present in each fieldwork. Redundancy analysis (RDA) was applied to evaluate the influence of physicochemical variables on the variability of pico- and nanophytoplankton abundances. RDA is a multiple linear regression method between environmental and biological data (explanatory and response variables), considered an extension of the PCA (BORCARD; GILLET; LEGENDRE, 2018). PCA analysis was performed with the *FactoMinerR* package and the RDA analysis with the *vegan* package, followed by the ANOVA test of significance (anova.cca function), using R software, version 3.6.3.

As most of the data did not conform to a normal distribution, analysis of variance using the non-parametric Kruskal-Wallis test, followed by the Dunn's post hoc test, was applied to the pico-nanophytoplankton abundance data (log-transformed) to assess the variability between collection sites and depth layers. The tests were implemented in the PAST software (version 4.02) and a significance level of 5% was used (p-value <0.05). Spearman's rank correlation was also performed between biological and environmental data, using R software (version 3.6.3).

4.4. Results

Meteorological and oceanographic conditions

During the fieldwork on December 4 and January 8, winds were predominantly from NE and ENE, with mean speeds of 2.19 and 2.10 m s^{-1}, respectively (Fig. 4.2 B and E). In the days before the collections, the mean wind speed was 1.77 m s^{-1} on December 3, coming from the S-SW on average (Fig. 4.2 A), and 1.93 m s^{-1} on January 7, with predominant winds from ENE (Fig. 4.2 D). The TS diagram for both campaigns showed the predominance of shelf waters (SW) at the surface (T>20° and 34<S<36.4), resulting from a mixture between the coastal water (T>20°C and S<34) and the tropical water (T>20°C and S>36.40); and the presence of SACW (T<20°C; S <36.4; Miranda & Katsuragawa, 1991) below ~15 m depth (Fig. 4.2 C and F).

In January, the presence of SACW in the bottom layer was stronger, reaching lower temperatures, around 17°C (Fig. 4.2 F). In both campaigns, spatial stations were carried out during spring tides in flooding periods, when tidal currents generally flow to the west-northwest in this region (BATISTA; HARARI, 2017).

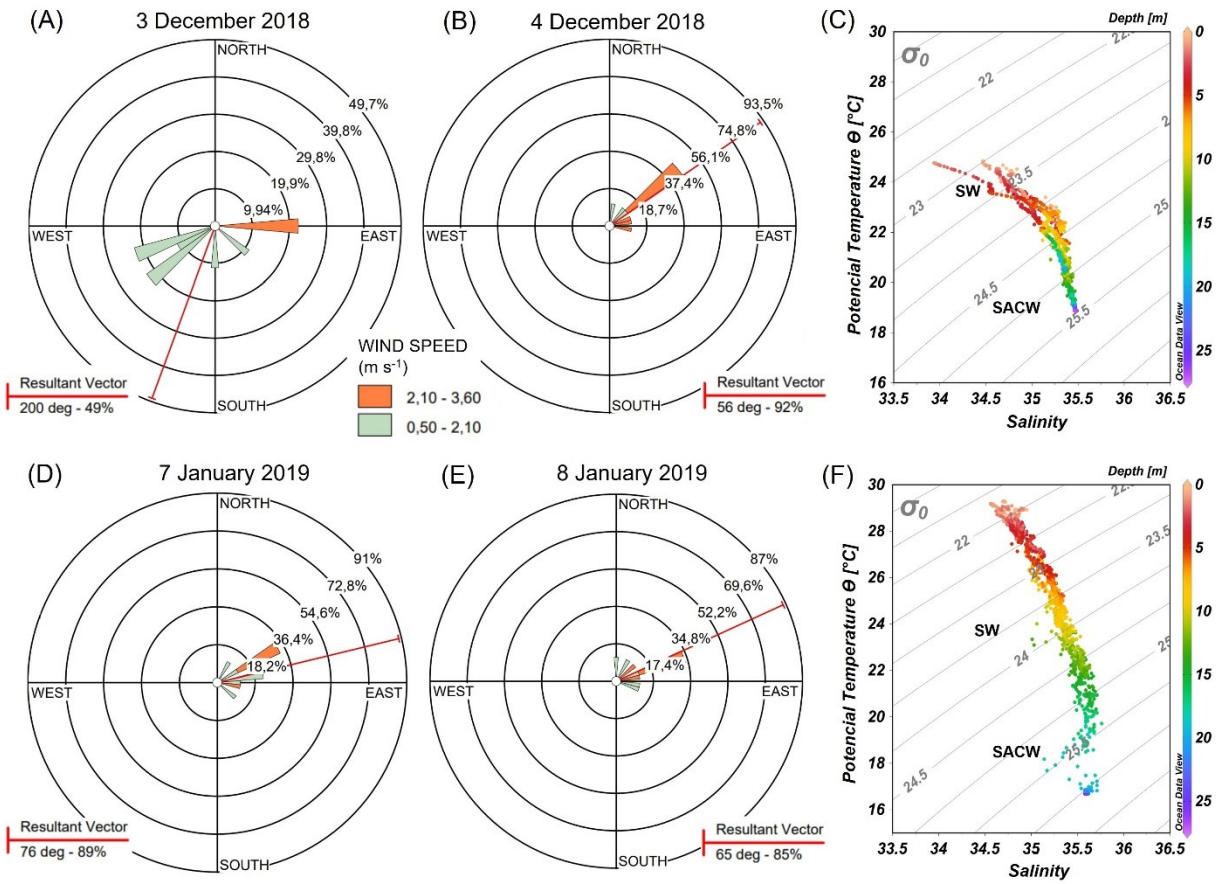

Fig. 4.2. Speeds, direction frequencies and mean direction (resultant vector) of wind (coming from) for: (A) December 3, 2018, (B) December 4, 2018, (D) January 7, 2019, and (E) January 8, 2019 (data from CFSv2/NCEP). Wind speed range is indicated on the color bar (light green: 0.50-2.10 m s^{-1}; orange: 2.10-3.60 m s^{-1}). TS-Diagram for (C) December 4, 2018, and (F) January 8, 2019, with depth in gradient color (SW-Shelf Water; SACW-South Atlantic Central Water).

Spatial distributions of environmental variables

December 4, 2018:

December is a transitional month between spring and summer in the Southern Hemisphere. The seawater temperature reached about 25°C in the surface layer, and 18.6°C at the bottom (Fig. 4.3 A1). Temperatures below 20°C were recorded below 13 m depth. The distribution of isotherms indicated greater mixing of water masses, less thermal stratification, and a less pronounced seasonal thermocline (Fig. 4.3 B1). Salinity varied between 34.4, in the most superficial layers, and 35.5 in the deepest layers.

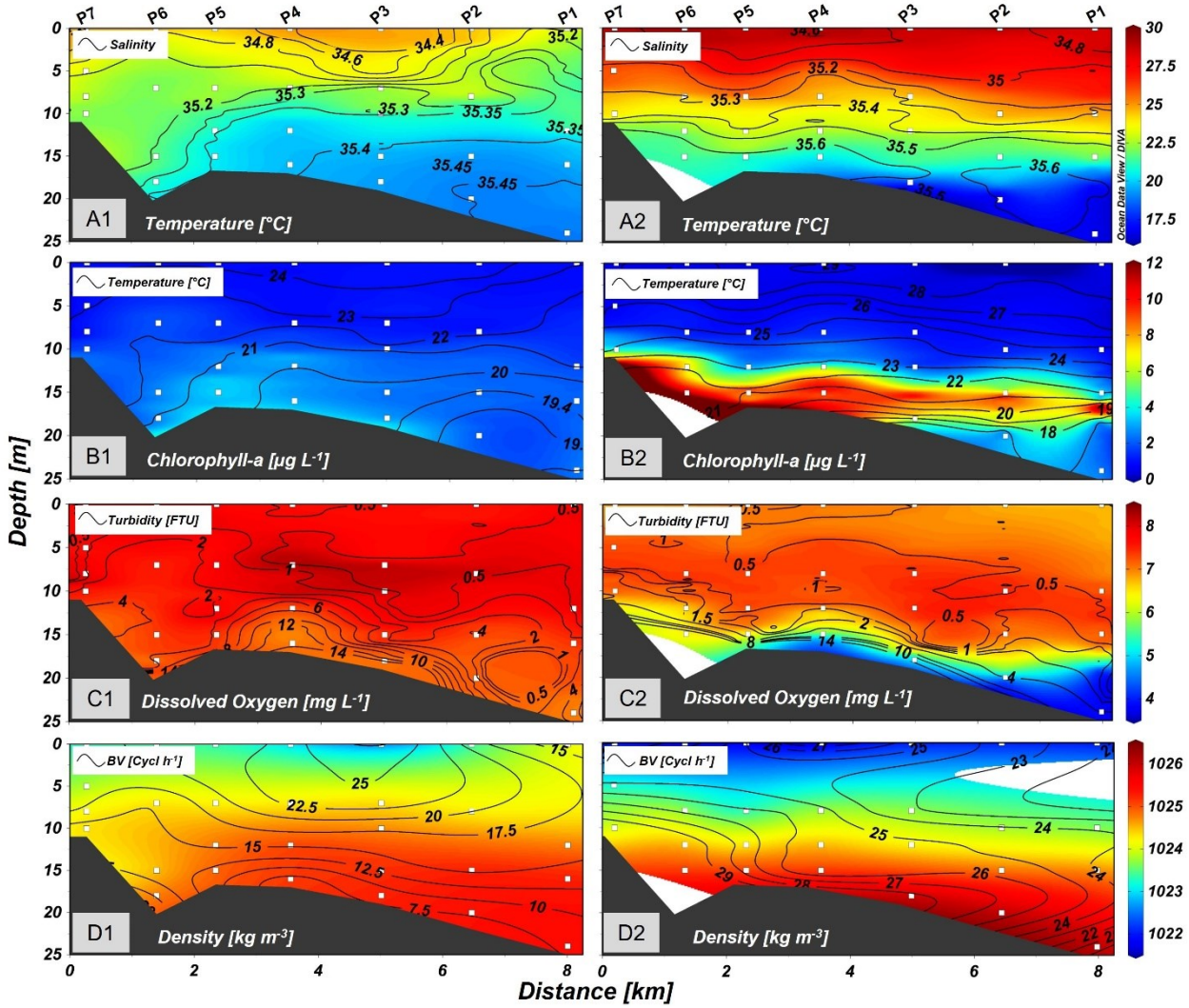

Fig. 4.3. Cross-shore distributions of environmental variables for December 4 (A1-D1) and January 8 (A2-D2): (A1-2) Temperature (°C; in gradient color) and salinity (black isolines); (B1-2) Chlorophyll-a (µg L^{-1}; in gradient color) and temperature (black isolines); (C1-2) Dissolved oxygen (mg L^{-1}; in gradient color) and turbidity (black isolines); (D1-2) Density (in gradient color) and Brunt-Väisälä frequency (cycles h^{-1}; black isolines). The white squares indicate the approximate depths of the collection bottles in each sampling station.

An increase in the concentration of Chl-a was observed between 10 and 17 m, reaching average concentrations of about 3.0 µg L^{-1} in the outermost stations (P1-P2). In the intermediate stations (P3 to P5), Chl-a reached 4.0 µg L^{-1} below 10 m depth (Fig. 4.3 B1), where an increase in the concentration of suspended particles (i.e., turbidity) was also observed (Fig. 4.3 C1). Dissolved oxygen (DO) had minimum values at the bottom (~ 7.0 mg L^{-1}) and maximum values in the surface layer, with values around 8.0 mg L^{-1} (Fig. 4.3 C1).

Lower values of N along the water column were observed on December 4, reaching higher values around 25 cycles h^{-1} near the surface, and lower values around 7.5 cycles h^{-1} in the bottom layer (Fig. 4.3 D1). For the dissolved nutrients, there was an increase in their concentrations towards the bottom. The average values for the surface (bottom) on December 4 were: 0.08 (0.17) µM for nitrite, 0.16 (1.09) µM for nitrate, 0.13 (0.30) µM for phosphate, and 3.90 (8.75) µM for silicate. The innermost stations had lower mean nutrient concentrations than the outermost stations (Table 4.1).

Table 4.1. Euphotic zone depth (Zeu, in meters), mean and standard deviation of nutrient concentration (µM), AOU (µmol kg^{-1}) and picophytoplankton biomass (µgC L^{-1}), and total abundance (cell mL^{-1}) for each collection station along the inner shelf off Ubatuba on December 4, 2018, and January 8, 2019.

	Stt	Zeu (m)	Nitrite (µM)	Nitrate (µM)	Phosphate (µM)	Silicate (µM)	AOU (µmol kg^{-1})	Pico_biomass (µgC L^{-1})	Total abundance (cell mL^{-1})
December/2018	P1	16.5	0.10 ± 0.05	0.43 ± 0.37	0.2 ± 0.03	4.05 ± 0.27	222.3 ± 6.7	12.5 ± 2.70	112,906
	P2	15.3	0.12 ± 0.06	0.72 ± 0.76	0.22 ± 0.08	7.43 ± 7.00	219.7 ± 9.6	8.23 ± 0.06	66,258
	P3	12.9	0.12 ± 0.07	0.44 ± 0.42	0.20 ± 0.10	4.03 ± 2.42	219.0 ± 7.7	17.07 ± 16.42	208,667
	P4	17.6	0.18 ± 0.16	0.80 ± 0.86	0.24 ± 0.13	4.79 ± 2.75	218.6 ± 8.6	28.08 ± 27.11	245,808
	P5	10.6	0.09 ± 0.08	0.49 ± 0.71	0.23 ± 0.10	5.39 ± 3.88	217.4 ± 5.5	42.6 ± 30.72	490,258
	P6	10.6	0.12 ± 0.01	0.51 ± 0.38	0.23 ± 0.09	5.00 ± 2.31	216.7 ± 3.8	42.43 ± 27.41	488,400
	P7	14.1	0.07 ± 0.05	0.19 ± 0.09	0.15 ± 0.04	3.75 ± 0.75	212.8 ± 3.5	17.55 ± 21.88	191,482
January/2019	P1	27.0	0.15 ± 0.15	3.21 ± 5.20	0.48 ± 0.36	5.62 ± 4.12	214.2 ± 18.7	19.76 ± 23.44	175,416
	P2	25.9	0.18 ± 0.15	3.07 ± 2.54	0.54 ± 0.20	4.14 ± 2.57	215 ± 18.5	18.80 ± 12.38	155,432
	P3	15.3	0.16 ± 0.21	1.75 ± 1.17	0.48 ± 0.34	4.61 ± 4.40	212.3 ± 17.2	24.25 ± 23.97	204,312
	P4	15.3	0.11 ± 0.09	0.56 ± 0.55	0.28 ± 0.12	4.83 ± 1.53	209 ± 12.3	20.53 ± 21.05	198,624
	P5	14.1	0.06 ± 0.07	0.24 ± 0.36	0.24 ± 0.15	3.49 ± 1.71	207.4 ± 11.6	15.96 ± 18.61	152,512
	P6	14.1	0.04 ± 0.03	0.13 ± 0.07	0.22 ± 0.09	4.13 ± 0.82	205.4 ± 11.2	15.09 ± 20.18	127,544
	P7	10.6	0.04 ± 0.03	0.15 ± 0.07	0.31 ± 0.24	4.06 ± 1.11	201.5 ± 8.1	23.37 ± 32.03	189,320

January 8, 2019:

In January, the sampling period was marked by a stable climate, with low precipitation and high temperatures. The temperature results showed a well-stratified water column, with

temperatures lower than 20°C below 18 m depth, and a maximum of 30°C in surface waters. Salinity varied between 34.5, at the surface, and 35.75, near the bottom (Fig 4.3 A1). The SCM formed around 16 m inside the seasonal thermocline at stations P1 to P3, and high values of Chl-a (10-12 µg L^{-1}) were observed at the bottom at the shallowest stations, P4 to P7 (Fig 4.3 B2). DO reached maximum values around 7.5 mg L^{-1} in the surface layer, and minimum values around 3.5 mg L^{-1} at the bottom (Fig 4.3 C2). The turbidity was higher in the bottom layer at the intermediary stations, P3 to P5 (Fig 4.3 C2).

N values were higher (above 22 cycles h^{-1}) along the water column, compared to December data, reaching maximum values around 26 cycles h^{-1} in the seasonal thermocline, in the SACW intersection zone. (Fig. 4.3 D2). In January some nutrients had higher mean concentrations at the bottom compared to the previous month, mainly nitrate. The mean nutrient concentrations for the surface (bottom) on January 8 were: 0.06 (0.23) µM for nitrite, 0.78 (3.17) µM for nitrate, 0.28 (0.57) for µM phosphate, and 3.90 (6.80) µM for silicate. The outermost stations had higher mean concentrations than the innermost stations (see Table 4.1).

Spatial distributions of biological variables

December 4, 2018:

In December, in general, the abundance of pico- and nanophytoplankton cells increased with depth (Fig. 4.4 A1-D1). Syne reached the highest mean abundance among the groups analyzed (around 48,372 cell mL^{-1}) and was higher between stations P5 and P7 (Fig. 4.4 A1). Pro abundance was higher between stations P3 and P5 (8,805 cell mL^{-1} on average) reaching maximum values near the bottom at P5 (Fig. 4.4 B1). The PicoEuk mean abundance was around 4,300 cell mL^{-1}, reaching 11,500 cell mL^{-1} between P4 and P5 (Fig. 4.4 C1). NanoEuk abundance was 700 cell mL^{-1} on average, with a slight increase in the region between 10 and 15 m, coinciding with the SCM depths. The NanoEuk maximum abundance was 1,592 cell mL^{-1} around 15 m at P3 (Fig. 4.4 D1).

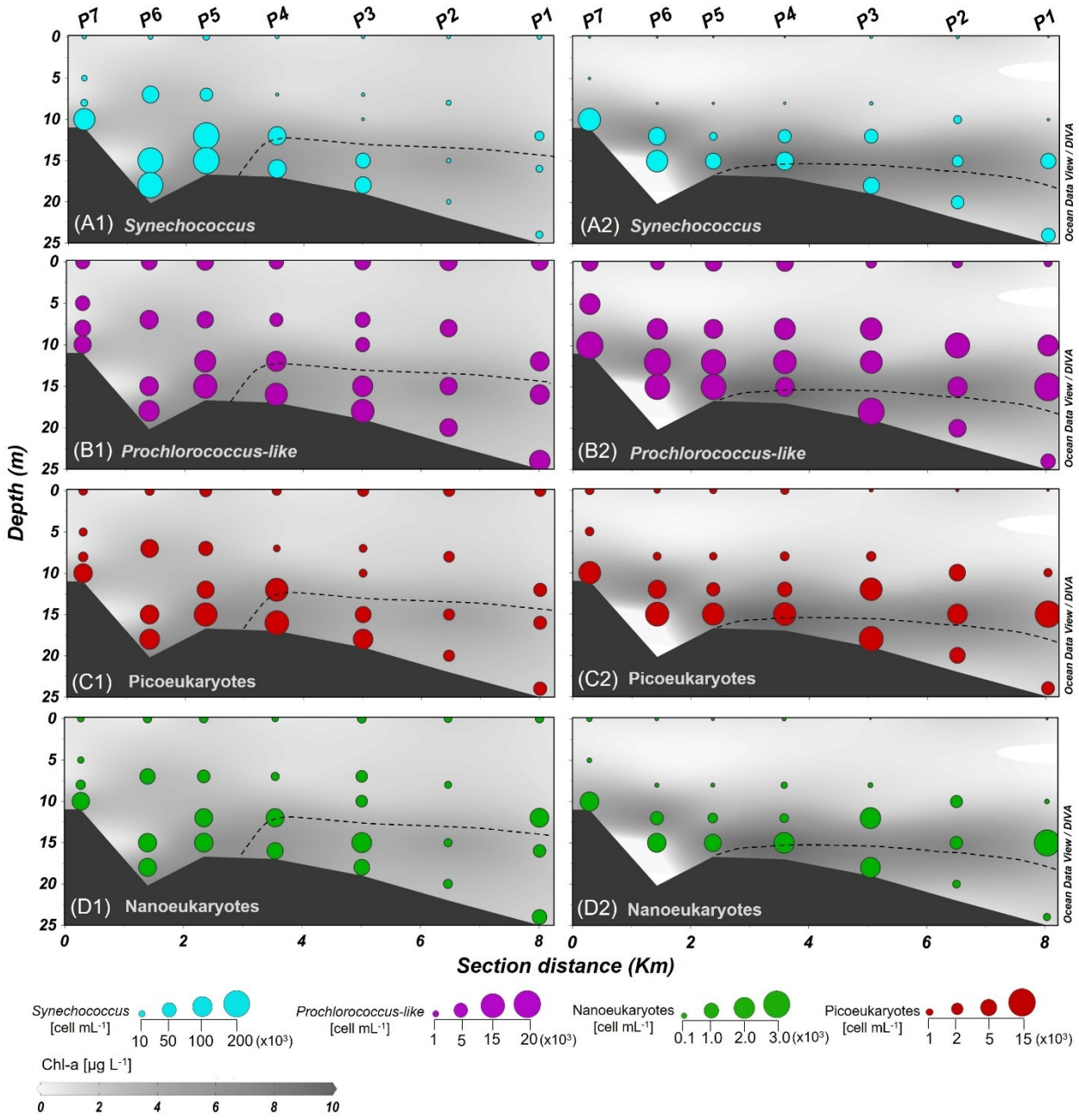

Fig. 4.4. Cross-shore distribution of biological variables for December 4, 2018 (A1-D1), and January 8, 2019 (A2-D2): (A) *Synechococcus* (cell mL^{-1}), (B) *Prochlorococcus* (cell mL^{-1}), (C) Picoeukaryotes (cell mL^{-1}), and (D) Nanoeukaryotes (cell mL^{-1}). The dashed line represents the 20°C isotherm at the interface with the SACW.

January 8, 2019:

In January, Syne was the most abundant group (30,000 cell mL^{-1}), reaching the highest values at the innermost station P7 (a maximum of 133,000 cell mL^{-1}) (Fig. 4.4 A2). Pro and PicoEuk mean abundances were 11,000 cell mL^{-1} and 4,500 cell mL^{-1}, respectively (Fig. 4.4 B2-C2). NanoEuk was the least abundant group, with a mean of 555 cell mL^{-1} (Fig. 4.4 D2). Pro, PicoEuk, and NanoEuk abundance peaks were recorded in the SCM region at the outermost station (P1). In general, the vertical distribution of pico- and nanoplankton populations was more heterogeneous on January 8, with very low values in the most superficial layers, and increased considerably in the SCM's vicinities at the outermost stations (P1 to P3), and close to the bottom at the innermost stations (P4 to P7).

The average picophytoplankton biomass was higher in January at the stations where the SCM was observed (P1 to P3), compared to the same stations in December (Table 4.1). Overall, in December, the total cell abundance and mean picophytoplankton biomass increased towards the coast, reaching maximum values at P5 and P6 stations. On the other hand, in January, the total abundance and average picophytoplankton biomass showed a downward trend from P3 to P6. The AOU decreased towards the coast, in both scenarios, but December presented higher mean values (Table 4.1). In addition, Zeu decreased towards the coast, and was higher on January 8, on average, mainly at P1-P3 (Table 4.1).

The distribution of the relative abundances along the transect carried out on December 4 indicated that Pro, PicoEuk- and NanoEuk abundances increased towards the mid/outer shelf, while the abundance of Syne increased towards the coast (Fig. 4.5 A). On January 8 the distribution was more homogeneous (Fig. 4.5 B). Pro showed the opposite trend to that observed in December, with a slight increase towards the coast, while the PicoEuk and NanoEuk populations maintained the trend observed in the previous month, decreasing towards the coast. Among the four populations analyzed, the population of Syne had the highest abundance in both scenarios (65% in January and 77% in December), followed by Pro (24% in January and 14% in December), and PicoEuk (9.7 % in January and 7% in December). NanoEuk presented the lowest relative abundances (approx.1.2% in both months).

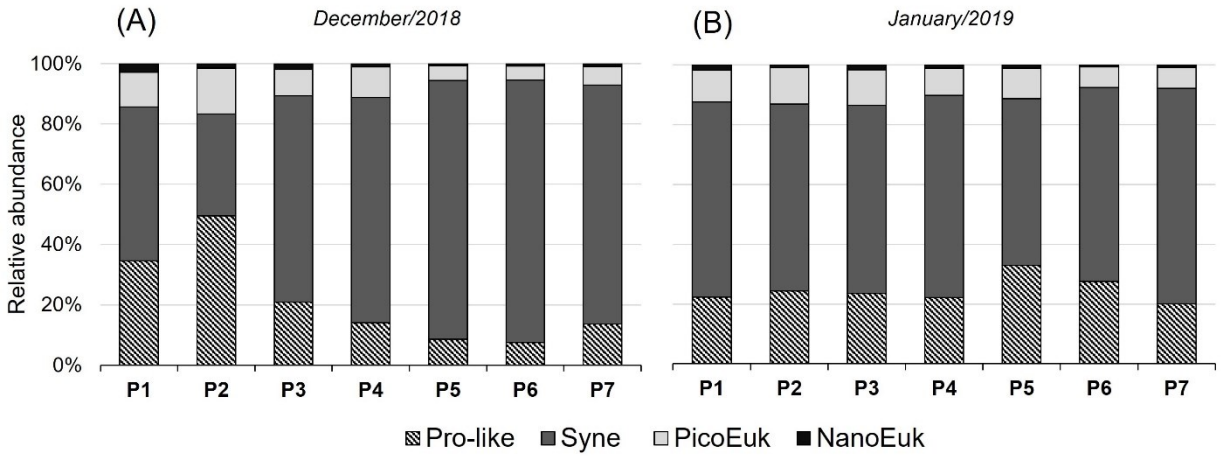

Fig. 4.5. Relative abundance (%) distribution of *Prochlorococcus* (Pro), *Synechococcus* (Syne), picoeukaryotes (PicoEuk), and nanoeukaryotes (NanoEuk) along the transect in (A) December 4, 2018, and (B) January 8, 2019.

An analysis of the vertical distributions at station P1 (the outermost) showed that picoplankton biomass peaked in the SCM's vicinities, within the seasonal thermocline in January (Fig. 4.6 A-B). The increase in Chl-a concentration along the thermocline was accompanied by a marked increase in AUO (Fig. 4.6 A). The vertical distribution of dissolved nutrients showed a decrease in the vicinity of the SCM (Fig. 4.6 C1). Vertical profiles for P1 in December indicate a slight increase in Chl-a concentration towards the bottom, without SCM formation (Fig. 4.6 A2), and a slight increase in Syne and NanoEuk populations in the vicinity of the less accentuated thermocline (Fig. 4.6 B2).

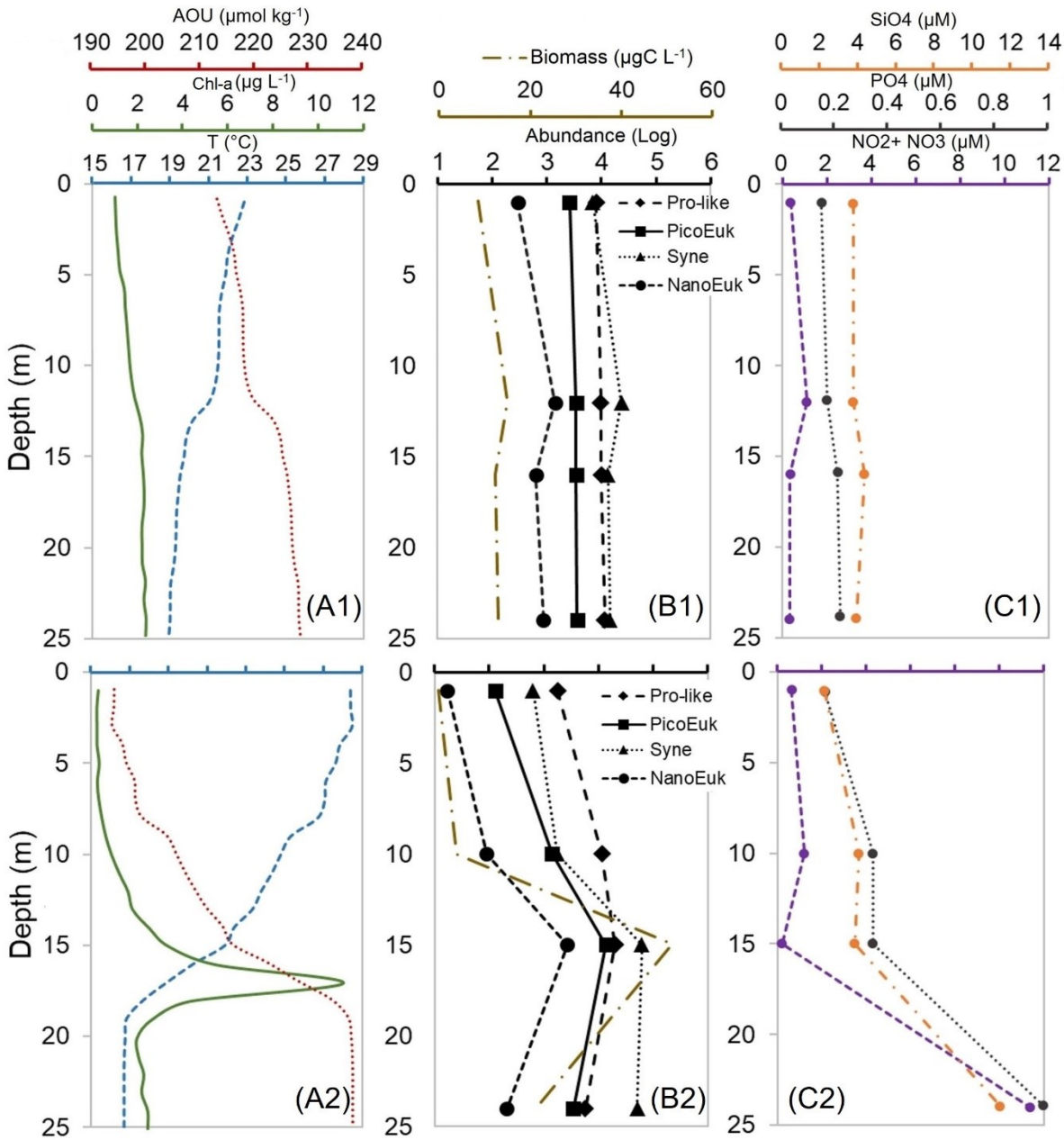

Fig. 4.6. Vertical profiles of environmental and biological variables for P1 on December 4 (A1-C1) and on January 8 (A2-C2): (A) Apparent oxygen utilization (AOU; µmol kg $^{-1}$), Chlorophyll-a (Chl-a; µg L^{-1}), and Temperature (T; °C); (B) picophytoplankton biomass (µgC L^{-1}; dash-dotted line) and Phytoplankton abundance (Log) (*Prochlorococcus* = long-dashed line with diamonds, picoeukaryotes = solid line with squares, *Synechococcus* = dotted line with triangles, and nanoeukaryotes = dashed line with points); (C) dissolved nutrients (silicate (SO4); phosphate (PO4); and nitrate (NO2) + nitrite (NO3)), in µM.

To evaluate the population's variabilities between the transect stations and depth levels, variance tests were performed between the surface, midwater, SCM, and bottom. In December there were no significant differences in the abundances between the depths or between the transect

stations. In January, there was significant variability in abundances along the water column. Syne and Pro abundances had higher medians at the bottom, but there were significant differences between surface and SCM (Fig. 4.7 A-B). PicoEuk and NanoEuk abundances showed higher medians in the SCM, with very significant variability ($p<0.001$) between surface and SCM, and significant ($p<0.05$) between midwater and SCM (Fig. 4.7 C-D).

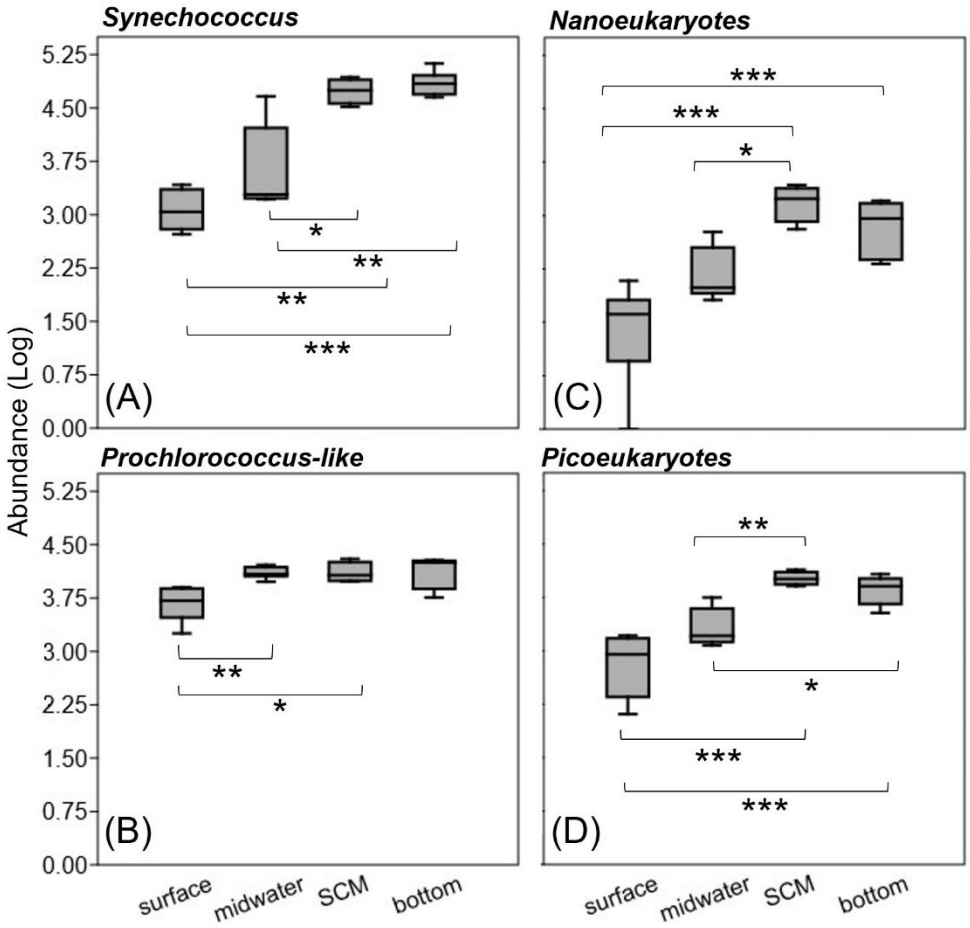

Fig. 4.7. Boxplots of abundance (Log_{10}) of (A) *Synechococcus*, (B) *Prochlorococcus*, (C) Nanoeukaryotes, and (D) Picoeukaryotes for January 8, 2019. Data are grouped according to depth layers (surface, midwater, SCM, and bottom). The p-values of pairwise comparisons between the groups are summarized with asterisks (* = $p\leq0.05$; ** = $p\leq0.01$; *** = $p\leq0.001$). The boxes display (from lower to upper limit) the first, second (median), and third quartiles; the lower whiskers extend from the first quartile to the minimum value, and the upper whiskers extend from the third quartile to the maximum value.

Multivariate analyses

Multivariate analysis was used to analyze and identify patterns and the degree of relationship between the environmental parameters in the two scenarios studied. The PCA for December 4 indicated that the first two principal components were sufficient to explain 70.16% of

the relationships between environmental and biological variables. The first component (PC1) explained 54.22% of the data variability and the second component (PC2) explained 15.94% of the variability (Fig. 4.8 A). The variables that most contributed to PC1 were phosphate, turbidity, and temperature; for PC2 were salinity, N (stratification), and density. Nutrients, turbidity, Chl-a, and AOU had a strong positive correlation with each other and a strong negative correlation with temperature; stratification was inversely correlated with salinity and density.

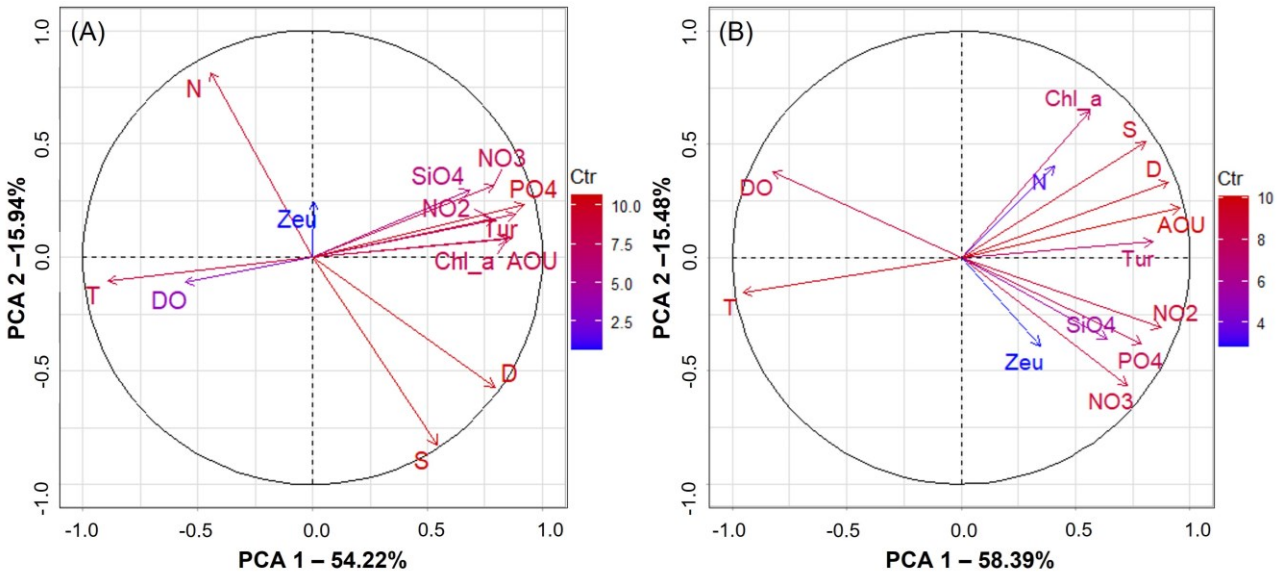

Fig. 4.8. PCA of environmental variables for December 4, 2018 (A) and January 8, 2019 (B). The color bar and the arrows' size indicate the contribution of the components (where the red color indicates the highest contribution, and the dark blue the lowest). T = temperature; D = density; S = salinity; N = Brunt-Väisälä frequency; Chl_a = chlorophyll-a; Tur = turbidity; PO4 = phosphate; NO3 = nitrate; NO2 = nitrite; SiO4 = silicate; DO = dissolved oxygen; AOU = apparent oxygen utilization; and Zeu=Euphotic zone depth.

On January 8, the PCA indicated that the first two principal components explained 73.87% of the relationships between environmental and biological variables. PC1 explained 58.39% of the data variability, while PC2 explained 15.48%. The highest contributions to PC1 were AOU, temperature, and density, while the highest contributions to PC2 were Chl-a, nitrate, and salinity. Chl-a was positively correlated with N. The AOU shows a strong negative connection with temperature and a strong positive connection with density and turbidity. Nutrients were positively correlated with each other, with nitrate having the highest positive correlation with the euphotic zone (Zeu). In addition, nutrients had weaker (negative) correlations with temperature compared

to the previous scenario. Spearman's rho matrices for each fieldwork can be viewed in APPENDIX C.

The redundancy analysis (RDA) with all samples indicated that 83% of the variation in biological parameters can be explained by the physical-chemical parameters (Fig. 4.9); RDA1 explained 78% of the variability, while RDA2 explained 5%. The influence of explanatory variables on response variables was very significant ($p<0.001$). Syne, PicoEuk and Pro populations were very connected with AUO, density, and Chl-a. All the pico- and nanoplankton populations were positively correlated with each other and negatively correlated with temperature. The distribution of samples in the RDA graph indicated the influence of depth on sampling variability; bottom samples (>15 m) had higher correlations with high concentrations of Chl-a, turbidity, nutrients, and phytoplankton abundance (Fig. 4.9).

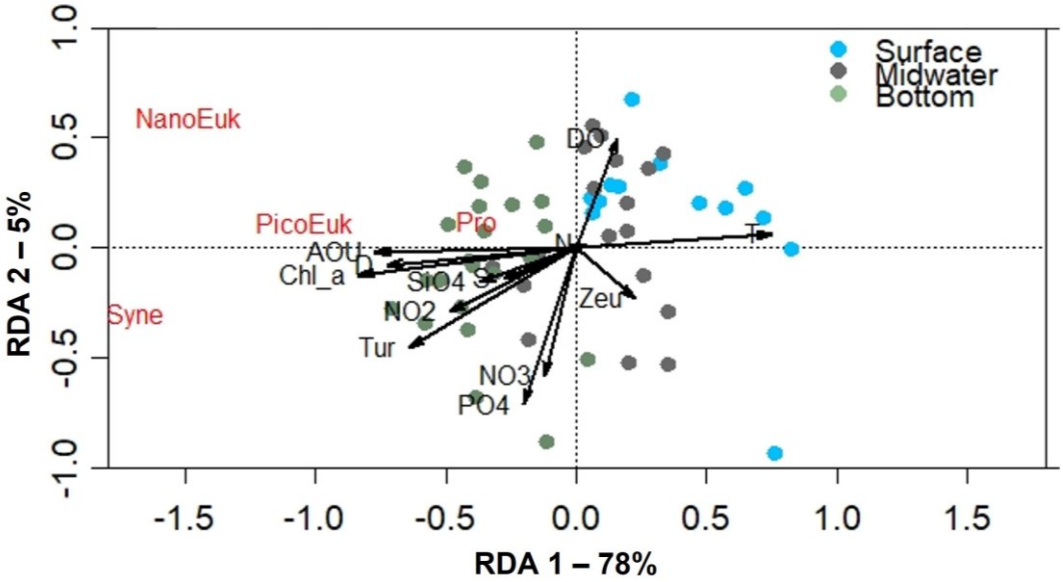

Fig. 4.9. RDA showing ecological relationships between environmental (black arrows) and biological variables (gray arrows). The blue dots represent the samples collected at the surface (0-5 m), the gray ones represent the samples collected in the midwater (5-15 m) and the green ones represent the samples collected at the bottom (> 15m). T = temperature; D = density; S = salinity; N = Brunt-Väisälä frequency; Chl_a = chlorophyll-a; Tur = turbidity; PO4 = phosphate; NO3 = nitrate; NO2 = nitrite; SiO4 = silicate; DO = dissolved oxygen; PicoEuk = Picoeukaryotes; NanoEuk = Nanoeukaryotes; Pro = Prochlorococcus; Syne = Synechococcus. AOU = Apparent oxygen utilization; and Zeu=Euphotic zone depth.

4.5.Discussion and conclusion

On the Brazilian continental shelf between 20°S and 30°S, the winds are predominantly from the E-NE (REBOITA et al., 2019) during the spring and summer months favoring the SACW upwelling via Ekman transport (CASTRO et al., 2006) and the formation of the seasonal thermocline (CASTRO FILHO; MIRANDA; MIYAO, 1987). The wind direction on December 3 indicated that there was a decrease in wind speed and a change in direction (coming from south-southwest), which probably generated instabilities in the water column and weakened the SACW intrusion towards the coast (Fig. 4.2 A).

As in shallow waters the local wind can induce rapid changes in the water column from a few hours to a few days (MAHADEVAN; TANDON; FERRARI, 2010), on December 4, although the mean wind direction is from NE, the water column showed less stratification as a result of the instabilities generated on the previous day. Changes in wind direction occur frequently in the study region (DOTTORI; CASTRO, 2009), and are associated with mixing processes and changes in the abundance and structure of phytoplankton communities (GAETA et al., 1999) and benthic macrofauna. (QUINTANA et al., 2015).

Environmental data indicated the presence of SACW near the bottom, in the December (late spring) and January (summer) campaigns. However, the temperature and density distribution, as well as the N values, corroborate the scenario of lower water column stratification and seasonal thermocline erosion on December 4. There was no formation of a prominent SCM, although there was an increase in Chl-a concentration in midwater and near the bottom (Fig. 4.3 A1-D1). On January 8, the water column showed greater stability. The onshore SACW intrusion caused a strong thermocline below 16 m and the SCM formation in the SACW intrusion region, in the seasonal thermocline. In addition to the SCMs, higher Chl-a concentrations were observed near the bottom at stations P4 to P7, probably due to the SACW intrusion and the resuspension of bottom sediments (Fig 4.3 A2-D2).

Nutrients are the controllers of the primary productivity in the study region (TEIXEIRA, 1973). The nutrient concentrations were relatively low in the more superficial layers and corroborate with values found in previous studies in the region (AIDAR et al., 1993; BRAGA; MÜLLER, 1998). In January, the increase in nutrient concentration was noted below 15 m, and the averages were higher than those observed in the previous month. The increase in nutrients, mainly

nitrate, provided by the SACW leads to the formation of SCMs at the base of the euphotic zone (BRANDINI et al., 2014; BRANDINI, 2006), and are considered nuclei of high photosynthetic production (GAETA, S. A.; BRANDINI, 2006).

SCMs are associated with thermoclines due to the accumulation of cells at neutral density depths along a vertical temperature gradient (DURHAM; STOCKER, 2012), and due to thermal stratification regulating the mixing of nutrients from deeper waters in the euphotic zone, being an important factor in determining nutricline (CULLEN, 2015; LEACH et al., 2018). Penninck et al., (2021), using an imaging system, found a great abundance of diatoms (microphytoplankton) in the SCM region, which developed in the form of a thin layer, on the inner shelf of Ubatuba. Our results indicate a great contribution of pico- and nanoplankton populations to the SCM, mainly Syne, PicoEuk, and NanoEuk. The dominance of these organisms in the Ubatuba coastal area was recorded by Frazão (2001), who indicated that picoplankton accounted for 68% of the total phytoplankton abundance, and nanoplankton corresponded to 29% of the total abundance.

Multivariate analyzes indicated different environmental conditions between the collection days. In the December scenario there were stronger negative correlations between nutrients and temperature. In January, although the correlations between nutrients and temperature were weaker, some profiles showed a decrease in nutrient concentration in the seasonal thermocline region and an increase at the bottom, suggesting a depletion in nutrients due to the greater assimilation by phytoplankton in the region of the SCM. In addition, density stratification and Chl-a concentration were more closely connected, with strong negative correlations being found between Syne, NanoEuk, and PicoEuk populations and temperature, suggesting that the thermocline presence and the strong SACW intrusion had a great positive impact on cell proliferation.

The greater availability of nitrate (> 1 μM on average) in January probably favored the primary production of phytoplankton (new production), and the increase in biomass, mainly the Syne, NanoEuk, and PicoEuk populations (Fig. 4.7). The Pro populations, although did not show a high correlation with temperature in January, were probably favored by the stability of the water column, showing greater abundance. Studies show that *Prochlorococcus* is mainly limited by the temperature and stability of the fluid (PARTENSKY; HESS; VAULOT, 1999; SCHMOKER; HERNÁNDEZ-LEÓN, 2013). Silovic et al. (2018) showed that *Prochlorococcus* cells appeared to be a much more sensitive and reactive population to changes in hydrodynamics. Rocap et al. (2003) point out that, depending on the light levels to which it adapts better, *Prochlorococcus* could use

ammonia in surface waters and nitrite in deep layers, and may have genes for assimilating nitrate and nitrite according to the availability of nitrogen in the area.

Synechococcus can also use different nitrogen sources (MOORE et al., 2002), however, it can adapt to different temperatures (MACKEY et al., 2013) and proliferate despite the water column instability. With great diversity and wide distribution, *Synechococcus* has been recorded in mesotrophic and oligotrophic regions, from polar to tropical oceans (SOHM et al., 2016; ZUBKOV et al., 2000). This may explain the higher abundances of Syne on December 4, despite the greater instability and relatively low nutrient levels. It is important to highlight that pico-nanophytoplankton populations have genotypic differences (ecotypes) that provide better adaptation to certain temperatures and nutrient conditions (SOHM et al., 2016).

Our results corroborate previous work showing that populations of Syne, PicoEuk, and NanoEuk can be favored by the influx of nutrient-rich waters, showing an increase in abundance in the SCMs in offshore and coastal waters (BERGO et al., 2017; RIBEIRO et al., 2016). Pico- and nanoeukaryotes communities have been linked to great variability in physiologies and life strategies (WORDEN; NOT, 2008). The greater abundance of PicoEuk compared to NanoEuk in the SCM region and close to the bottom may be related to the better adaptation of the picoeukaryotes to lower light intensities.

In addition to SCMs, events of water bodies intrusions in coastal areas have been linked to the formation of zooplankton aggregates (BENOIT-BIRD; SHROYER; MCMANUS, 2013; MARCOLIN; LOPES; JACKSON, 2015). Our results indicate an increase in suspended particles and AOU in the thermocline region, associated with maximum Chl-a. The high correlations found between the AOU and the phytoplankton abundance probably indicate an increase in heterotrophic activity in the seasonal thermocline. Oxygen utilization is related to the remineralization of organic matter by microbial respiration, zooplankton, and other heterotrophic marine organisms (CALLEJA; AL-OTAIBI; MORÁN, 2019). Zooplankton populations were probably favored by phytoplankton growth, being the main factor controlling the phytoplankton community through grazing (LOPES; MARCOLIN; BRANDINI, 2016).

Concluding remarks

Our results allowed us to assess the cross-shore distribution of pico- and nanophytoplankton abundance in the coastal region of Ubatuba in response to different environmental and hydrodynamic conditions. These differences were likely forced by meteorological changes since the circulation is strongly determined by the action of local winds on the inner shelf (CASTRO, 1997). The previous relaxation of the E-NE winds on December 3 probably increased the turbulence, promoting the mixing of water masses (SW and SACW) and the dissipation of the seasonal thermocline, resulting in the scenario seen on December 4. In January, prevailing winds from the E-NE favored the greater penetration of SACW in the inner shelf, the increase of stratification, and the formation of the SCM, as observed on January 8.

The planktonic system on the inner shelf of Ubatuba is influenced by meso- and sub-mesoscale processes (wind dynamics), inducing changes in coastal upwelling dynamics and forcing vertical mixing, at spatial scales of a few kilometers and temporal scales from a few hours to days. Pico- and nanophytoplankton abundance were likely affected by vertical mixing and lower nutrient concentrations in December, except for *Synechococcus* populations, which have shown to thrive despite the physical conditions. The greater stability and availability of nutrients favored populations in January, with an increase in biomass in the SCM region, inside the seasonal thermocline formed by the intrusion of the SACW.

Thus, given the scenarios studied, we conclude that the vertical and spatial distribution of pico-nanoplankton populations in the coastal region of Ubatuba is likely controlled by sub-mesoscale physical processes, associated with wind dynamics, which drive the water column stratification and the increase in nutrient concentrations through the SACW intrusion. Future research with greater detail on the pico-nanoplankton ecotypes and their seasonal distribution would help to improve our understanding of the ecological forces and environmental preferences of each population in the study area. The understanding of the abundance and distribution of planktonic, autotrophic, and heterotrophic organisms, and their interaction with the physical-chemical conditions in coastal areas, can assist in the exploitation of fisheries resources sustainably, as well as serve as a database for future monitoring to assess changes in the planktonic community.

5. General conclusion

Understanding the phytoplankton distribution in the ocean represents a long-standing challenge in oceanography, due to the complex interactions between biotic and abiotic processes at multiple scales (BARTON et al., 2010). In the coastal zone of Ubatuba, there is an interaction between meso- and submesoscale processes that influence the water column stability and the structure of the planktonic communities throughout the year. The SACW upwelling is forced by the Ekman transport (mesoscale geostrophic flow) and its lateral advection onto the shelf influences physical and biological processes at smaller scales (CALIL et al., 2021). The entire region of the Southern Brazilian shelf has its circulation controlled by the same meteorological conditions on a synoptic scale (CASTRO FILHO; MIRANDA; MIYAO, 1987) and the passage of low-pressure frontal systems is a recurrent mesoscale phenomenon that can induce submesoscale instabilities, such as fronts and mixing processes (DOTTORI; CASTRO, 2018; WHITT; TAYLOR; LÉVY, 2017).

The works presented in this thesis had an observational and descriptive character with the objective of evaluating the spatiotemporal plankton distribution in different environmental conditions on the inner shelf off Ubatuba, considering high vertical and spatial resolutions. The research efforts in this work relied on field observation techniques at fixed and spatial stations, continuous profiling using high-resolution optical and acoustic sensors, and discrete sample collection for analysis in laboratory techniques. The abundance of the main groups of the micro- and mesoplankton above 100 µm was estimated by an *in situ* shadowgraphic imaging system (In Chapters II and III), and the autotrophic microorganisms of the picoplankton (0.2-2.0 µm) and nanoplankton (2-20 µm) were quantified by flow cytometry (Chapter IV).

Aiming to investigate the occurrence of plankton aggregations on a fine scale (from centimeters to a few meters) and the physical processes involved in their formation and dissipation, the work presented in Chapter II evaluated the temporal evolution of thin phytoplankton layers over two days. The thin layers observed were associated with mesoscale and submesoscale flows, related to Ekman transport and the lateral advection of water bodies in the coastal zone. Physical mechanisms of stratification and current shear were attributed to the formation of the thin layers, in addition to biological mechanisms, such as *in situ* growth and mobility of dinoflagellates. The dissipation of the thin layers was associated with changes in the regional wind patterns that affected

the presence of SACW, leading to changes in the water column stability. The impact of the thin layers at higher trophic levels was indicated by the greater presence of crustaceans in their surroundings.

The work presented in Chapter III aimed to investigate the spatial and short-term variation in the plankton abundance distribution. The spatial distribution investigation was conducted along the inner shelf between stations roughly at 1.5 km intervals. The temporal variability observed in phytoplankton abundance (significant increase in diatoms) over a 24-h period in July/2018 was probably caused by the intensification of mixing processes. In January/2019, the SACW intrusion intensification and the increase in stratification were the main factors that led to variations in the vertical plankton distribution over a 12-h period. Spatially, the results for winter/2018 suggest that submesoscale instabilities induced by a frontal system passing probably led to a significant increase in plankton abundance at the outermost stations of the inner shelf; in summer, the increase in stratification and nutrient concentration promoted by the SACW led to a local increase in phytoplankton abundance and diversity.

In chapter IV, the study aimed to evaluate the influence of the wind-driven environmental conditions on the abundances of *Synechococcus*, *Prochlorococcus*, pico- and nanoeukaryotes, along the inner shelf (stations at ~1.5 km intervals), in December/2018 and January/2019. The results suggest that variations in wind patterns in December led to intensified vertical mixing, seasonal thermocline erosion, and lower nutrient concentrations, leading to lower abundances of *Prochlorococcus*, picoeukaryotes, and nanoeukaryotes. In January, the greater stratification and availability of nutrients caused by the strong SACW intrusion favored the microbial populations, leading to variability in the abundances along the water column, with a significant increase in the pico- and nanoeukaryote abundances in the SCM.

It is concluded that the present thesis has achieved the general objectives, bringing new insights into the influence of physical processes on the high-resolution spatiotemporal distribution of plankton in a subtropical coastal ecosystem on the southern Brazilian shelf. The general results showed evidence that the wind is the main driver of the variability in the abundance and vertical distribution of plankton in the inner shelf off Ubatuba, driving submesoscale phenomena related to the SACW onshore intrusion or offshore retraction, and vertical mixing processes associated with unsteady winds.

Submesoscale processes have been shown to be fundamental in the transport of properties, generation of spatial heterogeneities, and transfer of energy from meso- to small scales (GULA et al., 2022; LÉVY; FRANKS; SMITH, 2018), being, however, particularly difficult to observe in the field or through models, due to their smaller time and spatial scales (hours to days, 0.1–10 km) (THOMAS; TANDON; MAHADEVAN, 2008). As the intensification of cold frontal systems and changes in stratification, circulation, and coastal upwellings are some of the predicted impacts of climate change on the oceans (ANDRADE et al., 2012; COOLEY et al., 2022; FOX-KEMPER et al., 2021), greater research efforts in the search for solutions and parameterization of movements on smaller scales are increasingly relevant in studies on the structure of marine planktonic communities.

6. References

AIDAR, E. et al. Ecossistema costeiro subtropical: nutrientes dissolvidos, fitoplâncton e clorofllla-a e suas relações com as condições oceanográficas na região de Ubatuba, SP. **Publicação Especial do Instituto Oceanográfico**, v. 10, p. 9–43, 1993.

ALLDREDGE, A. L. et al. Occurrence and mechanisms of formation of a dramatic thin layer of marine snow in a shallow Pacific fjord. **Marine Ecology Progress Series**, v. 233, p. 1–12, 2002.

ALVES, M. A. **Correntes subinerciais na Plataforma Continental interna entre Peruíbe e São Sebastião: observações.** [s.l.] University of São Paulo, 1992.

ANDRADE, K. M. et al. Avaliação de mudanças na frequência de sistemas frontais sobre o sul da América do Sul em projeções do clima futuro. v. 37, n. 1, p. 15–26, 2012.

BAEK, S. H. et al. Growth of dinoflagellates, Ceratium furca and Ceratium fusus in Sagami Bay, Japan: The role of vertical migration and cell division. **Harmful Algae**, v. 8, n. 6, p. 843–856, 2009.

BARNETT, M. L. et al. Shelf sea subsurface chlorophyll maximum thin layers have a distinct phytoplankton community structure. **Continental Shelf Research**, v. 174, p. 140–157, 2019.

BARTON, A. D. et al. Patterns of Diversity in Marine Marine Phytoplankton. **Marine Phytoplankton**, v. 327, p. 1509–1511, 2010.

BASEDOW, S. L. et al. Remote sensing of zooplankton swarms. **Scientific Reports**, v. 9, n. 1, p. 1–10, 2019.

BASTERRETXEA, G.; FONT-MUÑOZ, J. S.; TUVAL, I. Phytoplankton Orientation in a Turbulent Ocean: A Microscale Perspective. **Frontiers in Marine Science**, v. 7, p. 185, 2020.

BATISTA, S. S.; HARARI, J. Modelagem da dispersão de coliformes termotolerantes e enterococos em duas enseadas na região costeira de Ubatuba (SP), Brasil. **Engenharia Sanitaria e Ambiental**, v. 22, n. 2, p. 403–414, 2017.

BENEDETTI, F. et al. Major restructuring of marine plankton assemblages under global warming. **Nature Communications 2021 12:1**, v. 12, n. 1, p. 1–15, 2021.

BENOIT-BIRD, K. J. et al. Integrated measurements of acoustical and optical thin layers I: Vertical scales of association. **Continental Shelf Research**, v. 30, n. 1, p. 17–28, 2010.

BENOIT-BIRD, K. J.; COWLES, T. J.; WINGARD, C. E. Edge gradients provide evidence of ecological interactions in planktonic thin layers. **Limnology and Oceanography**, v. 54, n. 4, p. 1382–1392, 2009.

BENOIT-BIRD, K. J.; SHROYER, E. L.; MCMANUS, M. A. A critical scale in plankton aggregations across coastal ecosystems. **Geophysical Research Letters**, v. 40, n. 15, p. 3968–3974, 2013.

BERGO, N. M. et al. The Partitioning of Carbon Biomass among the Pico- and Nano-plankton Community in the South Brazilian Bight during a Strong Summer Intrusion of South Atlantic Central Water. **Frontiers in Marine Science**, v. 4, p. 1–12, 2017.

BOCHDANSKY, A. B. et al. Effect of the heterotrophic dinoflagellate Oxyrrhis marina and the copepod Acartia tonsa on vertical carbon flux in and around thin layers of the phytoflagellate Isochrysis galbana. **Marine Ecology Progress Series**, v. 402, p. 179–196, 2010.

BORCARD, D.; GILLET, F.; LEGENDRE, P. **Numerical ecology with R**. 2. ed. New York: [s.n.].

BRAGA, E. D. S.; MÜLLER, T. J. Observation of regeneration of nitrate, phosphate and silicate during upwelling off Ubatuba, Brazil, 23°S. **Continental Shelf Research**, v. 18, n. 8, p. 915–922, 1998.

BRANDINI, F. et al. Deep chlorophyll maximum and plankton community response to oceanic bottom intrusions on the continental shelf in the South Brazilian Bight. **Continental Shelf Research**, v. 89, p. 61–75, 2014.

BRANDINI, F. P. Hidrografia e Produçao Biológica na regiao Sudeste-Sul do Brasil no contexto do Programa REVIZEE. In: EDUSP (Ed.). . **O ambiente oceanográfico da plataforma continental e do talude na região sudeste-sul do Brasil**. São Paulo, SP: [s.n.]. p. 447–460.

BUITENHUIS, E. T. et al. Earth System Science Data Picophytoplankton biomass distribution in the global ocean. **Earth Syst. Sci. Data**, v. 4, p. 37–46, 2012.

CALIL, P. H. R. et al. Filaments, fronts and eddies in the cabo frio coastal upwelling system, Brazil. **Fluids**, v. 6, n. 2, p. 54, 2021.

CALLEJA, M. L.; AL-OTAIBI, N.; MORÁN, X. A. G. Dissolved organic carbon contribution to oxygen respiration in the central Red Sea. **Scientific Reports 2019 9:1**, v. 9, n. 1, p. 1–12, 18 mar. 2019.

CARVALHO, M.; GIANESELLA, S. M. F.; SALDANHA-CORRÊA, F. M. P. Trichodesmium Erythraeum bloom on the continental shelf off Santos, Southeast Brazil. **Brazilian Journal of Oceanography**, v. 56, n. 4, p. 307–311, 2008.

CASTRO, B. M. **Correntes e massas de água da plataforma continental norte de São Paulo**. São Paulo: Universidade de São Paulo, 1997.

CASTRO, B. M. et al. Estrutura termohalina e circulação na região entre o Cabo de São Tomé (RJ) e o Chuí (RS). In: EDUSP (Ed.). . **O Ambiente Oceanográfico da Plataforma Continental e do Talude na Região Sudeste-Sul do Brasil**. [s.l: s.n.]. p. 11–120.

CASTRO, B. M.; MIRANDA, L. B. Physical oceanography of the western Atlantic continental shelf located between 4 N and 34 S. **The sea**, v. 11, n. 1, p. 209–251, 1998.

CASTRO, B. M. DE. **Subtidal response to wind forcing in the South Brazil Bight during winter**. Miami: University of Miami, USA, 1985.

CASTRO FILHO, B. M. DE; MIRANDA, L. B. DE; MIYAO, S. Y. Condições hidrográficas na plataforma continental ao largo de Ubatuba: variações sazonais e em média escala. **Boletim do Instituto Oceanográfico**, v. 35, n. 2, p. 135–151, 1987.

CERDA, C.; CASTRO, B. M. Hydrographic climatology of South Brazil Bight shelf waters between Sao Sebastiao (24°S) and Cabo Sao Tome (22°S). **Continental Shelf Research**, v. 89, p. 5–14, 2014.

CHASSOT, E. et al. Global marine primary production constrains fisheries catches. **Ecology Letters**, v. 13, n. 4, p. 495–505, 2010.

CHEN, Y. L. L. et al. Seasonal dynamics of new production from Trichodesmium N2 fixation and nitrate uptake in the upstream Kuroshio and South China Sea basin. **Limnology and Oceanography**, v. 53, n. 5, p. 1705–1721, 2008.

CHERITON, O. M. et al. Effects of mesoscale physical processes on thin zooplankton layers at four sites along the west coast of the U.S. **Estuaries and Coasts**, v. 30, n. 4, p. 575–590, 2007.

COMFORT, C. M. et al. Observations of the Hawaiian Mesopelagic Boundary Community in Daytime and Nighttime Habitats Using Estimated Backscatter. **AIMS Geosciences**, v. 3, n. 3, p. 304–326, 2017.

COOLEY, S. et al. Chapter 3: Oceans and Coastal Ecosystems and their Services | EPIC. In: **Climate Change 2022: Impacts, adaptation and vulnerability. Contribution of the WGII to the 6th assessment report of the intergovernmental panel on climate change, IPCC AR6 WGII**. [s.l.] Cambridge University Press, 2022. p. 1–236.

CORREDOR-ACOSTA, A. et al. The Influence of Diapycnal Nutrient Fluxes on Phytoplankton Size Distribution in an Area of Intense Mesoscale and Submesoscale Activity off Concepción, Chile. **Journal of Geophysical Research: Oceans**, v. 125, n. 5, 2020.

CORZO, A. et al. Synechococcus and Prochlorococcus populations detected by flow cytometry in a eutrophic reservoir in summer. **Journal of Plankton Research**, v. 21, n. 8, p. 1575–1581, 1999.

COWLES, T. J.; DESIDERIO, R. A.; CARR, M. E. Small-scale planktonic structure: Persistence and trophic consequences. **Oceanography**, v. 11, n. 1, p. 4–9, 1998.

CSANADY, G. T. Wind effects on surface to bottom fronts. **Journal of Geophysical Research**, v. 83, n. C9, p. 4633, 20 set. 1978.

CULLEN, J. J. Subsurface Chlorophyll Maximum Layers: Enduring Enigma or Mystery Solved? **Annual Review of Marine Science**, v. 7, n. 1, p. 207–239, 2015.

DAVIS, R. E.; BOGDEN, P. S. Variability on the California shelf forced by local and remote winds during the Coastal Ocean Dynamics Experiment. **Journal of Geophysical Research: Oceans**, v. 94, n. C4, p. 4763–4783, 15 abr. 1989.

DE VERNEIL, A.; FRANKS, P. J. S.; OHMAN, M. D. Frontogenesis and the Creation of Fine-Scale Vertical Phytoplankton Structure. **Journal of Geophysical Research: Oceans**, v. 124, n. 3, p. 1509–1523, 2019.

DEINES, K. L. Backscatter estimation using broadband acoustic Doppler current profilers. **Proceedings of the IEEE Working Conference on Current Measurement**, p. 249–253, 1999.

DEKSHENIEKS, M. M. et al. Temporal and spatial occurrence of thin phytoplankton layers in relation to physical processes. **Marine Ecology Progress Series**, v. 223, p. 61–71, 2001.

DETONI, A. M. S. et al. Trichodesmium latitudinal distribution on the shelf break in the southwestern Atlantic Ocean during spring and autumn. **Global Biogeochemical Cycles**, v. 30, n. 11, p. 1738–1753, 2016.

DONAGHAY, P. L.; RINES, H. M.; SIEBURTH, J. M. Simultaneous sampling of fine scale biological, chemical, and physical structure in stratified waters. **Arch. Hydrobiol. Beih. Ergebn. Limnol.**, v. 36, p. 97–108, 1992.

DOTTORI, M.; CASTRO, B. M. The response of the Sao Paulo continental shelf, Brazil, to synoptic winds. **Ocean Dynamics**, v. 59, n. 4, p. 603–614, 2009.

DOTTORI, M.; CASTRO, B. M. The role of remote wind forcing in the subinertial current variability in the central and northern parts of the South Brazil Bight. **Ocean Dynamics**, v. 68, n. 6, p. 677–688, 2018.

DURHAM, W. M.; STOCKER, R. Thin Phytoplankton Layers: Characteristics, Mechanisms, and Consequences. **Annual Review of Marine Science**, v. 4, n. 1, p. 177–207, 2012.

ECKART, C. An analysis of the stirring and mixing processes in incompressible fluids. **J. Mar. Res.**, v. 7, p. 265–75, 1948.

EHRNSTEN, E. et al. Benthic-pelagic coupling in coastal seas – Modelling macrofaunal biomass and carbon processing in response to organic matter supply. **Journal of Marine Systems**, v. 196, p. 36–47, 2019.

FENSOME, R. A. A classification of living and fossil dinoflagellates. **Micropaleontology,special publication**, v. 7, p. 1–351, 1993.

FERNÁNDEZ, A. et al. Latitudinal distribution of Trichodesmium spp. and N2 fixation in the Atlantic Ocean. **Biogeosciences**, v. 7, n. 10, p. 3167–3176, 2010.

FERREIRA, J. C. N. et al. Abundance and microbial diversity from surface to deep water layers over the Rio Grande Rise, South Atlantic. **Progress in Oceanography**, v. 201, p. 102736, 2022.

FOX-KEMPER, B. et al. Chapter 9: Ocean, Cryosphere and Sea Level Change. In: **Climate Change 2021: The Physical Science Basis. Contribution of Working Group I to the Sixth Assessment Report of the Intergovernmental Panel on Climate Change**. [s.l.] Cambridge University Press, 2021.

FRANKS, P. J. S.; WALSTAD, L. J. Phytoplankton patches at fronts: A model of formation and response to wind events. **Journal of Marine Research**, v. 55, n. 1, p. 1–29, 1997.

FRAZÃO, L. R. **Eutrofização por esgotos domésticos e sua relação com a ecologia e fisiologia do fitoplâncton marinho no litoral do Estado de São Paulo: Ubatuba, Praia Grande e Santos.** [s.l.] University of São Paulo, 2001.

FRAZÃO, L. R. et al. Microbial ecology of the South Atlantic Subtropical Gyre: a state-of-the-art review of an understudied ocean region. **Ocean and Coastal Research**, v. 69, p. 1–22, 2021.

FU, F. X.; BELL, P. R. F. Effect of salinity on growth, pigmentation, N2 fixation and alkaline phosphatase activity of cultured Trichodesmium sp. **Marine Ecology Progress Series**, v. 257, n. August, p. 69–76, 2003.

GAETA, S. A.; BRANDINI, F. P. Gaeta, S. A., & Brandini, F. P. (2006). Produção primária do fitoplâncton na região entre o Cabo de São Tomé (RJ) e o Chuí (RS). In: EDUSP (Ed.). . **O ambiente oceanográfico da plataforma continental e do talude na região sudeste-sul do Brasil**.

São Paulo, SP: [s.n.]. p. 219–264.

GAETA, S. A. et al. Size-fractionation of primary production and phytoplankton biomass on inshore waters of the Ubatuba region. **Publ. Esp. Inst. Oceanogr**, v. 11, p. 153–162, 1995.

GAETA, S. A. et al. Environmental forcing on phytoplankton biomass and primary productivity of the coastal ecosystem in Ubatuba region, southern Brazil. **Revista Brasileira de Oceanografia**, v. 47, n. 1, p. 11–27, 1999.

GREER, A. T. et al. Relationships between phytoplankton thin layers and the fine-scale vertical distributions of two trophic levels of zooplankton. **Journal of Plankton Research**, v. 35, n. 5, p. 939–956, 2013.

GUERRA, D. et al. Zooplankton diel vertical migration in the Corsica Channel (north-western Mediterranean Sea) detected by a moored acoustic Doppler current profiler. **Ocean Science**, v. 15, n. 3, p. 631–649, 2019.

GUIRY, M. D.; GUIRY, G. M. **AlgaeBase: World-wide electronic publication**. Galway: National University of Ireland, 2021.

GULA, J. et al. Submesoscale processes and mixing. **Ocean Mixing**, p. 181–214, 2022.

HAAS, S. et al. Physical mixing in coastal waters controls and decouples nitrification via biomass dilution. **Proceedings of the National Academy of Sciences**, v. 118, n. 18, p. e2004877118, 2021.

HARARI, J.; MESQUITA, A. R. Tábuas das marés de Ubatuba, Santos e Cananéia para os anos de 2004 e 2005. **Relatório Técnico do Instituto Oceanográfico**, n. 51, p. 1–28, 2003.

HERNÁNDEZ-HERNÁNDEZ, N. et al. Short-Term Spatiotemporal Variability in Picoplankton Induced by a Submesoscale Front South of Gran Canaria (Canary Islands). **Frontiers in Marine Science**, v. 8, p. 243, 2021.

HOECKER-MARTÍNEZ, M. S.; SMYTH, W. D. Trapping of gyrotactic organisms in an unstable shear layer. **Continental Shelf Research**, v. 36, p. 8–18, 15 mar. 2012.

HOLLIDAY, D. V.; GREENLAW, C. F.; DONAGHAY, P. L. Acoustic scattering in the coastal

ocean at Monterey Bay, CA, USA: Fine-scale vertical structures. **Continental Shelf Research**, v. 30, n. 1, p. 81–103, 2010.

HOSEGOOD, P. J. et al. Nutrient pumping by submesoscale circulations in the mauritanian upwelling system. **Progress in Oceanography**, v. 159, p. 223–236, 2017.

HUNT, B. P. V.; HOSIE, G. W. Zonal structure of zooplankton communities in the Southern Ocean South of Australia: Results from a 2150 km continuous plankton recorder transect. **Deep-Sea Research Part I: Oceanographic Research Papers**, v. 52, n. 7, p. 1241–1271, 2005.

ITSWEIRE, E. C.; OSBORN, T. R.; STANTON, T. P. **Horizontal Distribution and Characteristics of Shear Layers in the Seasonal ThermoclineJournal of Physical Oceanography**, 1989.

JOHNSON, K. S.; RISER, S. C.; KARL, D. M. Nitrate supply from deep to near-surface waters of the North Pacific subtropical gyre. **Nature**, v. 465, n. 7301, p. 1062–1065, 2010.

KASAI, A. et al. Salt-wedge intrusion of seawater and its implication for phytoplankton dynamics in the Yura Estuary, Japan. **Estuarine, Coastal and Shelf Science**, v. 86, n. 3, p. 408–414, 10 fev. 2010.

LEACH, T. H. et al. Patterns and drivers of deep chlorophyll maxima structure in 100 lakes: The relative importance of light and thermal stratification. **Limnology and Oceanography**, v. 63, n. 2, p. 628–646, 2018.

LEE, Y. et al. Physical-biological coupling in the Amundsen Sea, Antarctica: Influence of physical factors on phytoplankton community structure and biomass. **Deep-Sea Research Part I: Oceanographic Research Papers**, v. 117, p. 51–60, 2016.

LÉVY, M.; FRANKS, P. J. S.; SMITH, K. S. The role of submesoscale currents in structuring marine ecosystems. **Nature Communications**, v. 9, n. 1, p. 1–16, 2018.

LI, M.; GARGETT, A.; DENMAN, K. What determines seasonal and interannual variability of phytoplankton and zooplankton in strongly estuarine systems? Application to the semi-enclosed estuary of Strait of Georgia and Juan de Fuca Strait. **Estuarine, Coastal and Shelf Science**, v. 50,

n. 4, p. 467–488, 2000.

LONGHURST, A. R.; HARRISON, W. G. The biological pump : Profiles of plankton production and consumption in the upper ocean. **Progress in Oceanography**, v. 22, p. 47–123, 1989.

LOPES, R. M. et al. Zooplankton and ichthyoplankton distribution on the southern Brazilian shelf: An overview. **Scientia Marina**, v. 70, n. 2, p. 189–202, 2006.

LOPES, R. M. Marine zooplankton studies in Brazil - A brief evaluation and perspectives. **Anais da Academia Brasileira de Ciencias**, v. 79, n. 3, p. 369–379, 2007.

LOPES, R. M.; BRANDINI, F. P.; GAETA, S. A. Distribution patterns of epipelagic copepods off Rio de Janeiro (SE Brazil) in summer 1991/1992 and winter 1992. **Hydrobiologia**, v. 411, n. 0, p. 161–174, 1999.

LOPES, R. M.; MARCOLIN, C. R.; BRANDINI, F. P. Influence of oceanic fronts on mesozooplankton abundance and grazing during spring in the south-western Atlantic. **Marine and Freshwater Research**, v. 67, n. 5, p. 626–635, 2016.

LUHTALA, H.; TOLVANEN, H. Optimizing the Use of Secchi Depth as a Proxy for Euphotic Depth in Coastal Waters: An Empirical Study from the Baltic Sea. **ISPRS International Journal of Geo-Information 2013, Vol. 2, Pages 1153-1168**, v. 2, n. 4, p. 1153–1168, 2013.

MACÍAS, D. et al. Turbulence as a driver for vertical plankton distribution in the subsurface upper ocean. **Scientia Marina**, v. 77, n. 4, p. 541–549, 2013.

MACKEY, K. R. M. et al. Effect of temperature on photosynthesis and growth in marine Synechococcus spp. **Plant Physiology**, v. 163, n. 2, p. 815–829, 2013.

MAHADEVAN, A. The Impact of Submesoscale Physics on Primary Productivity of Plankton. **Annual Review of Marine Science**, v. 8, n. September 2015, p. 161–184, 2016.

MAHADEVAN, A.; TANDON, A.; FERRARI, R. Rapid changes in mixed layer stratification driven by submesoscale instabilities and winds. **Journal of Geophysical Research: Oceans**, v. 115, n. C3, p. 1–12, 2010.

MAHIQUES, M. M. DE. Dinâmica sedimentar atual nas enseadas da região de Ubatuba, Estado de São Paulo. **Boletim do Instituto Oceanográfico**, v. 43, n. 2, p. 111–122, 1995.

MANN, K. H.; LAZIER, J. R. N. Biological-Physical Interactions in the Oceans. In: **Dynamics of Marine Ecosystems**. third edit ed. Cambridge, Massachusetts: Blackwell Science, 2006.

MARCOLIN, C. R.; GAETA, S.; LOPES, R. M. Seasonal and interannual variability of zooplankton vertical distribution and biomass size spectra off Ubatuba, Brazil. **Journal of Plankton Research**, v. 37, n. 4, p. 808–819, 2015.

MARCOLIN, C. R.; LOPES, R. M.; JACKSON, G. A. Estimating zooplankton vertical distribution from combined LOPC and ZooScan observations on the Brazilian Coast. **Marine Biology**, v. 162, n. 11, p. 2171–2186, 2015.

MARGALEF, R. Life-forms of phytoplankton as survival alternatives in an unstable environment. **Oceanologica Acta**, v. 1, n. 4, p. 493–509, 1978.

MARIE, D.; SIMON, N.; VAULOT, D. Phytoplankton cell counting by flow cytometry. **Algal culturing techniques**, v. 1, p. 253–267, 2005.

MARTIN, A. P. Phytoplankton patchiness: the role of lateral stirring and mixing. **Progress in Oceanography**, v. 57, n. 2, p. 125–174, 2003.

MAZZINI, P. L. F. **Correntes Subinerciais na Plataforma Continental Interna entre Peruíbe e São Sebastião: Observações**. Master's thesis. São Paulo: University of São Paulo, 2009.

MCFARLAND, M. N. et al. Impact of phytoplankton size and physiology on particulate optical properties determined with scanning flow cytometry. **Marine Ecology Progress Series**, v. 531, p. 43–61, 2015.

MCMANUS, M. A. et al. Cryptic blooms: Are thin layers the missing connection? **Estuaries and Coasts**, v. 31, n. 2, p. 396–401, 2008.

MCMANUS, M. A. et al. Observations of Thin Layers in Coastal Hawaiian Waters. **Estuaries and Coasts**, v. 35, n. 4, p. 1119–1127, 2012.

MCMANUS, M. A. et al. Characterization of the biological, physical, and chemical properties of a toxic thin layer in a temperate marine system. **Marine Ecology Progress Series**, v. 678, p. 17-35, 2021.

MEDEIROS, M. **Development of an in situ image capture instrumentation to study the vertical distribution of plankton.** Master's thesis. São Paulo: University of São Paulo, 2017.

MELO JÚNIOR, M. et al. Temporal changes in pelagic copepod assemblages off Ubatuba, Brazil. **Marine Ecology**, v. 37, n. 4, p. 877–890, 2016.

MESQUITA, A. R. D.; HARARI, J. Tides and tide Gauges of Cananéia and Ubatuba-Brazil (lat, 24). **Relat. int. Inst. oceanogr. Univ. S Paulo**, v. 11, p. 1–14, 1983.

METZLER, P. M. et al. New and regenerated production in the South Atlantic off Brazil. **Deep-Sea Research Part I: Oceanographic Research Papers**, v. 44, n. 3, p. 363–384, 1997.

MIGLIETTA, M. P. et al. Approaches to the ethology of hydroids and medusae(Cnidaria, Hydrozoa). **Sci. Mar.**, v. 64, p. 63–71, 2000.

MIRANDA, L. B.; KATSURAGAWA, M. Estrutura térmica na região sudeste do Brasil (outubro/novembro de 1988). **Publicação especial do Instituto Oceanográfico**, v. 8, p. 1–14, 1991.

MIYASHITA, L. K. et al. Seasonal contrasts in abundance and reproductive parameters of Penilia avirostris (Cladocera, Ctenopoda) in a coastal subtropical area. **Marine Biology**, v. 157, n. 11, p. 2511–2519, 2010.

MIYASHITA, L. K.; LOPES, R. M. Larvacean (Chordata, Tunicata) abundance and inferred secondary production off southeastern Brazil. **Estuarine, Coastal and Shelf Science**, v. 92, n. 3, p. 367–375, 2011.

MÖLLER, K. O. et al. Marine snow, zooplankton and thin layers: Indications of a trophic link from small-scale sampling with the Video Plankton Recorder. **Marine Ecology Progress Series**, v. 468, p. 57–69, 2012.

MOORE, L. R. et al. Utilization of different nitrogen sources by the marine cyanobacteria Prochlorococcus and Synechococcus. **Limnology and Oceanography**, v. 47, n. 4, p. 989–996, 2002.

MULLIN, M. M.; BROOKS, E. R. Some consequences of distributional heterogeneity of phytoplankton and zooplankton. **Limnology and Oceanography**, v. 21, n. 6, p. 784–796, 1976.

NAGATA, R. M. et al. Spatial and temporal variation of planktonic cnidarian density in subtropical waters of the Southern Brazilian Bight. **Journal of the Marine Biological Association of the United Kingdom**, v. 94, n. 7, p. 1387–1400, 2014.

NAYAK, A. R. et al. On plankton distributions and biophysical interactions in diverse coastal and limnological environments. **SPIE-Intl Soc Optical Eng**, v. 10631, p. 27, 2018.

NOGUEIRA JR, M.; BRANDINI, F. P.; CODINA, J. C. U. Distribution of planktonic cnidarians in response to South Atlantic Central Water intrusion in the South Brazilian Bight. **Continental Shelf Research**, v. 89, p. 93–102, 2014.

NOGUEIRA, M.; BRANDINI, F. P. Community Structure and Spatiotemporal Dynamics of the Zooplankton in the South Brazilian Bight: A Review. **Plankton Ecology of the Southwestern Atlantic: From the Subtropical to the Subantarctic Realm**, p. 149–170, 2018.

ONITSUKA, G. et al. Development of a thin diatom layer observed in a stratified embayment in Japan. **Journal of Oceanography**, v. 74, n. 4, p. 351–365, 2018.

PANNARD, A. et al. Short-term variability of the phytoplankton community in coastal ecosystem in response to physical and chemical conditions' changes. **Estuarine, Coastal and Shelf Science**, v. 80, n. 2, p. 212–224, 2008.

PARTENSKY, F.; HESS, W. R.; VAULOT, D. Prochlorococcus, a Marine Photosynthetic Prokaryote of Global Significance. **Microbiology and Molecular Biology Reviews**, v. 63, n. 1, p. 106–127, 1999.

PEÑA, M. A.; MASSON, D.; CALLENDAR, W. Annual plankton dynamics in a coupled physical–biological model of the Strait of Georgia, British Columbia. **Progress in Oceanography**,

v. 146, p. 58–74, 2016.

PENNINCK, S. B. et al. Thin layers in the coastal zone of Ubatuba, Brazil: Mechanisms of formation and dissipation. **Limnology and Oceanography**, v. 66, n. 2, p. 558–574, 2021.

PÉREZ, V. et al. Latitudinal distribution of microbial plankton abundance, production, and respiration in the Equatorial Atlantic in autumn 2000. **Deep Sea Research Part I: Oceanographic Research Papers**, v. 52, n. 5, p. 861–880, 2005.

PIANKA, E. R. **Evolutionary ecology**. Seventh ed ed. [s.l: s.n.].

PIELOU, E. C. The measurement of diversity in different types of biological collections. **Journal of Theoretical Biology**, v. 13, n. C, p. 131–144, 1 dez. 1966.

POND, S.; PICKARD, G. L. **Introductory dynamical oceanography**. 2nd ed. ed. Oxford: Butterworth-Heinemann, 1983.

PRAIRIE, J. C. et al. Biophysical interactions in the plankton: A cross-scale review. **Limnology and Oceanography: Fluids and Environments**, v. 2, n. 1, p. 121–145, 2012.

PRAIRIE, J. C.; WHITE, B. L. A model for thin layer formation by delayed particle settling at sharp density gradients. **Continental Shelf Research**, v. 133, p. 37–46, 2017.

QUINTANA, C. O. et al. Effects of coastal upwelling on the structure of macrofaunal communities in SE Brazil. **Journal of Marine Systems**, v. 143, p. 120–129, 2015.

REBOITA, M. S. et al. The south atlantic subtropical anticyclone: Present and future climate. **Frontiers in Earth Science**, v. 7, n. February, p. 1–15, 2019.

REYNOLDS, C. S. **The ecology of phytoplankton**. [s.l.] Cambridge University Press, 2006.

RIBEIRO, C. G. et al. Pico and nanoplankton abundance and carbon stocks along the Brazilian Bight. **PeerJ**, v. 2016, n. 11, p. e2587, 2016.

RICHARDSON, A. J. Plankton and Climate. **Encyclopedia of Ocean Sciences**, p. 464–472, 2009.

RINES, J. E. B. et al. Thin layers and camouflage: Hidden Pseudo-nitzschia spp. (Bacillariophyceae) populations in a fjord in the San Juan Islands, Washington, USA. **Marine Ecology Progress Series**, v. 225, p. 123–137, 2002.

ROCAP, G. et al. Genome divergence in two Prochlorococcus ecotypes reflects oceanic niche differentiation. **Nature**, v. 424, n. 6952, p. 1042–1047, 2003.

RODRIGUES, M. L. G.; FRANCO, D.; SUGAHARA, S. Climatologia de frentes frias no litoral de Santa Catarina. **Revista Brasileira de Geofísica**, v. 22, n. 2, p. 135–151, 2004.

ROEMMICH, D.; MCGOWAN, J. Climatic warming and the decline of zooplankton in the California current. **Science**, v. 267, n. 5202, p. 1324–1326, 1995.

RYAN, J. P. et al. Phytoplankton thin layers caused by shear in frontal zones of a coastal upwelling system. **Marine Ecology Progress Series**, v. 354, p. 21–34, 2008.

RYAN, J. P.; MCMANUS, M. A.; SULLIVAN, J. M. Interacting physical, chemical and biological forcing of phytoplankton thin-layer variability in Monterey Bay, California. **Continental Shelf Research**, v. 30, n. 1, p. 7–16, 2010.

SABINE, C. L. et al. The oceanic sink for anthropogenic CO2. **Science**, v. 305, n. 5682, p. 367–371, 2004.

SALDANHA-CORRÊA, F. M. P.; GIANESELLA, S. M. F. A microcosm approach on the potential effects of the vertical mixing of water masses over the primary productivity and phytoplankton biomass in the southern Brazilian coastal region. **Brazilian Journal of Oceanography**, v. 52, n. 3–4, p. 167–182, 2004.

SASSI, R.; KUTNER, M. B. B. Variação sazonal do fitoplâncton da região do Saco da Ribeira (Lat. 23º30'S; Long. 45º07'W), Ubatuba, Brasil. **Boletim do Instituto Oceanográfico**, v. 31, n. 2, p. 29–42, 1982.

SCHLITZER, R. Ocean Data View. **odv.awi.de**, 2021.

SCHMOKER, C.; HERNÁNDEZ-LEÓN, S. Stratification effects on the plankton of the

subtropical Canary Current. **Progress in Oceanography**, v. 119, p. 24–31, 2013.

SENGUPTA, A.; CARRARA, F.; STOCKER, R. Phytoplankton can actively diversify their migration strategy in response to turbulent cues. **Nature**, v. 543, n. 7646, p. 555–558, 2017.

SEVADJIAN, J. C.; MCMANUS, M. A.; PAWLAK, G. Effects of physical structure and processes on thin zooplankton layers in Mamala Bay, Hawaii. **Marine Ecology Progress Series**, v. 409, p. 95–106, 2010.

SHANNON, C. E. A mathematical theory of communication. **The Bell system technical journal**, v. 27, n. 3, p. 379–423, 1948.

SHROYER, E. L. et al. Stratification and mixing regimes in biological thin layers over the Mid-Atlantic Bight. **Limnology and Oceanography**, v. 59, n. 4, p. 1349–1363, 2014.

SILOVIC, T. et al. Picoplankton distribution influenced by thermohaline circulation in the southern Adriatic. **Continental Shelf Research journal**, v. 155, p. 21–33, 2018.

SOHM, J. A. et al. Co-occurring Synechococcus ecotypes occupy four major oceanic regimes defined by temperature, macronutrients and iron. **ISME Journal**, v. 10, n. 2, p. 333–345, 2016.

SOMERFIELD, P. J.; CLARKE, K. R.; WARWICK, R. M. Simpson Index. **Encyclopedia of Ecology, Five-Volume Set**, p. 3252–3255, 2008.

SONTEK-YSI INC. **SonTek Doppler current meters - using signal strength to monitor suspended sediment concentration**. San Diego: SonTek Application Notes, 1997.

STACEY, M. T.; MCMANUS, M. A.; STEINBUCK, J. V. Convergences and divergences and thin layer formation and maintenance. **Limnology and Oceanography**, v. 52, n. 4, p. 1523–1532, 2007.

STEINBUCK, J. V. et al. Observations of turbulent mixing in a phytoplankton thin layer: Implications for formation, maintenance, and breakdown. **Limnology and Oceanography**, v. 54, n. 4, p. 1353–1368, 2009.

STEWART, R. H. **Introduction to physical oceanography**. [s.l.] Texas A & M University,

College Station, 2008.

SULLIVAN, J. M. et al. Layered organization in the coastal ocean: An introduction to planktonic thin layers and the LOCO project. **Continental Shelf Research**, v. 30, n. 1, p. 1–6, 2010.

SULLIVAN, J. M.; DONAGHAY, P. L.; RINES, J. E. B. Coastal thin layer dynamics: Consequences to biology and optics. **Continental Shelf Research**, v. 30, n. 1, p. 50–65, 2010.

TALAPATRA, S. et al. Characterization of biophysical interactions in the water column using in situ digital holography. **Marine Ecology Progress Series**, v. 473, p. 29–51, 2013.

TARRAN, G. A.; HEYWOOD, J. L.; ZUBKOV, M. V. Latitudinal changes in the standing stocks of nano- and picoeukaryotic phytoplankton in the Atlantic Ocean. **Deep Sea Research Part II: Topical Studies in Oceanography**, v. 53, n. 14–16, p. 1516–1529, 2006.

TEIXEIRA, C. Preliminary studies of primary production in Ubatuba region (Lat. 23°30'S - Long. 45°06'W). **Bolm Inst. oceanogr., São Paulo**, v. 22, p. 49–58, 1973.

TEIXEIRA, C.; GAETA, A. S. Variação nictemeral da clorofila a, produção primária do fitoplâncton e fatores ambientais da região de Ubatuba (Lat.23°30'5 Long. 45°06'W). v. 39, n. 1, p. 15–24, 1991.

THOMAS, L. N.; TANDON, A.; MAHADEVAN, A. Submesoscale processes and dynamics. **Geophysical Monograph Series**, v. 177, p. 17–38, 2008.

THOMSON, R. E.; EMERY., W. J. **Data analysis methods in physical oceanography**. 3rd. ed. [s.l: s.n.].

TRUCCOLO, E. C. Assessment of the wind behavior in the northern coast of Santa Catarina. **Revista Brasileira de Meteorologia**, v. 26, n. 3, p. 451–460, 2011.

TURNER, J. T. The importance of small planktonic copepods and their roles in pelagic marine food webs. **Zool. Stud.**, v. 43, p. 255–266, 2004.

URBAN-RICH, J.; FERNÁNDEZ, D.; ACUÑA, J. L. Grazing impact on chromophoric dissolved organic matter (CDOM) by the larvacean Oikopleura dioica. **Marine Ecology Progress Series**, v.

317, p. 101–110, 2006.

VELO-SUÁREZ, L. et al. Hydrodynamic conditions associated with the formation, maintenance and dissipation of a phytoplankton thin layer in a coastal upwelling system. **Continental Shelf Research**, v. 30, n. 2, p. 193–202, 2010.

VILLAC, M. C.; CABRAL-NORONHA, V. A. D. P.; PINTO, T. D. O. The phytoplankton biodiversity of the coast of the state of São Paulo, Brazil. **Biota Neotrop.**, v. 8, n. 3, p. 151–173, 2008.

VILLAMAÑA, M. et al. The role of mixing in controlling resource availability and phytoplankton community composition. **Progress in Oceanography**, v. 178, p. 102181, 2019.

VILLAREAL, T. A.; CARPENTER, E. J. Diel buoyancy regulation in the marine diazotrophic cyanobacterium Trichodesmium thiebautii. **Limnology and Oceanography**, v. 35, n. 8, p. 1832–1837, 1990.

WEISS, R. F. The solubility of nitrogen, oxygen and argon in water and seawater. **Deep-Sea Research**, v. 17, p. 721–735, 1970.

WELSCHMEYER, N. Fluorometric analysis of Chlorophyll a in the presence of Chlorophyll b and pheopigments. **Limnology and Oceanography**, v. 39, p. 1985–1992, 1994.

WHITE, J. W. et al. Connectivity, dispersal, and recruitment. **Oceanography**, v. 32, n. 3, p. 50-59, 2019.

WHEELER, J. D. et al. Not just going with the flow: The effects of fluid flow on bacteria and plankton. **Annual Review of Cell and Developmental Biology**, v. 35, p. 213–237, 2019.

WHITT, D. B.; TAYLOR, J. R.; LÉVY, M. Synoptic-to-planetary scale wind variability enhances phytoplankton biomass at ocean fronts. **Journal of Geophysical Research: Oceans**, v. 122, n. 6, p. 4602–4633, 2017.

WOODSON, C. B. et al. Observations of internal wave packets propagating along-shelf in northern Monterey Bay. **Geophysical Research Letters**, v. 38, n. 1, 2011.

WOODSON, C. B. et al. Coastal fronts set recruitment and connectivity patterns across multiple taxa. **Limnology and Oceanography**, v. 57, n. 2, p. 582–596, 2012.

WORDEN, A. Z.; NOT, F. Ecology and Diversity of Picoeukaryotes. **Microbial Ecology of the Oceans**, v. 2, p. 159–205, 2008.

WORMS EDITORIAL BOARD. **World Register of Marine Species**, https://www.marinespecies.org/, acessed on 06-30-2022.

YANG, D.; YE, H.; WANG, G. Impacts of internal waves on chlorophyll a distribution in the northern portion of the South China Sea. **Chinese Journal of Oceanology and Limnology**, v. 28, n. 5, p. 1095–1101, 2010.

YIN, K. et al. Effect of wind events on phytoplankton blooms in the Pearl River estuary during summer. **Continental Shelf Research**, v. 24, n. 16, p. 1909–1923, 2004.

YOSHIDA, J.; NAGASHIMA, H.; MA, W. J. A double diffusive lock-exchange flow with small density difference. **Fluid Dynamics Research**, v. 2, n. 3, p. 205–215, 1987.

ZUBKOV, M. V. et al. Picoplankton community structure on the Atlantic Meridional Transect: a comparison between seasons. **Progress in Oceanography**, v. 45, n. 3–4, p. 369–386, 2000.

APPENDIX A - Supplementary material for Chapter II

Table A1. Collection time (UTC-3), euphotic zone depth (Z_{eu}, m), collection depth (m), physicochemical parameters (Temperature (Temp., °C), Salinity, Density (kg m^{-3}), Chlorophyll-a (Chl-a, µg L^{-1}), Turbidity (Tur., FTU), and Dissolved oxygen (DO, mg L^{-1})), and nutrients (Nitrite, Nitrate, Phosphate, and Silicate; µM) for February 20, 2019.

Time (UTC-3)	Z_{eu} (m)	Depth (m)	Temp. (°C)	Salinity	Density (Kg m^{-3})	Chl-a (µg L^{-1})	Tur. (FTU)	DO (mg L^{-1})	Nitrite (µM)	Nitrate (µM)	Phosphate (µM)	Silicate (µM)
08:00	25.9	0	27.46	34.24	1022.00	0.72	0.43	6.86	0.08	0.36	0.23	5.64
		5	27.21	34.50	1022.29	0.76	0.35	6.99	0.01	0.17	0.24	4.32
		10	25.98	34.94	1023.04	0.67	0.12	7.10	0.02	0.23	0.18	3.64
		15	23.77	35.31	1024.01	1.14	0.19	7.27	0.01	0.07	0.14	2.63
		17	22.02	35.70	1024.82	1.34	0.15	7.41	0.03	0.50	0.23	4.36
		19	20.37	35.79	1025.35	3.84	0.68	7.45	0.39	1.19	0.35	5.26
		21	19.61	35.74	1025.52	4.05	2.13	6.71	0.80	3.94	0.60	11.10
		23	19.34	35.75	1025.61	3.42	4.98	6.04	0.96	4.27	0.71	11.04
12:00	19.9	0	27.90	34.28	1021.89	0.52	0.46	6.66	0.02	0.09	0.09	4.73
		5	26.86	34.57	1022.46	1.01	0.66	6.84	0.03	0.22	0.16	3.91
		10	25.29	35.08	1023.36	1.07	0.25	7.00	0.12	0.25	0.18	3.04
		15	22.44	35.67	1024.67	2.03	0.68	6.75	0.02	0.03	0.21	3.92
		17	20.33	35.75	1025.32	2.67	0.48	7.28	0.15	0.50	0.23	4.27
		19	19.57	35.72	1025.51	5.57	1.16	7.04	0.38	0.98	0.35	4.67
		21	19.33	35.72	1025.58	4.62	2.40	6.05	0.72	2.11	0.50	7.30
		23	19.20	35.73	1025.63	3.68	2.15	5.94	1.09	3.20	0.66	9.65
16:00	18.8	0	27.55	34.44	1022.12	0.66	0.27	6.83	0.15	0.87	0.20	6.51
		5	26.06	34.93	1022.98	0.64	0.06	6.97	0.17	0.55	0.11	5.73
		10	25.27	35.13	1023.40	1.04	0.12	7.09	0.01	0.11	0.13	1.96
		15	19.91	35.66	1025.35	3.91	0.56	7.16	0.16	0.34	0.24	5.57
		17	19.24	35.70	1025.57	5.12	1.74	6.26	0.20	0.31	0.23	4.34
		19	18.90	35.69	1025.66	3.65	7.27	5.71	0.64	1.80	0.42	5.99
		21							1.08	3.95	0.66	13.61
		23							0.73	2.52	0.51	8.74
20:00		0	27.44	34.50	1022.20	0.64	0.17	6.79	0.05	1.06	0.20	4.86
		5	27.35	34.52	1022.26	0.73	0.25	6.82	0.10	0.24	0.15	3.96
		10	26.53	34.84	1022.79	0.79	0.19	6.89	0.01	0.08	0.09	2.40
		15	22.54	35.58	1024.58	2.57	0.64	6.66	0.06	0.10	0.30	5.64
		17	20.48	35.77	1025.29	3.47	0.93	7.09	0.12	0.35	0.21	3.84
		19	19.82	35.75	1025.47	4.76	1.10	6.84	0.14	0.36	0.42	7.71
		21	19.58	35.73	1025.52	4.69	2.13	6.67	0.62	1.48	0.41	6.15
		23	19.31	35.72	1025.59	4.02	6.30	5.53	0.93	2.63	0.66	10.58

Table A2. Collection time (UTC-3), euphotic zone depth (Z_{eu}, m), collection depth (m), physicochemical parameters (Temperature (Temp., °C), Salinity, Density (kg m^{-3}), Chlorophyll-a (Chl-a, µg L^{-1}), Turbidity (Tur., FTU), and Dissolved Oxygen (DO, mg L^{-1})), and nutrients (Nitrite, Nitrate, Phosphate, and Silicate; µM) for February 21, 2019.

Time (UTC-3)	Z_{eu} (m)	Depth (m)	Temp. (°C)	Salinity	Density (Kg m^{-3})	Chl-a (µg L^{-1})	Tur. (FTU)	DO (mg L^{-1})	Nitrite (µM)	Nitrate (µM)	Phosphate (µM)	Silicate (µM)
08:00	25.9	0	27.40	33.98	1021.82	0.85	0.27	6.76	0.03	0.18	0.15	6.97
		5	27.35	34.42	1022.19	0.67	0.21	6.70	0.01	0.07	0.19	5.03
		10	27.22	34.74	1022.50	0.67	0.10	6.74	0.13	0.13	0.23	3.59
		15	25.64	35.07	1023.27	1.11	0.23	6.96	0.18	1.43	0.31	5.04
		17	24.67	35.19	1023.66	3.47	2.62	6.03	0.18	0.82	0.34	7.42
		19	23.46	35.42	1024.20	4.16	4.36	5.43	0.29	1.13	0.38	6.76
		21	22.33	35.57	1024.65	4.51	6.75	4.58	0.86	3.22	0.71	13.99
		23	20.84	35.74	1025.20	4.01	6.53	4.74	0.92	3.35	0.73	14.58
12:00	27.0	0	27.69	33.80	1021.60	0.85	0.39	6.81	0.16	0.37	0.11	5.73
		5	27.32	34.49	1022.25	0.79	0.17	6.75	0.00	0.20	0.12	3.26
		10	26.93	34.77	1022.61	0.84	0.14	6.76	0.03	0.11	0.23	6.36
		15	24.95	35.41	1023.73	2.81	1.20	6.21	0.26	0.87	0.24	4.82
		17	23.89	35.50	1024.13	2.86	1.36	5.86	0.14	0.69	0.37	7.61
		19	23.29	35.51	1024.32	2.55	1.39	6.10	0.60	1.48	0.45	8.75
		21	22.34	35.67	1024.72	2.69	1.72	5.64	0.82	3.10	0.68	13.39
		23	20.90	35.79	1025.23	3.47	6.71	4.81	0.73	2.74	0.63	12.38
16:00	23.5	0	28.22	33.70	1021.35	1.02	0.27	6.92	0.01	0.13	0.12	5.34
		5	27.36	34.58	1022.31	0.92	0.19	6.85	0.00	0.04	0.14	3.97
		10	26.48	34.76	1022.74	1.50	0.46	6.68	0.00	0.07	0.19	5.78
		15	23.90	35.39	1024.03	2.67	2.21	6.36	0.10	0.15	0.27	6.72
		17	23.07	35.51	1024.38	2.92	2.01	6.13	0.16	0.25	0.29	7.42
		19	22.36	35.62	1024.67	2.87	1.38	6.00	0.09	0.34	0.31	5.83
		21	20.59	35.75	1025.27	2.93	2.40	5.63	0.91	2.11	0.59	10.69
		23	20.00	35.77	1025.45	3.09	3.02	5.14	1.02	3.34	0.78	13.44
20:00		0	27.72	33.87	1021.64	0.93	0.27	6.95	0.04	0.89	0.19	7.70
		5	27.12	34.59	1022.39	1.13	0.23	6.83	0.21	0.83	0.18	5.14
		10	25.62	35.18	1023.33	1.44	0.31	6.92	0.14	0.55	0.17	4.72
		15	24.05	35.44	1024.02	3.79	2.01	6.18	0.04	0.16	0.26	6.28
		17	23.37	35.47	1024.26	3.55	2.50	5.75	0.07	0.33	0.24	5.23
		19	23.32	35.48	1024.29	3.71	2.46	5.96	0.10	0.25	0.33	6.96
		21	22.91	35.55	1024.47	3.36	2.17	6.04	0.69	2.37	0.61	12.14
		23	21.26	35.70	1025.06	2.58	3.93	5.78	0.20	0.68	0.35	6.81

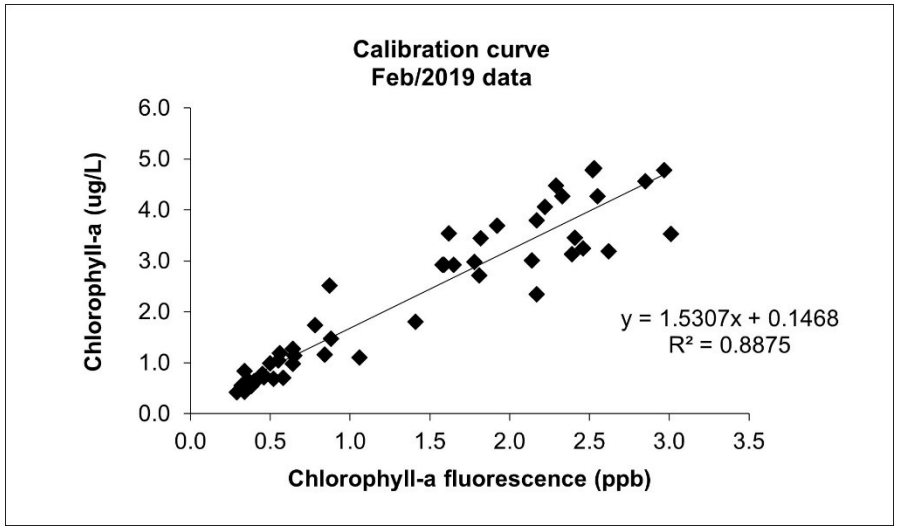

Fig. A1. Calibration curve for chlorophyll-a fluorescence data collected in February 2019 (n = 50). The data collected between the period of 10 am and 4 pm, and the outliers, were excluded.

APPENDIX B - Supplementary material for Chapter III

Table B1. Checklist of the specimens classified for diatom, dinoflagellate, and cyanobacteria group for the inner shelf off Ubatuba in winter/2018 and summer/2019. Taxonomic information was obtained from AlgaeBase, accessed through World Register of Marine Species at http://www.marinespecies.org on 2021-11-24.

Taxonomic groups	Winter 2018	Summer 2019
Chromista		
Phylum Ochrophyta		
Class Bacillariophyceae (diatoms)		
Order Achnanthales		
Genus *Achnanthes*		X
Order Bacillariales		
Genus *Nitzschia*	X	X
Order Chaetocerotanae incertae sedis		
Genus *Bacteriastrum*	X	X
Genus *Chaetoceros*		
Chaetoceros atlanticus	X	X
Chaetoceros coarctatus	X	X
Chaetoceros compressus	X	X
Chaetoceros curvisetum	X	X
Chaetoceros peruvianus	X	X
Chaetoceros sp.1	X	X
Chaetoceros sp.2		X
Chaetoceros sp.3		X
Order Corethrales		
Genus *Corethron*		
Corethron criophilum	X	X
Order Coscinodiscales		
Genus *Coscinodicus*		
Coscinodiscus sp.1	X	X
Coscinodiscus sp.2		X
Order Fragilariales		
Genus *Asterionellopsis*		
Asterionellopsis glacialis	X	X
Order Hemiaulales		
Genus *Cerataulina*	X	X
Genus *Hemiaulus*		
Hemiaulus sp.1	X	X
Hemiaulus sp.2	X	X
Order Leptocylindrales		
Genus *Leptocylindrus*		X
Order Lithodesmiales		
Genus *Ditylum*		X
Genus *Helicotheca*	X	X
Order Melosirales		
Genus *Melosira*	X	X
Genus *Stephanopyxis*		X

Order Naviculales		
Genus *Gyrosigma*		X
Order Rhizosoleniales		
Genus *Guinardia*		
Guinardia sp.1	X	X
Guinardia sp.2		X
Genus *Rhizosolenia*		
Rhizosolenia sp.1	X	X
Rhizosolenia sp.2		X
Rhizosolenia sp.3		X
Order Thalassionematales		
Genus *Thalassionema*		
Thalassionema frauenfeldii	X	X
Genus *Thalassiothrix*	X	X
Order Thalassiosirales		
Genus *Skeletonema*	X	X
Genus *Thalassiosira*		
Thalassiosira sp.1	X	X
Thalassiosira sp.2	X	X
Thalassiosira sp.3		X
Order Triceratiales		
Genus *Odontella*		X
Phylum Myzozoa		
Class Dinophyceae		
Order Dinophysiales		
Genus Dinophysis	X	X
Order Gonyaulacales		
Genus *Tripos*		
Tripos furca	X	X
Tripos fusus	X	X
Tripos brevis	X	X
Tripos sp.1	X	X
Tripos sp.2	X	X
Genus *Pyrophacus*	X	
Order Noctilucales		
Genus *Noctiluca*	X	
Order Peridiniales		
Genus *Protoperidinium*	X	X
Order Prorocentrales		
Genus *Prorocentrum*		X
Order Pyrocystales		
Genus *Pyrocystis*		
Pyrocystis lunula		X
Bacteria		
Phylum Cyanobacteria		
Class Cyanophyceae		
Order Oscillatoriales		
Genus *Trichodesmium*		
Trichodesmium erythraeum		X
Trichodesmium thiebautii		X

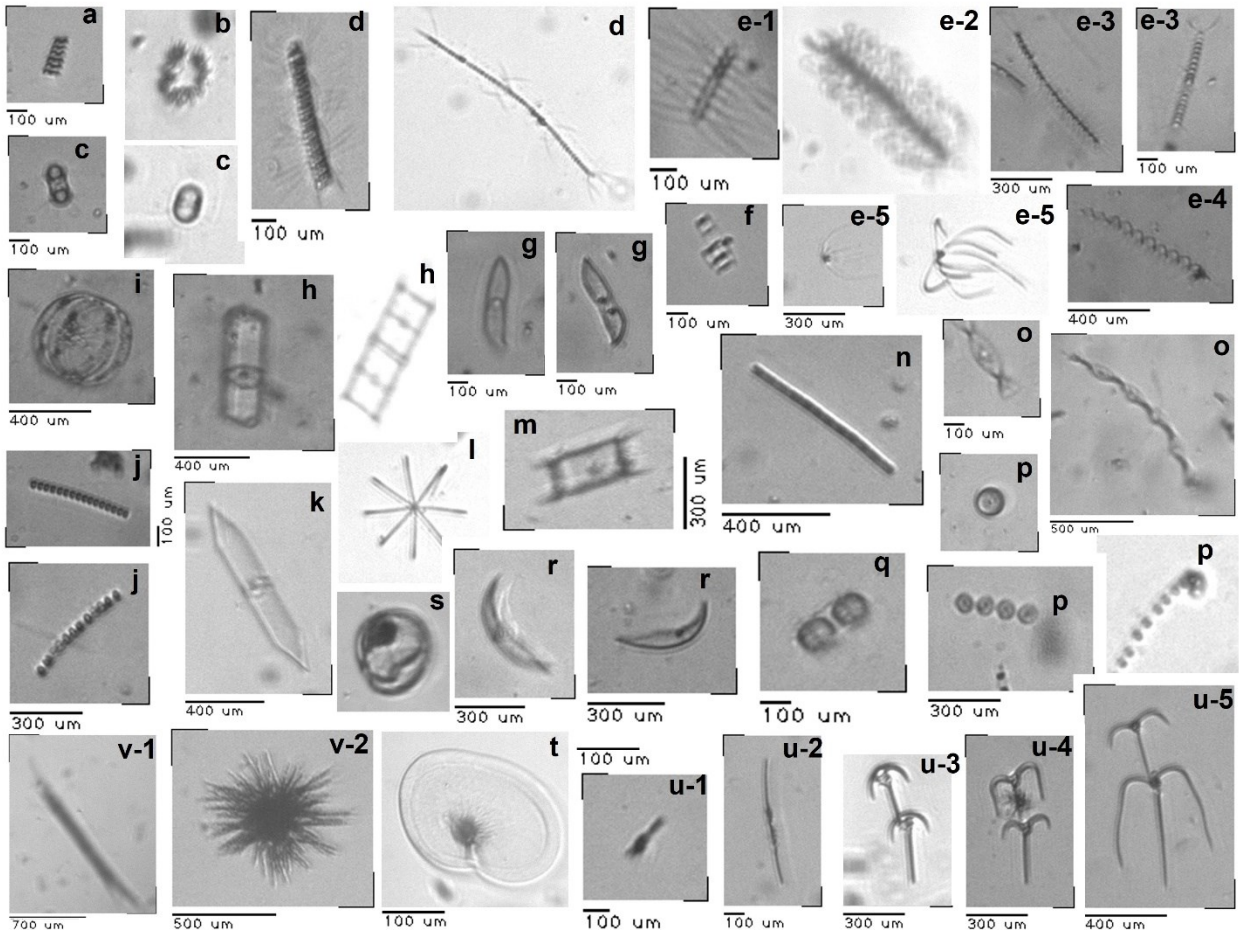

Fig. B1. ROIs depicting some plankton organisms obtained by the imaging system. Diatoms: a) *Achnanthes* sp., b) *Asterionellopsis* sp., c) *Corethron criophilum,* d) *Bacteriastrum* spp., e-1) *Chaetoceros atlanticus,* e-2) *Chaetoceros coarctatus,* e-3) *Chaetoceros compressus*, e-4) *Chaetoceros curvisetus,* e-5) *Chaetoceros peruvianus*, f) *Hemiaulus* sp., g) *Gyrosigma* sp. h) *Guinardia* sp., i) *Coscinodiscus* sp., j) *Melosira* sp., k) *Rhizosolenia* sp., l) *Thalassionema frauenfeldii*, m) *Odontella* sp., n) *Leptocylindrus* sp. o) *Helicotheca* sp., p) *Thalassiosira spp.*, q) *Stephanopyxis* sp.; Dinoflagellates: r) *Pyrocystis lunula,* s) *Noctiluca* sp, t) *Pyrophacus* sp., u-1) *Tripos furca,* u-2) *Tripos fusus,* u-3) *Tripos brevis* sp., u-4) *Tripos* sp.1, u-5) *Tripos* sp.2; Cyanobacteria: v-1) *Trichodesmium erythraeum*, v-2) *Trichodesmium thiebautii.*

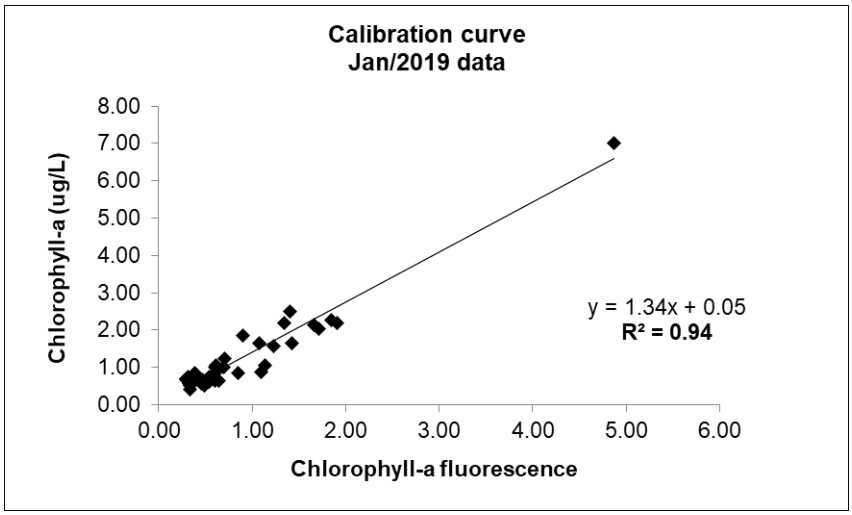

Fig. B2. Calibration curve for chlorophyll-a fluorescence data collected in January 2019 (n = 38). The data collected between the period of 10 am and 4 pm, and the outliers, were excluded.

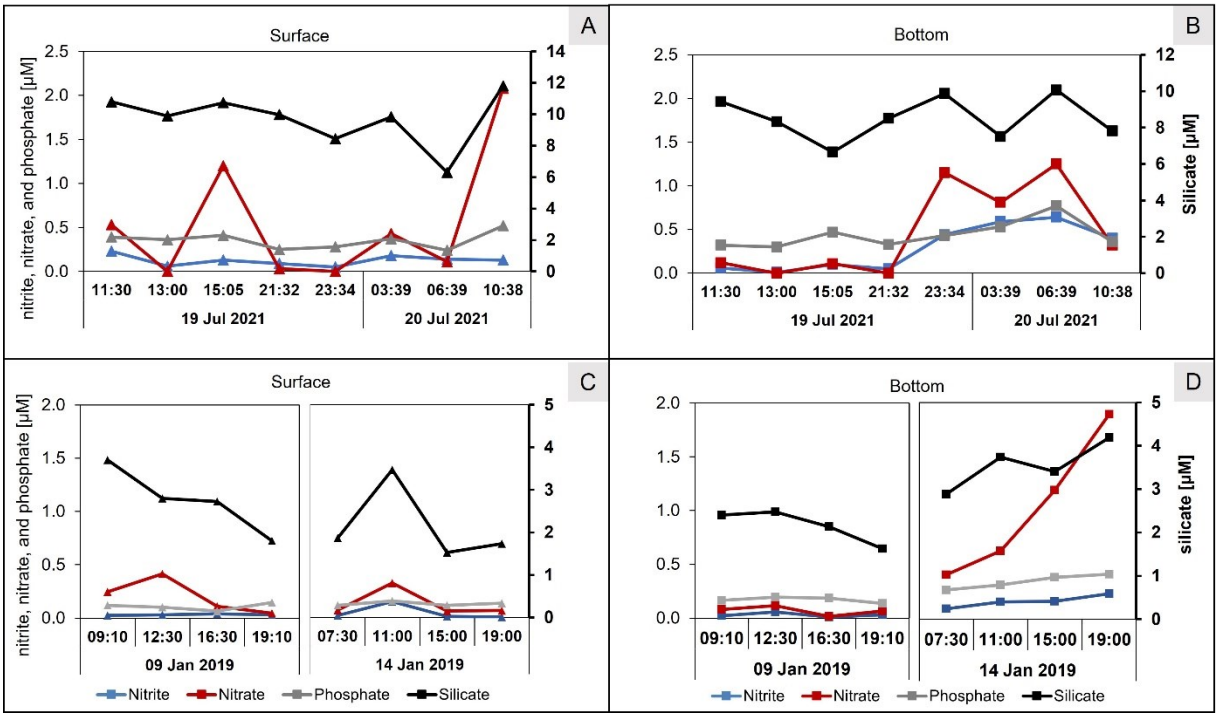

Fig. B3. Temporal distribution of nutrients (µM): (A) fixed station on July 19-20, 2018, in the surface layer; (B) fixed station on July 19-20, 2018, in the bottom layer; (C) fixed stations on January 9 and 14, 2019, in the surface layer; and (D) fixed stations on January 9 and 14, 2019, in the bottom layer. The axis on the right corresponds to the concentration of silicate and the axis on the left, to the concentration of nitrite, nitrate, and phosphate.

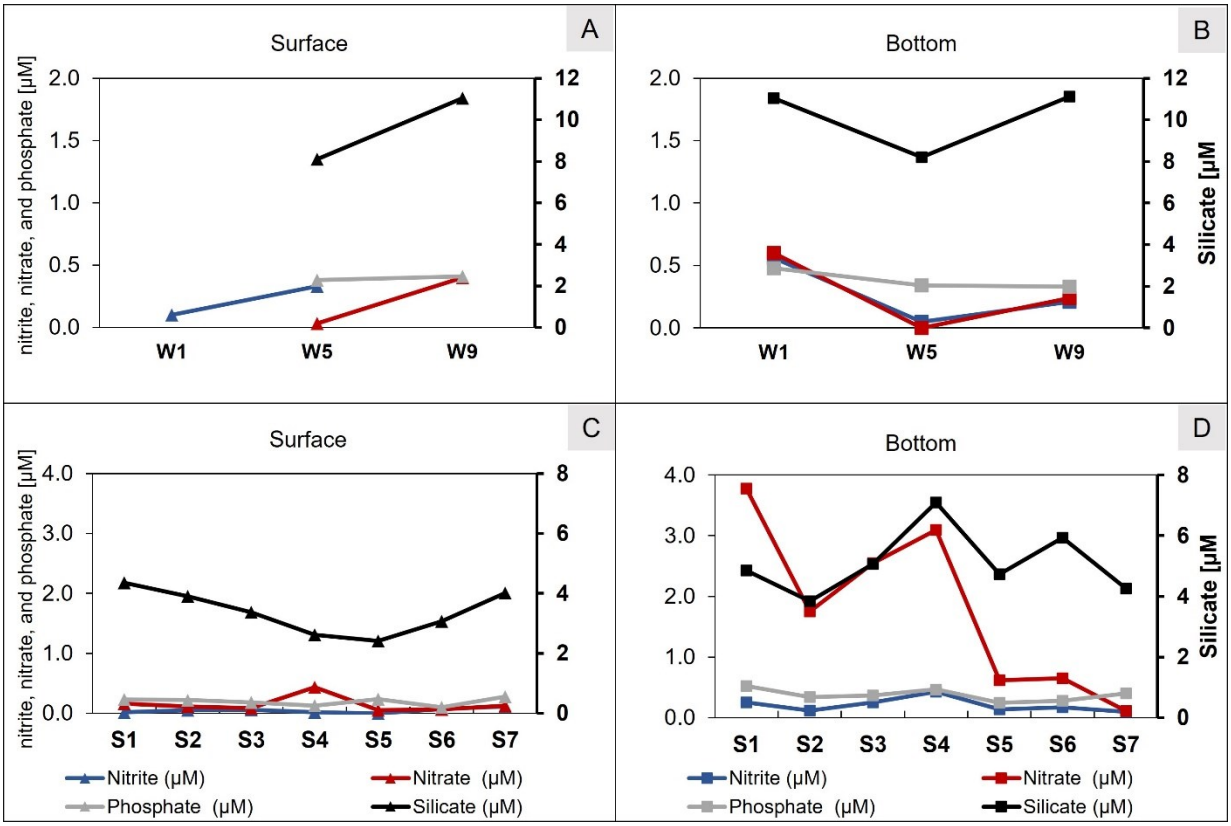

Fig. B4. Spatial distribution of nutrients. (A) Transect stations on July 25, 2018, in the surface layer; (B) Transect stations on July 25, 2018, in the bottom layer; (C) Transect stations on January 11, 2019, in the surface layer; and (D) Transect stations on January 11, 2019, in the bottom layer. The axis on the right corresponds to the concentration of silicate and the axis on the left, to the concentration of nitrite, nitrate, and phosphate.

Table B2. The results for Kruskal–Wallis and Dunn's post-hoc tests with Bonferroni correction for phytoplankton, protozooplankton, and metazooplankton abundances between the transect sites on July 25, 2018. Values in bold are significantly different between the sites (p<0.05).

	Phytoplankton	**Protozooplankton**	**Metazooplankton**
Kruskal-Wallis	**1.82E-28**	**1.74E-04**	**9.56E-08**
Chi-square	149.00	19.72	24.70
Dunn's post hoc test sites			
W1-W2	1.28E-01	9.45E-01	8.78E-02
W1-W3	4.99E-01	**5.14E-03**	2.71E-01
W1-W4	**3.77E-14**	6.44E-01	**3.53E-04**
W1-W5	**1.86E-18**	2.95E-01	6.61E-03
W1-W6	**6.95E-07**	1.75E-01	**3.08E-03**
W1-W7	**3.63E-03**	2.77E-01	4.00E-01
W1-W8	5.57E-01	1.17E-01	4.62E-02
W1-W9	5.54E-01	**5.80E-05**	7.15E-01
W2-W3	4.46E-01	**1.39E-02**	**1.13E-02**
W2-W4	**9.28E-08**	7.28E-01	1.11E-01
W2-W5	**7.99E-11**	3.80E-01	3.75E-01
W2-W6	**1.16E-03**	2.38E-01	2.07E-01
W2-W7	1.62E-01	2.92E-01	5.15E-01
W2-W8	4.81E-01	1.66E-01	6.64E-01
W2-W9	8.53E-02	**2.30E-04**	3.29E-01
W3-W4	**8.70E-10**	**2.73E-02**	**2.39E-05**
W3-W5	**3.58E-13**	1.08E-01	**5.67E-04**
W3-W6	**7.35E-05**	2.59E-01	**2.75E-04**
W3-W7	**3.54E-02**	**8.77E-04**	9.11E-02
W3-W8	9.90E-01	3.95E-01	**6.22E-03**
W3-W9	2.85E-01	1.14E-01	2.35E-01
W4-W5	1.75E-01	5.75E-01	4.90E-01
W4-W6	1.03E-01	3.71E-01	8.52E-01
W4-W7	**5.40E-04**	1.59E-01	**3.26E-02**
W4-W8	**2.94E-08**	2.66E-01	3.22E-01
W4-W9	**3.33E-10**	**4.82E-04**	**1.88E-02**
W5-W6	4.88E-03	7.13E-01	6.60E-01
W5-W7	**4.55E-06**	6.10E-02	1.40E-01
W5-W8	**3.98E-11**	5.49E-01	7.14E-01
W5-W9	**3.56E-13**	**3.05E-03**	8.20E-02
W6-W7	8.86E-02	**3.59E-02**	7.32E-02
W6-W8	**2.61E-04**	8.19E-01	4.57E-01
W6-W9	**8.06E-06**	**1.28E-02**	**4.28E-02**
W7-W8	5.14E-02	**2.35E-02**	3.14E-01
W7-W9	4.47E-03	**1.13E-05**	7.24E-01
W8-W9	3.25E-01	**2.67E-02**	1.98E-01

Table B3. The results for Kruskal–Wallis and Dunn's post-hoc tests with Bonferroni correction for phytoplankton, protozooplankton, and metazooplankton abundances between the transect sites on January 11, 2019. Values in bold are significantly different between the sites ($p<0.05$).

	Phytoplankton	**Protozooplankton**	**Metazooplankton**
Kruskal-Wallis	**2.50E-11**	**1.41E-18**	**6.33E-03**
Chi-square	59.17	35.04	15.30
Dunn's post hoc test sites			
S1-S2	**1.53E-05**	**1.52E-08**	3.42E-01
S1-S3	**3.41E-03**	**6.51E-04**	1.33E-01
S1-S4	**1.99E-02**	**2.85E-04**	7.79E-01
S1-S5	**2.33E-07**	**6.53E-04**	5.33E-02
S1-S6	**1.32E-07**	**1.65E-04**	**9.56E-04**
S1-S7	**2.96E-04**	**1.67E-04**	4.44E-01
S2-S3	2.33E-01	4.66E-01	5.71E-01
S2-S4	**3.62E-09**	**7.74E-13**	5.98E-01
S2-S5	8.30E-01	6.32E-01	2.97E-01
S2-S6	7.43E-01	7.01E-01	**2.11E-02**
S2-S7	9.56E-01	8.44E-01	1.31E-01
S3-S4	**2.71E-06**	**2.43E-13**	3.11E-01
S3-S5	3.78E-01	8.40E-01	6.22E-01
S3-S6	4.03E-01	7.38E-01	9.26E-02
S3-S7	2.90E-01	4.21E-01	5.12E-02
S4-S5	**1.28E-07**	**4.95E-10**	1.56E-01
S4-S6	**4.95E-08**	**3.24E-11**	**1.10E-02**
S4-S7	**2.53E-07**	**1.80E-10**	3.62E-01
S5-S6	9.27E-01	9.09E-01	2.74E-01
S5-S7	8.14E-01	5.53E-01	**2.14E-02**
S6-S7	7.41E-01	6.07E-01	**6.40E-04**

APPENDIX C - Supplementary material for Chapter IV

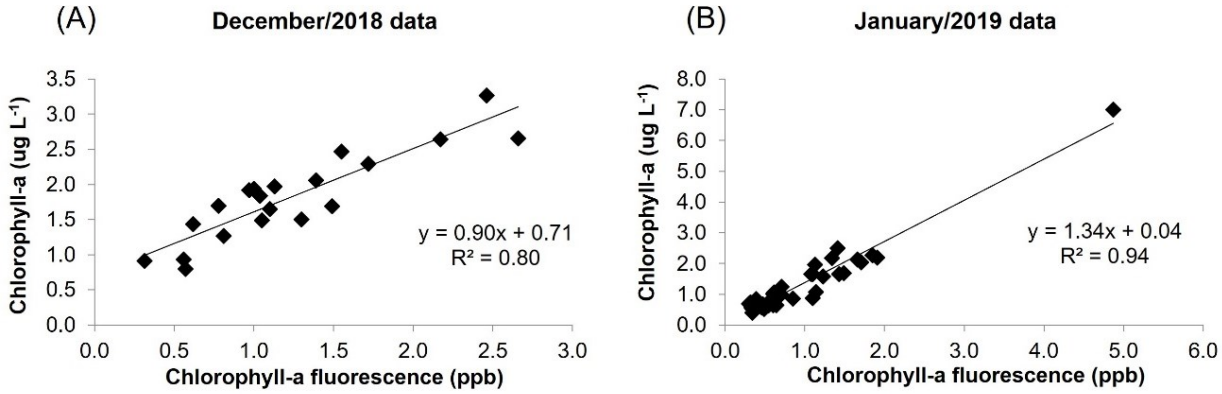

Fig. C1. Calibration curve for chlorophyll-a fluorescence data collected in (A) December 2018 (n= 20) and (B) January 2019 (n=40). The data collected between the period of 10 am to 4 pm and the outliers were excluded.

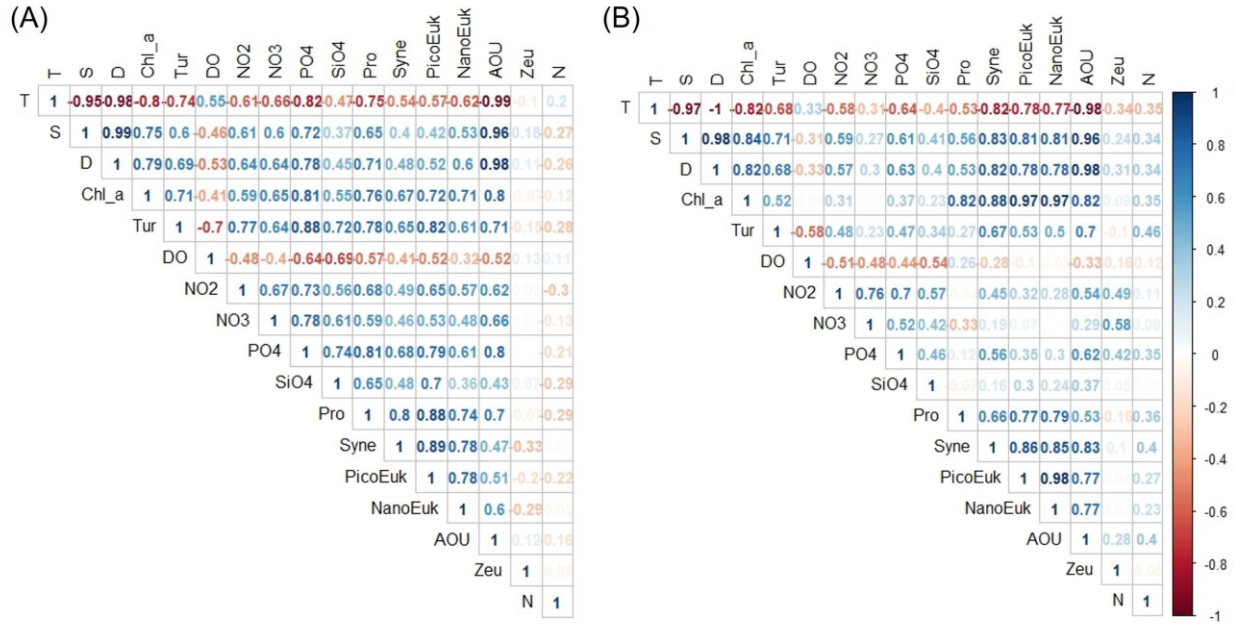

Fig. C2. Spearman`s rho matrices between environmental and biological data for (A) December 4 e (B) January 8. T = temperature; D = density; S = salinity; N = Brunt-Väisälä frequency; Chl_a = chlorophyll-a; Tur = turbidity; PO4 = phosphate; NO3 = nitrate; NO2 = nitrite; SiO4 = silicate; DO = dissolved oxygen; PicoEuk = Picoeukaryotes; NanoEuk = Nanoeukaryotes; Pro = *Prochlorococcus*; Syne = *Synechococcus*. AOU = Apparent oxygen utilization; and Zeu = Euphotic zone depth.

Table C1. Summary of the Principal Component Analysis (PCA) results for the first five dimensions for December 4 data.

	Dim.1	**Dim.2**	**Dim.3**	**Dim.4**	**Dim.5**
Eigenvalues	7.05	2.07	1.22	0.80	0.76
Explained variance (%)	54.22	15.94	9.39	6.13	5.83
Cumulative % of var.	54.22	70.16	79.55	85.68	91.51
Variables	*Contribution to each dimension (%)*				
T	11.25	0.50	2.90	8.90	7.88
S	4.17	32.74	0.32	0.17	0.22
D	8.93	15.82	1.31	0.73	1.15
Tur	11.10	1.72	0.40	0.75	0.16
DO	4.35	0.58	18.26	48.44	2.41
NO2	8.91	1.36	2.91	8.06	1.58
NO3	8.89	4.80	0.21	9.94	4.85
PO4	12.11	2.63	0.81	1.22	0.37
SiO4	6.63	4.20	7.88	0.00	33.10
N	2.81	32.07	0.02	0.14	13.36
Chl-a	10.15	0.32	0.55	8.14	5.85
AOU	10.71	0.36	4.61	5.84	12.97
Zeu	0.00	2.92	59.83	7.66	16.10

Table C2. Summary of the Principal Component Analysis (PCA) results for the first five dimensions for January 8 data.

	Dim.1	**Dim.2**	**Dim.3**	**Dim.4**	**Dim.5**
Eigenvalues	7.59	2.01	1.12	0.92	0.40
Explained variance (%)	58.39	15.48	8.61	7.08	3.08
Cumulative % of var.	58.39	73.87	82.49	89.57	92.64
Variables	*Contribution to each dimension (%)*				
T	11.90	1.17	0.52	1.75	11.62
S	8.55	12.94	0.81	2.17	1.10
D	10.83	5.55	0.98	2.57	6.34
Tur	9.26	0.25	6.73	11.82	2.10
DO	8.91	7.22	2.27	1.58	14.05
NO2	10.03	4.73	1.42	0.30	13.24
NO3	6.96	15.80	3.97	0.85	0.04
PO4	8.21	7.21	0.20	2.06	9.08
SiO4	5.37	6.44	24.19	2.43	0.69
N	2.18	8.06	8.01	57.10	1.51
Chl-a	4.17	20.70	0.97	8.64	31.31
AOU	12.04	2.43	0.21	0.68	4.69
Zeu	1.58	7.51	49.72	8.06	4.23

Table C3. Summary of the Redundancy Analysis (RDA) results for all the samples.

	RDA1	**RDA2**	**RDA3**	**RDA4**	**PC1**	**PC2**
Eigenvalue	0.95	0.06	0.01	0	0.12	0.05
Proportion Explained	0.78	0.05	0.01	0	0.1	0.04
Cumulative Proportion	0.78	0.83	0.84	0.84	0.94	0.98
		Scores for constraining variables				
Pro	0.38	0.00	0.20	-0.09	0.01	-0.22
Syne	1.69	0.42	-0.08	-0.03	0.79	0.25
PicoEuk	1.04	0.01	0.14	0.11	0.25	-0.25
NanoEuk	1.49	-0.48	-0.06	-0.02	0.33	-0.39
T	-0.75	-0.06	0.40	-0.07	0.00	0.00
S	0.28	0.14	0.08	-0.24	0.00	0.00
D	0.73	0.08	-0.23	-0.13	0.00	0.00
Chl-a	0.84	0.13	0.39	0.05	0.00	0.00
Tur	0.65	0.46	-0.07	0.22	0.00	0.00
DO	-0.16	-0.50	0.04	-0.33	0.00	0.00
NO2	0.49	0.30	-0.17	0.56	0.00	0.00
NO3	0.12	0.59	-0.19	0.46	0.00	0.00
PO4	0.20	0.72	0.07	0.24	0.00	0.00
SiO4	0.37	0.16	0.18	0.60	0.00	0.00
N	-0.04	-0.02	0.08	-0.05	0.00	0.00
AOU	0.77	0.02	-0.36	0.04	0.00	0.00
Zeu	-0.23	0.23	0.07	0.25	0.00	0.00
Permutation test (anova)	*Df*	*Variance*	*F*	*p-value*		
Model	13	1.020	16.95	0.001		

Table C4. Sampling stations with geographic coordinates, collection time (UTC-3), euphotic zone depth (Zeu, m), collection depth (m), physicochemical parameters (Chlorophyll-a (Chl-a, µg L^{-1}), Temperature (Temp., °C), Salinity, Density (kg m^{-3}), Turbidity (Tur., FTU), Dissolved oxygen (DO, mg L^{-1}), and Apparent oxygen utilization (AOU, µmol Kg^{-1})), nutrients (Nitrite, Nitrate, Phosphate, and Silicate; µM), and abundance (cell mL^{-1}) of *Synechococcus*, *Prochlorococcus*, picoeukaryotes, and nanoeukaryotes populations for December 4, 2018.

Station	Time (UTC-3)	Z_{eu} (m)	Depth (m)	Chl-a (µg L^{-1})	Temp. (°C)	Salinity	Density (Kg m^{-3})	Tur. (FTU)	DO (mg L^{-1})	AOU (µmol Kg^{-1})	Nitrite (µM)	Nitrate (µM)	Phosphate (µM)	Silicate (µM)	Pro (cell mL^{-1})	Syne (cell mL^{-1})	PicoEuk (cell mL^{-1})	NanoEuk (cell mL^{-1})
P1	10:00	16.5	0	1.05	23.07	35.20	1024.07	0.64	7.65	213.64	0.04	0.33	0.16	3.87	7966.3	6923.2	2620.5	292.5
-45.0922°W			12	1.88	21.02	35.36	1024.81	0.54	7.69	220.43	0.12	0.97	0.18	3.88	9660.0	23308.0	3468.0	1420.0
-23.5886°S			16	2.26	19.54	35.42	1025.31	1.38	7.19	226.45	0.1	0.23	0.22	4.44	9994.0	13113.7	3450.8	625.4
			24	2.39	19.02	35.46	1025.47	4.90	6.80	228.64	0.15	0.17	0.23	4.02	11480.0	14156.0	3564.0	864.0
P2	10:35	15.3	0	1.11	24.33	34.78	1023.38	0.85	7.40	208.59	0.1	0.18	0.16	4.26	8421.9	4458.3	2652.9	251.0
-45.0939°W			8	1.22	22.51	35.22	1024.28	0.33	7.99	214.81	0.07	0.18	0.14	3.31	7976.2	7182.5	2357.1	198.4
-23.5749°S			15	2.34	19.38	35.43	1025.32	3.86	7.13	227.10	0.2	0.72	0.32	4.24	8036.0	5304.0	2520.0	272.0
			20	2.16	19.08	35.45	1025.44	2.85	6.95	228.36	0.09	1.79	0.26	17.91	8332.0	5436.0	2528.0	332.0
P3	12:05	12.9	0	1.17	24.76	33.95	1022.62	0.91	7.46	208.03	0.11	0.12	0.14	5.26	7100.0	3208.0	2660.0	316.0
-45.0939°W			7	1.21	22.38	35.34	1024.40	0.25	8.01	215.16	0.02	0.11	0.1	0.55	6031.7	3285.7	1269.8	547.6
-23.5618°S			10	2.06	21.22	35.33	1024.73	0.68	7.94	219.68	0.11	0.65	0.15	3.29	5328.0	2304.0	1304.0	544.0
			15	2.47	19.74	35.43	1025.22	2.58	7.22	225.60	0.16	0.25	0.27	3.96	11064.0	59272.0	5152.0	1592.0
			18	3.10	19.47	35.43	1025.31	15.42	6.88	226.75	0.2	1.08	0.33	7.08	14080.0	74712.0	7904.0	992.0
P4	13:30	17.6	0	0.94	24.77	34.47	1023.01	0.39	7.48	207.68	0.05	0.07	0.13	4.45	5760.0	3856.0	1824.0	176.0
-45.0947°W			7	1.21	22.27	35.16	1024.30	0.50	8.20	215.80	0.03	0.08	0.13	1.38	4648.0	2736.0	984.0	272.0
-23.5487°S			12	2.87	20.03	35.39	1025.10	7.12	7.06	224.46	0.32	1.28	0.32	5.27	10584.0	87392.0	10440.0	1304.0
			16	3.06	19.85	35.39	1025.17	13.80	8.28	226.35	0.32	1.76	0.38	8.07	13488.0	89720.0	11560.0	1064.0
P5	14:10	10.6	0	0.97	24.13	34.66	1023.35	0.64	7.57	210.45	0.02	0.03	0.12	3.43	7712.0	13080.0	2920.0	304.0
-45.0952°W			7	1.70	22.35	35.13	1024.25	1.55	7.56	215.52	0.03	0.14	0.22	3.39	7336.0	44456.0	4056.0	640.0
-23.5378°S			12	2.71	20.93	35.32	1024.81	1.98	7.56	220.84	0.11	0.22	0.21	3.52	12264.0	181400.0	6064.0	1312.0
			15	3.43	20.49	35.36	1024.97	4.21	7.20	222.60	0.19	1.55	0.36	11.21	15039.7	181531.7	10761.9	1381.0
P6	14:40	10.6	0	1.04	24.53	34.83	1023.36	0.62	7.69	211.52	0.12	0.23	0.12	2.75	6888.0	6384.0	1712.0	296.0
-45.0961°W			7	1.98	22.03	35.13	1024.34	3.18	7.34	216.76	0.12	0.32	0.2	4.69	9168.0	74936.0	6400.0	944.0
-23.5293°S			15	2.66	21.73	35.20	1024.51	4.03	7.13	217.83	0.13	0.43	0.29	4.32	9512.0	171232.0	7096.0	1344.0
			18	2.58	20.97	35.31	1024.82	3.90	6.93	220.71	0.1	1.07	0.32	8.23	11280.0	171888.0	8024.0	1296.0
P7	15:00	14.1	0	1.07	24.55	34.72	1023.27	0.60	7.58	208.04	0.09	0.15	0.11	3.36	5488.0	5120.0	1608.0	184.0
-45.0996°W			5	1.04	23.25	34.93	1023.83	0.58	7.47	212.39	0.04	0.29	0.18	3.97	5608.0	8780.0	1328.0	166.0
-23.5197°S			8	1.17	22.59	35.18	1024.22	0.60	7.74	214.57	0.02	0.08	0.12	2.98	6976.0	12936.0	1848.0	352.0
			10	1.77	22.17	35.18	1024.35	2.15	7.37	216.15	0.12	0.22	0.18	4.69	8144.0	124680.0	7040.0	1224.0

Table C5. Sampling stations with geographic coordinates, collection time (UTC-3), euphotic zone depth (Zeu, m), collection depth (m), physicochemical parameters (Chlorophyll-a (Chl-a, µg L^{-1}), Temperature (Temp., °C), Salinity, Density (kg m^{-3}), Turbidity (Tur., FTU), Dissolved oxygen (DO, mg L^{-1}), and Apparent oxygen utilization (AOU, µmol Kg^{-1})), nutrients (Nitrite, Nitrate, Phosphate, and Silicate; µM), and abundance (cell mL^{-1}) of *Synechococcus*, *Prochlorococcus*, picoeukaryotes, and nanoeukaryotes populations for January 8, 2019.

Station	Time (UTC-3)	Zeu (m)	Depth (m)	Chl-a (µg L^{-1})	Temp. (°C)	Salinity	Density (Kg m^{-3})	Tur. (FTU)	DO (mg L^{-1})	AOU (µmol Kg^{-1})	Nitrite (µM)	Nitrate (µM)	Phosphate (µM)	Silicate (µM)	Pro (cell mL^{-1})	Syne (cell mL^{-1})	PicoEuk (cell mL^{-1})	NanoEuk (cell mL^{-1})
P1	10:00	27.0	0	0.50	28.43	34.71	1022.04	0.31	6.77	194.90	0.06	0.59	0.18	2.47	1792.0	624.0	128.0	16.0
-45.0922°W			10	0.99	24.80	35.30	1023.67	0.54	7.23	206.31	0.09	1.12	0.36	4.28	11584.0	1744.0	1400.0	88.0
-23.5886°S			15	3.51	21.90	35.56	1024.74	0.68	7.18	216.73	0.07	0.14	0.36	4.05	19888.0	61784.0	13728.0	2680.0
			24	1.25	16.69	35.60	1026.15	4.21	3.82	238.83	0.37	10.99	1	11.68	5720.0	50616.0	3416.0	208.0
P2	11:00	25.9	0	1.27	28.62	34.83	1022.06	1.98	6.81	194.86	0.09	1.96	0.55	1.92	2984.0	2632.0	224.0	0.0
-45.0939°W			10	1.27	24.46	35.36	1023.82	0.46	7.48	207.44	0.02	0.14	0.25	1.93	16280.0	16920.0	5584.0	584.0
-23.5749°S			15	7.56	21.25	35.48	1024.86	1.05	7.16	219.38	0.36	4.29	0.63	5.93	10384.0	32832.0	8128.0	640.0
			20	2.81	16.82	35.58	1026.09	5.47	4.70	238.25	0.25	5.9	0.72	6.76	8296.0	44696.0	5000.0	248.0
P3	11:47	15.3	0	0.43	28.67	34.84	1022.05	0.31	6.99	193.84	0.09	1.84	0.71	3.67	3088.0	2264.0	336.0	8.0
-45.0939°W			8	0.96	24.49	35.25	1023.72	0.60	7.44	207.46	0.02	1.99	0.17	0.65	13048.0	3440.0	1888.0	96.0
-23.5618°S			12	2.01	22.94	35.38	1024.29	0.62	7.50	212.98	0.07	0.17	0.22	3.22	13288.0	50624.0	9992.0	1728.0
			18	5.52	17.48	35.69	1026.01	13.28	5.01	235.07	0.47	2.98	0.83	10.91	18712.0	72296.0	11896.0	1608.0
P4	12:30	15.3	0	0.64	29.13	34.57	1021.70	0.46	7.02	192.92	0.07	0.55	0.19	6.54	7976.0	696.0	1496.0	64.0
-45.0947°W			8	1.39	24.65	35.34	1023.74	0.83	7.34	206.79	0.08	0.25	0.23	4.16	12168.0	1920.0	1632.0	160.0
-23.5487°S			12	5.29	22.57	35.57	1024.54	1.45	6.88	214.14	0.04	0.1	0.25	3.07	14312.0	46056.0	4320.0	320.0
			15	9.33	20.57	35.62	1025.15	5.37	5.54	221.93	0.25	1.33	0.45	5.56	9616.0	85768.0	10416.0	1704.0
P5	12:50	14.1	0	0.52	28.93	34.66	1021.83	0.48	7.06	193.52	0.01	0.1	0.12	4.66	7640.0	528.0	1056.0	40.0
-45.0952°W			8	1.00	25.72	35.16	1023.28	1.08	7.35	203.26	0.03	0.01	0.17	1.89	9544.0	1648.0	1192.0	64.0
-23.5378°S			12	2.92	23.04	35.43	1024.30	0.91	7.26	212.55	0.02	0.06	0.22	2.17	16368.0	16176.0	3576.0	392.0
			15	8.32	20.94	35.71	1025.12	3.58	6.36	220.32	0.16	0.78	0.46	5.25	16760.0	66592.0	9760.0	1176.0
P6	13:20	14.1	0	0.62	29.29	34.71	1021.75	0.77	6.95	193.12	0.02	0.21	0.13	3.19	5152.0	1096.0	888.0	56.0
-45.0961°W			8	1.27	24.31	35.29	1023.81	0.60	7.40	208.06	0.07	0.1	0.23	4.61	11392.0	1680.0	1272.0	72.0
-23.5293°S			12	7.44	22.33	35.53	1024.58	2.07	6.63	215.11	0.03	0.07	0.3	4.6	18656.0	79888.0	6696.0	696.0
P7	13:40	10.6	0	0.46	28.96	34.91	1022.02	0.70	6.93	192.95	0.05	0.22	0.12	4.79	7464.0	1592.0	1640.0	120.0
-45.0996°W			5	0.75	25.98	35.21	1023.22	0.68	7.29	202.31	0.01	0.08	0.58	4.61	11352.0	1704.0	1536.0	88.0
-23.5197°S			10	4.14	23.98	35.36	1023.96	2.87	7.15	209.17	0.07	0.16	0.23	2.78	19088.0	133392.0	9904.0	1440.0

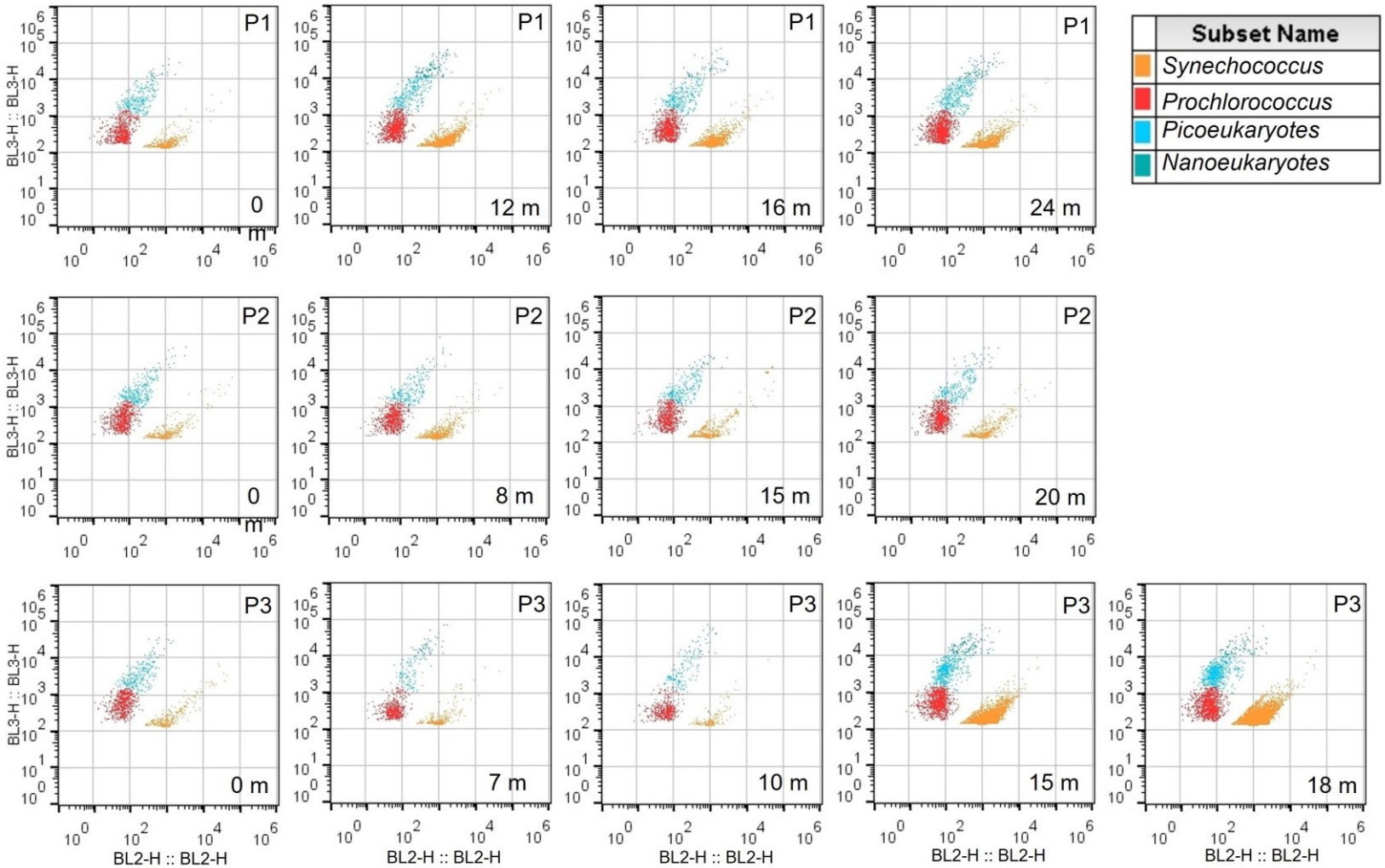

Fig. C3. Cytograms (phycoerythrin orange fluorescence/BL2-H vs. chlorophyll red fluorescence/BL3-H) discriminating the four populations for the samples collected in December/2018 at stations P1 to P3: *Synechococcus* (orange), *Prochlorococcus* (red), picoeukaryotes (light blue), and nanoeukaryotes (green).

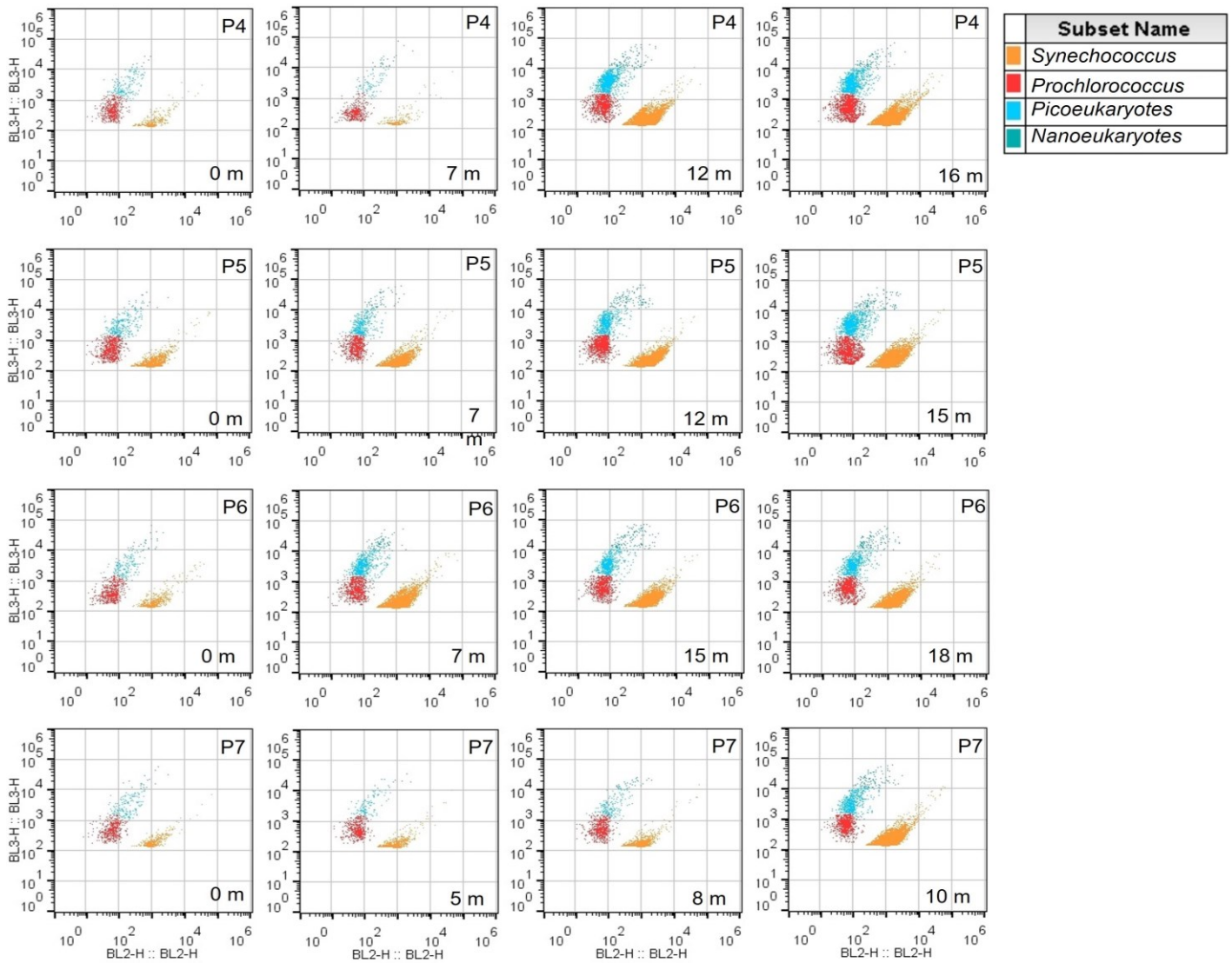

Fig. C4. Cytograms (phycoerythrin orange fluorescence/BL2-H vs. chlorophyll red fluorescence/BL3-H) discriminating the four populations for the samples collected in December/2018 at stations P4 to P7: *Synechococcus* (orange), *Prochlorococcus* (red), picoeukaryotes (light blue), and nanoeukaryotes (green).

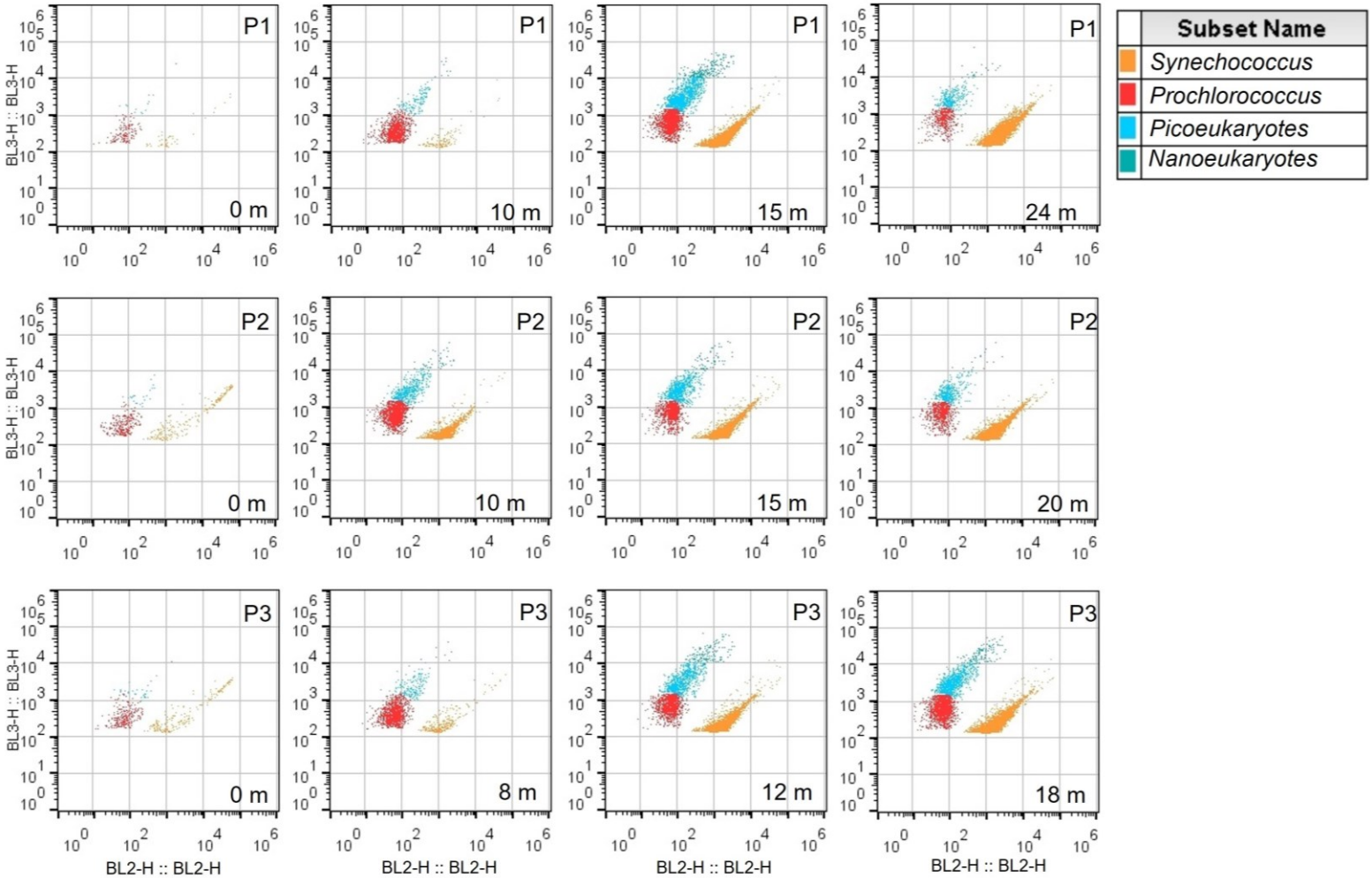

Fig. C5. Cytograms (phycoerythrin orange fluorescence/BL2-H vs. chlorophyll red fluorescence/BL3-H) discriminating the four populations for the samples collected in January/2019 at Stations P1 to P3: *Synechococcus* (orange), *Prochlorococcus* (red), picoeukaryotes (light blue), and nanoeukaryotes (green).

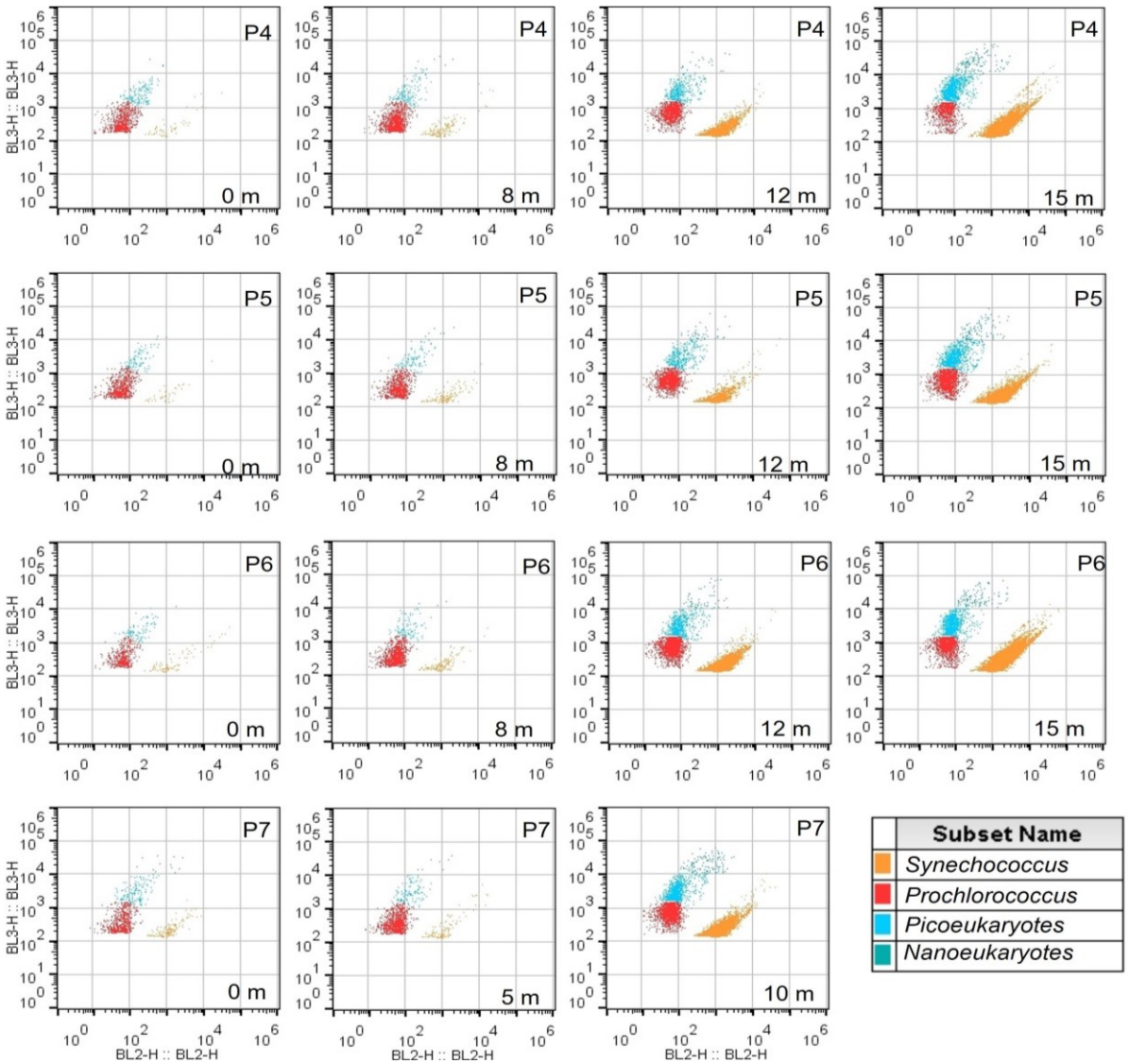

Fig. C6. Cytograms (phycoerythrin orange fluorescence /BL2-H vs. chlorophyll red fluorescence/BL3-H) discriminating the four populations for the samples collected in January/2019 at stations P4 to P7: *Synechococcus* (orange), *Prochlorococcus* (red), picoeukaryotes (light blue), and nanoeukaryotes (green).